UNIVERSITY OF OKLAHOMA

GRADUATE COLLEGE

SYNTHESIS AND CHARACTERIZATION OF POROUS HYDROXYAPATITE CERAMICS FOR BATCH AND COLUMN TREATMENT OF FLUORIDE-IMPACTED GROUND WATER

A DISSERTATION

SUBMITTED TO THE GRADUATE FACULTY

in partial fulfillment of the requirements for the

Degree of

DOCTOR OF PHILOSOPHY

By

ANISHA NIJHAWAN

Norman, Oklahoma

2019

SYNTHESIS AND CHARACTERIZATION OF POROUS HYDROXYAPATITE CERAMICS FOR BATCH AND COLUMN TREATMENT OF FLUORIDE-IMPACTED GROUND WATER

A DISSERTATION APPROVED FOR THE
SCHOOL OF CIVIL ENGINEERING AND ENVIRONMENTAL SCIENCE

BY

Dr. David A. Sabatini, Chair

Dr. Elizabeth C. Butler, Co-chair

Dr. Jim Chamberlain

Dr. Robert Nairn

Dr. Jadwiga Ziolkowska

Acknowledgement

None of this work would have been possible without the incredible support and encouragement of Dr. David Sabatini. He has been a constant source of guidance for nearly six years and the best doctoral advisor I could have asked for. My time as Dr. Sabatini's student has not only made me a more confident researcher, but also taught me the importance of grace and compassion in my professional life. I will forever be grateful for his faith in me.

I'd also like to thank Mrs. Frances Sabatini for making me feel at home in Norman with her warmth, friendship and support.

I'd like to express my gratitude to Dr. Elizabeth Butler for mentoring me at every step of my research and helping to sharpen my academic and writing skills. Her inputs in to my presentations and journal articles have been invaluable. I would also like to thank her for giving me the opportunity to serve as her teaching assistant, which was a great learning experience and instilled a lot of confidence in me.

I'd like to thank Dr. Jim Chamberlain for his mentorship all these years. He has given me innumerable opportunities to develop my skills outside the lab, especially through interaction with the WaTER Minor students. His contribution to my learning experience at OU has been immense.

I'd like to especially express my thanks to Dr. Robert Nairn and Dr. Jadwiga Ziolkowska for taking the time to serve as my committee members and their invaluable inputs in refining this dissertation.

I also thank Dr. Preston Larson at the Electron Microscopy lab for the hours he spent helping me develop micrographs of my materials which were essential to my research.

I'm grateful to the wonderful staff of the School of Civil Engineering and Environmental Science and the WaTER Center, Susan Williams, Molly Smith and Cindy Murphy for their help with paperwork, scheduling meetings, making sure I met important deadlines and stayed on track to graduate.

I owe a huge thanks to my former lab mates Dr. Laura Brunson, Dr. Junyi Du and Dr. Teshome Yami for their incredible support and guidance at each step of my doctoral program. Many thanks also to my talented undergraduate researchers, Stephanie Vo and Tri Pham, who spent time working with me in the lab. I admire their curiosity and drive.

I have many people to thank for the role they played in ensuring my personal well-being over the years. My wonderful friends and lab mates – Rajan Jha, Balwinder Singh, Conner Flansburg, Erin Thornton, Dan Markman, Juan Arango, Ian Thom, Parichat Phaodee (Tam), Philip Deal, Nusrat Sharmin, Yifan Ding and Brandi Dittrich for all the great times over the past five years. I feel truly fortunate to have met such an incredible group of people who made Norman special for me.

I am deeply grateful for the unwavering support of my family who helped me become the person I am today and who never stopped believing in me. I'd like to specially mention my beautiful niece and nephew who make me the world's proudest aunt.

Finally, I'd like to thank Pratik Samant, who supports me and inspires me with his brilliance, empathy and humor every day.

Table of Contents

List of Tables

List of Figures

Abstract

Elevated levels of naturally occurring fluoride affect the drinking water of approximately 200 million people worldwide in the Eastern Rift Valley of Africa, India, China and parts of North and South America. Intake of fluoride above the World Health Organization (WHO) guideline value of 1.5 mg/L causes dental and skeletal fluorosis. Dental fluorosis results in the darkening and mottling of teeth while skeletal fluorosis leads to joint stiffness, bone deformation and limited mobility. Two widely used fluoride removal adsorbents – activated alumina and bone char – suffer from limitations including low fluoride adsorption capacity, high cost and physical and chemical instability at extreme pH values. Moreover, bone char can impart an unpleasant color and taste to treated water and is considered culturally unacceptable in parts of south-Asia.

In recent years, porous clay ceramics have become popular for point-of-use water filtration to remove solids and filter out or inactivate bacteria and viruses. However, their fluoride removal capacity is low. Therefore, this research focused on developing porous ceramics from hydroxyapatite, a material with known affinity for fluoride. Porous ceramics were made by mixing hydroxyapatite powders with different types of starches and firing the mixture in a kiln at 1200 ^{o}C which left behind a well-connected porous ceramic structure. The maximum fluoride adsorption capacities of these ceramics, determined by fitting isotherm data to Langmuir parameters, ranged from 6 to 18 mg/g, depending on the volume ratio of hydroxyapatite and starches as well as their size.

The ceramic made with 50% hydroxyapatite and 25% each of insoluble rice starch and soluble starch (by volume) had the best adsorption performance. Using finer hydroxyapatite (d_{50} of 100 μm) had 50% higher fluoride adsorption than larger hydroxyapatite particles (d_{50} of 240 μm).

Scanning electron micrographs showed that the pore sizes of these ceramics ranged from 0.11 – 2.6 μm and 0.11 – 6.9 μm, respectively.

The best performing ceramic, with a maximum adsorption capacity of 18 mg/g, was regenerated with 1 M NaOH, while retaining 70% of its original adsorption capacity for up to four adsorption cycles. Further, it had good selectivity for fluoride and, of several compounds evaluated, only chloride competed for adsorbent sites at concentrations commonly found in groundwater.

The kinetic performance of these adsorbents was tested through batch kinetic tests and continuous-flow columns studies. Equilibrium fluoride concentration and time to reach equilibrium were found to be independent of adsorbent size, suggesting that the effective intraparticle diffusivity is independent of adsorbent size. Continuous-flow columns studies revealed that the breakthrough curves, plotting the effluent fluoride concentration versus number of bed volumes treated, were dependent on flow rate. As flow rate was increased, the number of bed volumes treated to breakthrough (when C_{eff} = 1.5 mg/L) decreased. Interrupting the column flow led to a decrease in effluent concentration suggesting that the column was run under non-equilibrium conditions and that mass transport was limited by intraparticle diffusion, i.e., diffusion of fluoride ions into the pores and along the surface of the pores inside the ceramic.

The Rapid Small-Scale Columns Tests (RSSCT) approach was also applied and validated for this adsorbent. The RSSCT approach is used to design small-scale columns that can be tested in the lab in a fraction of the time and consume much less resources compared to a pilot study. If done correctly, the breakthrough curves of these columns should accurately predict the performance of larger and full-scale columns. Smaller column designed under the assumption of constant effective

diffusivity was found to be a good predictor of the breakthrough curve of a larger column, confirming the validity of the RSSCT approach.

On a bed volume basis, the ceramic performed six to seven times better than activated alumina and bone char. The cost of manufacturing this media was found to be approximately $1.6 per kg, estimated from bulk raw material costs and electricity consumption, which is comparable to the cost of commercially available activated alumina, demonstrating that this media has the potential to be very cost-effective.

Overall, this research adds to the body of knowledge on the use of porous hydroxyapatite ceramic adsorbents for water treatment. Smaller size of starting powders resulted in smaller pores and higher internal surface area, which led to higher adsorption capacity. The ceramic showed strong affinity for fluoride and chloride, with no interference from nitrate, sulfate, bicarbonate and phosphate and, retained 70% of its adsorption capacity for up to four adsorption cycles when regenerated with 1 M NaOH. Intraparticle diffusion-limited adsorption in continuous-flow columns was scaled up using the Rapid Small-Scale Column Test (RSSCT) approach, establishing the applicability of this ceramic in community-level treatment systems. Preliminary cost analyses showed that this media has the potential to be technically and economically competitive with commonly used activated alumina and should be further developed and evaluated for full scale implementation.

Chapter 1 Introduction

Fluoride in drinking water

The Sustainable Development Goals (SDGs) aim to achieve universal access to safe and affordable drinking water by 2030 and improve water quality by reducing pollution and eliminating untreated, hazardous waste from being released into the environment (United Nations, 2015). Although 2.6 billion people have gained access to improved drinking water sources in the past two decades, an estimated 663 million still live without access to safe drinking water, predominantly in rural areas (United Nations 2016, 2017). Most water-related diseases arise from microbial contamination; however, a significant number of health issues occur as a result of chemical contamination of drinking water (WHO, 2017). Of these, fluoride poses a considerable risk because the contribution of drinking water to overall fluoride intake is considered important in preventing adverse health effects (WHO, 2017).

Nearly 200 million people worldwide are exposed to elevated levels of naturally occurring (geogenic) fluoride in their drinking water (Fewtrell et al., 2006). High fluoride concentrations are found in regions with volcanic activity and in areas where groundwater comes in contact with igneous rocks such as granite and basalt that are rich in fluoride minerals (Amini et al., 2008). Regions affected by geogenic fluoride include parts of China, India, the Rift Valley of East Africa, South Africa, Mexico and the southwest United States (Meenakshi and Maheshwari, 2006; Amini et al., 2008; Brindha et al., 2010; Odiyo and Makungo, 2012). Fluoride has a strong affinity for the inorganic component of bones and teeth – hydroxyapatite, a calcium phosphate salt with very low solubility (K_{sp} at 25°C = $10^{-116.8}$) (McCann, 1953; Dorozhkin, 2007). Adults retain 36% of ingested fluoride while children can retain up to 50% (Buzalaf and Whitford, 2011). Drinking-

water is a major contributor to overall fluoride intake. While at low concentrations, fluoride helps to strengthen tooth enamel and prevent caries, at high concentrations it is known to cause dental and skeletal fluorosis (Fawell et al., 2006). Dental fluorosis results in the darkening and mottling of teeth, which can cause problems resulting from social stigma such as reduced employability and eligibility for marriage (Narayana et al., 2004). Skeletal fluorosis symptoms include joint stiffness, bone deformation and limited mobility (Kaseva, 2006; Meenakshi and Maheshwari, 2006). This can impair the livelihood of those employed in manual labor and farm work. The World Health Organization recommends 1.5 mg/L of fluoride in drinking water below which the risk of fluorosis is minimal (WHO, 2011).

Fluoride removal technologies

Fluoride water treatment technologies that have been tested and optimized for field application include activated alumina (Ghorai and Pant, 2005; Brunson and Sabatini, 2014), bone char (Brunson and Sabatini, 2009; Medellin-Castillo et al., 2016; Shahid et al., 2019), electrocoagulation (Gwala et al., 2011), Nalgonda technique (Dahi, 2016; Fawell et al., 2006; Meenakshi and Maheshwari, 2006) and membrane processes (Mohapatra et al., 2009; Sehn, 2008; Shen et al., 2015). Activated alumina and bone char are adsorbent media that can be packed in a column through which fluoride-rich water flows. Electrocoagulation and the Nalgonda technique, both developed in India, involve precipitating fluoride with dissolved aluminum ions. The dissolved aluminum is introduced via aluminum electrode plates in the electrocoagulation method (Gwala et al., 2011), with aluminum dissolving when electric current is applied to the plates. In the Nalgonda technique, alumina and lime are added to fluoride-rich groundwater under constant stirring (Nawlakhe and Paramasivam, 1993). In both electrocoagulation and Nalgonda

technologies, aluminum forms a complex with fluoride to form a fluoride-rich precipitate (floc) which must be periodically removed and disposed of. Membrane processes such as reverse osmosis (Ndiaye et al., 2005, Hu et al., 2006) and electrodialysis (Sahli et al., 2007) require skilled operators and significant financial inputs that make them cost-prohibitive in low-income settings (Ayoob et al., 2008).

Activated alumina (γ-Al_2O_3) is an extensively studied commercially available fluoride removal material. Hydrous aluminum oxides found in bauxite are 'activated' by heating between 600 and 750^oC in the presence of oxygen (a process called calcination). The loss of water molecules at these temperatures creates a porous material with surface areas up to 350 m^2/g (Choi and Chen, 1976; Hao and Huang, 1986). The fluoride adsorption capacity of activated alumina varies depending on the adsorption pH and method of activation (Dahi, 2000; Leyva-Ramos et al., 2008). Bhatnagar et al. (2011) and Ku and Chiou (2002) found that the optimum pH range for fluoride removal is between 6 and 7.5. Below a pH of 6, soluble alumino-fluoro complexes dominate, while at more alkaline pH, hydroxide and bicarbonate ions compete with fluoride for surface sites (Hao and Huang, 1986). While the maximum adsorption capacity under laboratory conditions was 16 mg/g at a pH of 6.0 (Ku and Chiou, 2002), field studies have reported adsorption capacities as low as 1 mg/g because of incomplete activation of aluminum oxides (COWI, 1998). The solubility of alumina under acidic conditions puts further constraints on its applicability as a fluoride adsorbent. Studies have reported aluminum leaching at or below a pH of 6 because of formation of soluble aluminum species (Al Zubaidy et al., 2011). This can pose a real health hazard because aluminum and its complexes have been reported to increase the risk of Alzheimer's and cognitive decline (Davison et al., 1982, Rondeau et al. 2008).

Bone char is also commonly used to remove fluoride from drinking water in low-income settings. Animal or fish bones are heated in a low-oxygen or anoxic environment up to 700^{o}C (Mlilo et al., 2009). This drives off volatile organics, leaving behind a porous 'activated' material consisting of hydroxyapatite (60 - 80%), calcium carbonate (6 -10%) and carbon (7 - 10%) (Wilson et al., 2003). This process, known as thermal activation of bone, can produce chars with a high surface area of 100 – 150 m^2/g (Medellin-Castillo et al., 2007; Brunson and Sabatini, 2009). The chemical composition of bone char coupled with its high surface area make it an attractive option for adsorption of fluoride and heavy metal ions such as arsenic and lead (Fawell, 2006). Since the starting material can be procured from waste animal bones, it's also cost-effective in developing countries. Medellin-Castillo et al. (2007) and Levya-Ramos et al. (2010) reported a maximum fluoride adsorption capacity of 12 mg/g at a pH of 3, but it was reduced by half at a pH of 7. The pH dependence of the fluoride adsorption capacity of bone char indicates that electrostatic attraction between the surface of bone char and fluoride ions is the dominant mechanism of fluoride removal. Studies have reported a pH_{pzc} of 8.4 (Brunson and Sabatini, 2009). Below this pH, the hydroxyl groups of the hydroxyapatite are protonated, and fluoride ions can adsorb to the positively charged surface. The surface charge density increases as the pH is lowered below the pH_{pzc}, resulting in increased fluoride adsorption (Medellin-Castillo et al., 2007). Above the pH_{pzc}, the surface is net negatively charged and fluoride adsorption is negligible. This poses a potential problem for the applicability of bone char since fluoride-rich groundwaters with pH as high as 9.3 to 9.5 have been reported in Kenya and India (Coetsiers et al., 2008, Salve et al., 2008).

Additional limitations on the use of bone char arise from user acceptability. Dahi and Bregnhøj (1997) found that charring conditions were critical to the quality of water treated by bone char. In rural settings, charring is done in kilns, where control of oxygen poses a challenge. Improper

charring that doesn't eliminate volatile organics can lead to an unpleasant taste, smell and color in the treated water (Jacobsen and Dahi, 1998). In certain parts of the world, use of animal-based products to treat water is against cultural beliefs. For example, bone chars that are derived from cows or pigs would be unacceptable in south-Asian communities.

Low-cost adsorbent materials that are easy to fabricate, are stable at a range of pH values, show a high affinity towards fluoride and are not derived from animal products can be used to address these challenges. While fine, powdered adsorbents can disperse in water resulting in clogging and an eventual increase in head loss, granular adsorbents, such as porous ceramics, offer the advantage of better hydraulic performance in flow-through columns (Chen et al., 2010).

Viability of ceramics for water treatment

Porous ceramic filters have become a viable water treatment option in developing countries in recent years. They are made by mixing an inorganic material, usually clay, with an organic pore-forming agent such as saw dust, with compaction and firing at temperatures above 1000 ^{o}C (Lantagne, 2001). The organic materials burn off while the clay particles sinter to form a porous ceramic body (the coalescence of grains when heated to just below their melting point is referred to as sintering). Macro porous ceramics (with average pore size larger than 50 nm) have been used to filter and to remove suspended solids and bacterial pathogens (Lantagne, 2001; Oyanedel-Craver and Smith, 2008) or as ceramic tablets for the release of microbicidal ions (Ehdaie et al., 2014). Yang et al. (2005, 2007) fabricated silver-doped hydroxyapatite ceramics for removal of microorganisms but little research has been done to explore the potential of ceramics for fluoride removal. Clay-based ceramics have low fluoride adsorption (Hendrickson and Vik, 1984; Moges et al., 1996) due to low surface area and low affinity of fluoride toward clay. Chen et al. (2010,

2014) evaluated the fluoride removal capacity of granular ceramics made by combining clay and starch with ferric and aluminum salts and reported 90% fluoride removal with an initial concentration of 20 mg/L. However, a systematic study is yet to be done to test the fluoride adsorption capacity of ceramics made from materials with an intrinsic affinity for fluoride or to test the effect of properties such as pore size, total pore volume (or porosity), type of pore forming agent, grain size of raw materials, compaction pressure or sintering temperature on adsorbent performance.

For ceramics to be effective as fluoride adsorbents, materials with high specific surface areas and high adsorption affinities for fluoride are needed. These ceramics should have enough strength to withstand handling and operation and should be easy to synthesize and regenerate in order to minimize cost of manufacture and disposal.

Hydroxyapatite and its affinity for fluoride

As previously mentioned, hydroxyapatite is a non-toxic, low-solubility calcium phosphate mineral found in animal bones and teeth (Chao and Poon 1987; McCann, 1953; Dorozhkin, 2007). It is the most stable form of calcium phosphate above a pH of 4.8 (Somasundaran et al., 1985). Its suitability as a ceramic adsorbent is reinforced by the fact that it does not undergo phase change up to 1250^{o}C beyond which it is converted to tricalcium phosphate (Sato et al., 1979; Chen et al., 1989).

Hydroxyapatite is a versatile adsorbent, capable of removing chemical contaminants and microorganisms from aqueous systems by surface sorption or ion exchange. It can remove heavy metals (Jang et al., 2008; Piccirillo et al., 2013; Zendehdel et al., 2016), fluoride (Huang and Liu, 1999; Hammari et al., 2004), arsenic (Mirhosseini et al., 2014) and pathogenic bacteria (Berry and

Siragusa, 1997) from water. Zhang et al. (2012) reported a fluoride adsorption capacity of 40 mg/g at a pH of 3.0 which decreased to 20 mg/g above a pH 6.0. Lin et al (1981) and Sundaram et al. (2008) similarly reported a decrease in adsorption with increase in pH. This is explained by the net surface charge and electrostatic interactions between fluoride and hydroxyapatite, as discussed above. Hydroxyapatite has a point of zero charge (pH_{pzc}) between 7.8 and 8.5 (Bell et al., 1973; Sundaram et al., 2008). This refers to the pH at which the net surface charge of a solid is zero. Under acidic conditions, strong electrostatic attraction exists between fluoride ions and the positively charged hydroxyapatite surface, resulting in high fluoride uptake. Studies also suggest dissolution of calcium ions from the apatite lattice below a pH of 4 and the resulting precipitation of CaF_2 (Ramsay et al., 1973). As the solution pH approaches the pH_{pzc}, the surface of hydroxyapatite becomes less positive and the attractive forces between the surface and fluoride ions weaken. Hydroxide and bicarbonate ions also compete with fluoride for surface sites.

The mechanism of uptake of fluoride can be a combination of non-specific physical adsorption, resulting from electrostatic attraction, ion exchange between fluoride and hydroxide ions to form fluorapatite and the formation of calcium fluorite (CaF_2). The contribution of each mechanism depends on experimental conditions. Spinelli et al. (1971) studied the impact of pH, concentration and reaction time on the uptake of fluoride by hydroxyapatite and found that non-specific adsorption was the predominant mechanism at neutral pH but decreased as the pH was reduced below 5. Exchange of fluoride and hydroxide ions at the crystal surface occurred with long-term application of fluoride at acidic pH, leading to the formation of fluorapatite. Hydroxide and fluoride ions can readily exchange in solution because they have the same charge and similar ionic radii (1.40 and 1.36 Å, respectively) (Lin et al., 1981). Finally, CaF_2 precipitation occurs at fluoride

concentrations in a narrow range (between 500 and 1000 mg/L) and at very low pH (Spinelli et al., 1971).

While hydroxyapatite ceramics are widely used as biomedical implants, their potential applications for water treatment have not been explored. Yang et al. (2005, 2007) fabricated silver-doped hydroxyapatite ceramics with starch as pore-former and reported more than 99.9% removal of *E. coli* and 50% removal of Reovirus Type 3 cells. Yakub and Soboyejo (2013) developed a clay-hydroxyapatite composite ceramic for the simultaneous removal of fluoride and microorganisms. While the binding action of clay improved the strength of hydroxyapatite, the fluoride removal capacity of these composite ceramics decreased with increasing clay content.

The goal of this dissertation is to contribute to the existing knowledge on ceramics for water treatment by developing porous hydroxyapatite ceramics and testing their viability as a low-cost fluoride treatment option for emerging regions, where people depend on fluoride-impacted groundwater for drinking and for sustenance. Specifically, this research seeks to:

1) Synthesize porous hydroxyapatite ceramics using different types of insoluble and soluble starches and test their fluoride removal capacity (Chapter 2)

2) Study the impact of hydroxyapatite particle size on the pore morphology, surface area and fluoride adsorption capacity of these ceramics and test their regeneration potential and selectivity for fluoride (Chapter 3)

3) Evaluate the kinetic performance of these ceramics in batch kinetic and continuous-flow columns and test the Rapid Small-Scale Column Tests (RSSCT) approach for these adsorbents (Chapter 4)

Overview of chapters

Chapter 2 discusses the first objective of this research which was to develop porous hydroxyapatite ceramics with enough strength to withstand operation and handling while achieving desirable levels of fluoride uptake. Porous ceramic beads approximately 5 mm in diameter were made using hydroxyapatite powder (d_{50} 240 µm) along with different types of insoluble starches and soluble starch as pore-forming agents. The effect of varying the volume ratios of each component (hydroxyapatite and pore forming agents), the type of pore forming agent and ceramic fabrication conditions such as temperature and compaction pressure on fluoride adsorption was tested through batch adsorption studies. Results from the batch adsorption studies were fitted to the Langmuir isotherm and the maximum adsorption capacities ranged from 7 to 12 mg/g depending on the volume ratio of each component. The ceramic with 50% hydroxyapatite and 25% each of insoluble rice starch and soluble starch exhibited the best fluoride removal (12 mg/g). The fluoride adsorption directly correlated to open porosity (proportion of pores connected to the surface and therefore, accessible to fluoride ions).

In chapter 3, the goal of the second phase of this research was to improve upon the fluoride adsorption capacity of the ceramics by decreasing their pore size. It was hypothesized that smaller pores would improve fluoride adsorption by increasing the surface area of the ceramic. Since it has been reported in literature that pore size can be controlled by changing the particle size of the starting materials, finer hydroxyapatite particles (d_{50} of 100 µm as opposed to 240 µm) were used to make the ceramics. Some practical aspects of the adsorbent performance, such as their regeneration potential and selectivity for fluoride, were also assessed. NaOH solutions were used as regenerating solutions and the ceramics were subjected to repeated adsorption and desorption

cycles. Finally, the ceramic's selectivity for fluoride was examined by adding different concentrations of anions commonly found in groundwater and studying the change in fluoride removal. Finer hydroxyapatite grains showed a 50% improvement in maximum fluoride adsorption capacity. As hypothesized, the maximum pore diameter decreased from 6.9 to 2.6 μm and the maximum fluoride adsorption capacity increased from 12 mg/g to 18 mg/g. The ceramic showed high selectivity for fluoride relative to anions commonly found in groundwater and natural organic matter (NOM) and could be regenerated for up to five adsorption cycles using 0.05 M and 0.1 M sodium hydroxide.

Chapter 4 focused on studying the kinetics of fluoride adsorption with these ceramics. Kinetic studies were conducted using batch adsorption tests as well as continuous-flow column studies. Columns were operated at different flow rates to assess the impact of residence time on fluoride adsorption. Mass balances were conducted to determine the fluoride loading in each case. The mass loading at the point of exhaustion (C_{eff} = 0.85 C_0) increased with decrease in empty bed contact time (EBCT) while the mass loading at breakthrough (C_{eff} = 1.5 mg/L) showed the opposite trend. Interrupting the column flow led to a temporary decrease in the effluent fluoride concentration illustrating that these columns were under non-equilibrium conditions. This suggests that intraparticle diffusion plays a role in the kinetics of fluoride uptake. The Rapid Small-Scale Column Tests (RSSCT) approach was also tested and validated for these materials. This approach uses dimensionless equations to scale down from pilot-scale columns to small-scale columns that can be tested in the lab in a fraction of the time. Two small columns were designed using the constant diffusivity (CD) and proportional diffusivity (PD) RSSCT approaches, respectively. The CD approach was a better fit for these ceramics as there was more overlap between the breakthrough curves of the large column and the CD RSSCT column.

Chapter 5 discusses the main findings of this body of work on developing porous hydroxyapatite ceramic adsorbents and suggests potential for future research.

References

1. Al Zubaidy, E. A., Mohammad, F. S., & Bassioni, G. (2011). Effect of pH, salinity and temperature on aluminum cookware leaching during food preparation. *International Journal of Electrochemical Science*, *6*(12), 6424-6441.
2. Bell, L. C., Posner, A. M., & Quirk, J. (1973). The point of zero charge of hydroxyapatite and fluorapatite in aqueous solutions. *Journal of Colloid and Interface Science*, *42*(2), 250-261.
3. Berry, E. D., & Siragusa, G. R. (1997). Hydroxyapatite adherence as a means to concentrate bacteria. *Applied and Environmental Microbiology*, *63*(10), 4069-4074.
4. Bhatnagar, A., Kumar, E., Sillanpaa, M. (2011). Fluoride removal from water by adsorption-A review. *Chemical Engineering Journal*, *171*(3), 811-840.
5. Buzalaf, M. A. R., & Whitford, G. M. (2011). Fluoride metabolism. In *Fluoride and the oral environment* (Vol. 22, pp. 20-36). Karger Publishers.
6. Chao, S. Y., & Poon, C. K. (1987). Histologic study of tissue response to implanted hydroxylapatite in two patients. *Journal of oral and maxillofacial surgery*, *45*(4), 359-362.
7. Choi, W. W., & Chen, K. Y. (1979). The removal of fluoride from waters by adsorption. *Journal-American Water Works Association*, *71*(10), 562-570.
8. Coetsiers, M., Kilonzo, F., & Walraevens, K. (2008). Hydrochemistry and source of high fluoride in groundwater of the Nairobi area, Kenya/Hydrochimie et origine des fortes

concentrations en fluorure dans l'eau souterraine de la région de Nairobi, au Kenya. *Hydrological sciences journal*, *53*(6), 1230-1240.

9. COWI (1998) Review of Practical experiences with defluoridation in rural water supply programmes Part II 73 pp. Ministry of Foreign Affairs, Danida, Copenhagen.
10. Dahi, E. (2000). The state of art of small community defluoridation of drinking water. *Eli Dahi Sunsanee Rajchagool & Nipaphan Osiriphan*, 141.
11. Dahi, E., & Bregnhøj, H. (1995). Significance of oxygen in processing of bone char for defluoridation of water. In *Proceedings of the 1st international workshop on fluorosis and defluoridation of water, Ngurdoto, Tanzania*, 96-103.
12. Dahi, E. (2016). Africa's U-Turn in defluoridation policy: From the Nalgonda technique to bone char. *Fluoride*, *49*(4), 401.
13. Davison, A.M., Oli, H., Walker, G.S., Lewins, A.M. (1982). Water supply aluminium concentration, dialysis dementia, and effect of reverse–osmosis water treatment. *Lancet 320*, 785–787.
14. Dorozhkin, S. V. (2007). Calcium orthophosphates. *Journal of materials science*, *42*(4), 1061-1095.
15. Fawell, J., Bailey, K., Chilton, J., Dahi, E., & Magara, Y. (2006). *Fluoride in drinking-water*. IWA publishing.
16. Fulmer, M., & Brown, P. W. (1992). Low-Temperature Formation of Fluorapatite in Aqueous Solution. *Journal of the American Ceramic Society*, *75*(12), 3401-3407.
17. Hammari, L. E. L., Laghzizil, A., Barboux, P., Lahlil, K., & Saoiabi, A. (2004). Retention of fluoride ions from aqueous solution using porous hydroxyapatite: structure and conduction properties. *Journal of hazardous materials*, *114*(1-3), 41-44.

18. Hao, O. and Huang, C. (1986). Adsorption Characteristics of Fluoride onto Hydrous Alumina. *Journal of Environmental Engineering, 112* (6), 1054-1069.
19. Hu, K., & Dickson, J. M. (2006). Nanofiltration membrane performance on fluoride removal from water. *Journal of Membrane Science*, *279*(1-2), 529-538.
20. Huang C.J. and Liu J.C. (1999). Precipitate flotation of fluoride-containing wastewater from a semiconductor manufacturer. *Water Research, 33*(16), 3403-3412.
21. Reyes Bahena, J. L., Robledo Cabrera, A., López Valdivieso, A., & Herrera Urbina, R. (2002). Fluoride adsorption onto α-Al2O3 and its effect on the zeta potential at the alumina–aqueous electrolyte interface. *Separation Science and technology*, *37*(8), 1973-1987.
22. Jacobsen, P. and Dahi, E. 1998 Low cost domestic defluoridation of drinking water by means of locally charred bone. In: *Proceedings of the 2nd International Workshop on Fluorosis and Defluoridation of Water*. Nazareth, 19–22 November 1997, The International Society for Fluoride Research, Auckland.
23. Jang, S. H., Jeong, Y. G., Min, B. G., Lyoo, W. S., & Lee, S. C. (2008). Preparation and lead ion removal property of hydroxyapatite/polyacrylamide composite hydrogels. *Journal of Hazardous Materials, 159*(2), 294-299.
24. Ku, Y., & Chiou, H. M. (2002). The adsorption of fluoride ion from aqueous solution by activated alumina. *Water, air, and soil pollution*, *133*(1-4), 349-361.
25. Leyva-Ramos, R., Medellin-Castillo, N. A., Jacobo-Azuara, A., Mendoza-Barron, J., Landin-Rodriguez, L. E., Martinez-Rosales, J. M., & Aragon-Piña, A. (2008). Fluoride removal from water solution by adsorption on activated alumina prepared from pseudo-boehmite. *Journal of Environmental Engineering Management*, *18*(5), 301-309.

26. Leyva-Ramos, R., Rivera-Utrilla, J., Medellin-Castillo, N. A., & Sanchez-Polo, M. (2010). Kinetic modeling of fluoride adsorption from aqueous solution onto bone char. *Chemical Engineering Journal*, *158*(3), 458-467.

27. Lin, J., Raghavan, S., & Fuerstenau, D. W. (1981). The adsorption of fluoride ions by hydroxyapatite from aqueous solution. *Colloids and Surfaces*, *3*(4), 357-370.

28. Medellin-Castillo, N. A., Leyva-Ramos, R., Ocampo-Perez, R., Garcia de la Cruz, R. F., Aragon-Pina, A., Martinez-Rosales, J. M. & Fuentes-Rubio, L. (2007). Adsorption of fluoride from water solution on bone char. *Industrial & Engineering Chemistry Research*, *46*(26), 9205-9212.

29. Medellin-Castillo, N. A., Padilla-Ortega, E., Tovar-García, L. D., Leyva-Ramos, R., Ocampo-Pérez, R., Carrasco-Marín, F., & Berber-Mendoza, M. S. (2016). Removal of fluoride from aqueous solution using acid and thermally treated bone char. *Adsorption*, *22*(7), 951-961.

30. Mirhosseini, M., Biazar, E., & Saeb, K. (2014). Removal of Arsenic from Drinking Water by Hydroxyapatite Nano Particles. *Current World Environment, (9)2*, 331-338.

31. Mlilo, T. B., Brunson, L. R., & Sabatini, D. A. (2009). Arsenic and fluoride removal using simple materials. *Journal of Environmental Engineering*, *136*(4), 391-398.

32. Mohapatra, M., Anand, S., Mishra, B. K., Giles, D. E., & Singh, P. (2009). Review of fluoride removal from drinking water. *Journal of environmental management*, *91*(1), 67-77.

33. Narayana, A. S., Khandare, A. L., & Krishnamurthi, M. V. R. S. (2004, March). Mitigation of fluorosis in Nalgonda district villages. In *Proceedings of the fourth international workshop on fluorosis prevention and defluoridation of water* (pp. 2-6).

34. Nawlakhe, W. G., & Paramasivam, R. (1993). Defluoridation of potable water by Nalgonda technique. *Current Science*, *65*(10), 743-748.

35. Ndiaye, P. I., Moulin, P., Dominguez, L., Millet, J. C., & Charbit, F. (2005). Removal of fluoride from electronic industrial effluent by RO membrane separation. *Desalination*, *173*(1), 25-32.

36. Piccirillo, C., Pereira, S. I. A., Marques, A. P., Pullar, R. C., Tobaldi, D. M., Pintado, M. E., & Castro, P. M. (2013). Bacteria immobilisation on hydroxyapatite surface for heavy metals removal. *Journal of Environmental Management*, *121*, 87-95.

37. Rondeau, V., Jacqmin-Gadda, H., Commenges, D., Helmer, C., & Dartigues, J. F. (2008). Aluminum and silica in drinking water and the risk of Alzheimer's disease or cognitive decline: findings from 15-year follow-up of the PAQUID cohort. *American journal of epidemiology*, *169*(4), 489-496.

38. Sahli, M. M., Annouar, S., Tahaikt, M., Mountadar, M., Soufiane, A., & Elmidaoui, A. (2007). Fluoride removal for underground brackish water by adsorption on the natural chitosan and by electrodialysis. *Desalination*, *212*(1-3), 37-45.

39. Salve, P. R., Maurya, A., Kumbhare, P. S., Ramteke, D. S., & Wate, S. R. (2008). Assessment of groundwater quality with respect to fluoride. *Bulletin of environmental contamination and toxicology*, *81*(3), 289.

40. Shahid, M. K., Kim, J. Y., & Choi, Y. G. (2019). Synthesis of bone char from cattle bones and its application for fluoride removal from the contaminated water. *Groundwater for Sustainable Development*, *8*, 324-331.

41. Shen, J., Mkongo, G., Abbt-Braun, G., Ceppi, S. L., Richards, B. S., & Schäfer, A. I. (2015). Renewable energy powered membrane technology: Fluoride removal in a rural community in northern Tanzania. *Separation and Purification Technology*, *149*, 349-361.
42. Somasundaran, P., Amankonah, J. O., & Ananthapadmabhan, K. P. (1985). Mineral—solution equilibria in sparingly soluble mineral systems. *Colloids and Surfaces*, *15*, 309-333.
43. Spinelli, M. A., Brudevold, F., & Moreno, E. C. (1971). Mechanism of fluoride uptake by hydroxyapatite. *Archives of oral biology*, *16*(2), 187-203.
44. Sundaram, C. S., Viswanathan, N., & Meenakshi, S. (2008). Defluoridation chemistry of synthetic hydroxyapatite at nano scale: equilibrium and kinetic studies. *Journal of Hazardous Materials*, *155*(1-2), 206-215.
45. United Nations, 2015 Transforming our World: The 2030 Agenda for Sustainable Development. A/RES/70/1 (https://sustainabledevelopment.un.org, *Accessed 1-15-2019)*
46. United Nations, 2016 Progress towards the Sustainable Development Goals", E/2016/75
47. United Nations, 2017 Progress towards the Sustainable Development Goals", E/2017/66
48. WHO, 2017 Guidelines for drinking-water quality: fourth edition incorporating the first addendum. World Health Organization, Geneva.
49. Wilson, J. A., Pulford, I. D., & Thomas, S. (2003). Sorption of Cu and Zn by bone charcoal. *Environmental geochemistry and health*, *25*(1), 51-56.
50. Zendehdel, M., Shoshtari-Yeganeh, B., & Cruciani, G. (2016). Removal of heavy metals and bacteria from aqueous solution by novel hydroxyapatite/zeolite nanocomposite, preparation, and characterization. *Journal of the Iranian Chemical Society*, *13*(10), 1915-1930.

51. Zhang, D., Luo, H., Zheng, L., Wang, K., Li, H., Wang, Y., & Feng, H. (2012). Utilization of waste phosphogypsum to prepare hydroxyapatite nanoparticles and its application towards removal of fluoride from aqueous solution. *Journal of hazardous materials*, *241*, 418-426.

Chapter 2 Macroporous hydroxyapatite ceramic beads for fluoride removal from drinking water[1]

Abstract

This study evaluates the capacity of hydroxyapatite ceramics to remove fluoride from drinking water. Porous hydroxyapatite ceramic beads approximately five mm in diameter were fabricated using soluble potato starch as well as insoluble rice starch, wheat starch, corn starch, and cellulose as pore-forming agents. Calcination of hydroxyapatite particles, followed by mixing with starches and water, compaction, and sintering at 1200 ^{o}C resulted in formation of macroporous ceramic beads with maximum fluoride adsorption capacities ranging from 7 to 12 mg/g, depending on the relative proportions of different pore-forming agents. Increasing the insoluble starch content from 0 to 25% by volume in ceramics with 50% by volume hydroxyapatite led to a marked improvement in fluoride adsorption by creating interconnected macropores, as evidenced by scanning electron microscopy (SEM). Calcination of hydroxyapatite powder at or above 400 ^{o}C prior to ceramic preparation was required to obtain a ceramic material with sufficient structural integrity to withstand operation and handling after sintering.

[1] Nijhawan, A., Butler, E. C., & Sabatini, D. A. (2017). Macroporous hydroxyapatite ceramic beads for fluoride removal from drinking water. *Journal of Chemical Technology & Biotechnology*, *92*(8), 1868-1875.

Introduction

Naturally occurring elevated fluoride is estimated to affect the drinking water of up to 200 million people worldwide; regions impacted include South Africa, the Rift Valley of East Africa, China, India, and parts of the southwestern United States (Fewtrell et al., 2006; Meenakshi and Maheshwari, 2006; Amini et al., 2008; Brindha et al., 2010; Odiyo and Makungo, 2012). At low concentrations, fluoride helps prevent dental caries and strengthens tooth enamel, but at higher concentrations it can cause dental and skeletal fluorosis (Fawell et al., 2006). Dental fluorosis results in darkening or mottling of teeth, which can cause problems due to social stigma and reduced employability. Skeletal fluorosis can cause bones to become deformed or stiff, limiting mobility and/or causing pain (Kaseva, 2006; Meenakshi and Maheshwari, 2006), thus impairing the livelihood of those who depend on manual activities, including subsistence farming. For these reasons, the World Health Organization (WHO) recommends a fluoride concentration below 1.5 ppm in drinking water (WHO, 2011).

In recent years, ceramics have gained popularity as a viable water treatment option in developing countries. Clay ceramics, while effective for removal of microorganisms, have shown limited fluoride adsorption (Hendrickson and Vik, 1984; Moges et al., 1996) due to low specific surface area and low affinity for fluoride. Yakub and Soboyejo (2013) developed a clay-hydroxyapatite composite ceramic that can simultaneously remove fluoride and microbial pathogens. While the binding action of clay improved the strength of hydroxyapatite, the fluoride removal capacity of these composite ceramics decreased with increasing clay content. This highlights the need for ceramic materials with a high intrinsic affinity for fluoride. These ceramics should also have sufficient strength to withstand handling and operation and should be easy to synthesize and

regenerate in order to minimize cost of manufacture and disposal. A porous, granular adsorbent such as a ceramic also has the advantage of better hydraulic performance as a flow-through material during field operation. Fine powders can disperse in water resulting in clogging (Chen et al., 2010) and an eventual increase in head loss across a column. A porous ceramic bead adsorbent can potentially overcome these challenges.

The natural affinity of hydroxyapatite for fluoride is well documented (McCann, 1953; Spinelli et al., 1971; Lin et al., 1981; Huang and Liu, 1999; Hammari et al. 2004; Sundaram et al., 2008; Jiminéz-Ryes and Solache-Ríos, 2010; Bhatnagar et al., 2011) and porous hydroxyapatite ceramics have been prepared using different pore-forming agents. Tang et al. (2008) formed macroporous ceramic disks by compacting and firing hydroxyapatite powders mixed with polystyrene microspheres and found pores between 1 and 12 µm. Komlev et al. (2001) synthesized porous ceramic granules using a biopolymer as sacrificial template and reported pore sizes ranging from 4 nm to 14 µm. The starch consolidation method, using starch as the pore-forming agent, is a common technique to produce porous ceramics (Lyckfeldt et al., 2001). In addition to their gelling property, starches are inexpensive, non-toxic and available in both high-income and low-income countries. Slosarczyk et al. (1999) and Yang et al. (2005, 2007) fabricated macro-porous ceramics using water-soluble and insoluble starches. Water-soluble starches precipitated on hydroxyapatite particles before sintering, leaving small pores on the order of one to several micrometers, while insoluble starches optimized permeability by creating linkages between these small pores (Yang et al., 2005). Bhattacharjee et al. (2007) reported the use of soluble starch both as a thickener and a pore-forming agent.

Ceramics are made by compacting loose granular material or powders into desired shapes and then heating them to temperatures just below their melting point (Reed 1995) by a process called sintering (IUPAC, 2006). Under the influence of heat, atoms on the surface begin to diffuse towards the point of contact between two adjacent grains to minimize the surface curvature and surface energy (Herring, 1951; Zhang and Gladwell, 1998). This leads to neck formation between the two grains. As this process continues, a grain boundary develops and diffusion of atoms normal to this boundary results in densification (Ashby 1974; Zhang and Gladwell, 1998). The properties of sintered ceramics are influenced by the characteristics of the starting powders, including grain size, morphology and presence of impurities (Pask, 1979). Heating grains in the presence of air, or calcination (IUPAC 2006), prior to sintering is an important step in controlling these properties. Exter et al. (1994) and Wang et al. (2011) reported an increase in grain size during calcination. The larger grain sizes resulting from calcination lowered the driving force for surface diffusion but promoted grain boundary diffusion and densification (Landi et al., 2000), resulting in an increase in the density (Exter et al., 1994) and strength of the resulting ceramics (Juang and Hon, 1996). For example, Scalera et al. (2013) found that the compressive strength of porous hydroxyapatite scaffolds improved when calcination temperature was increased from 600 ^{o}C to 900 ^{o}C.

Although hydroxyapatite ceramics are widely used as biomedical implants, their potential application in water treatment has not been studied extensively. Yang et al. (2007) developed silver-doped hydroxyapatite ceramics for bacterial and viral filtration, while Yakub and Soboyejo (2013) evaluated the fluoride removal capacity of clay-hydroxyapatite composite ceramics. However, the fluoride adsorption capacity of pure hydroxyapatite ceramics prepared using starch as organic binder and pore forming agent has not been tested before. Specifically, the optimum ratio of hydroxyapatite to pore forming agent(s) and the effect of sintering and densification on

the capacity of hydroxyapatite for fluoride adsorption is unknown. Thus, the objectives of this research were to fabricate porous hydroxyapatite ceramics using different types of starches and cellulose as pore forming agents, and to test their fluoride adsorption capacity. Further, the effect of varying parameters such as percent volume of pore-forming agents, calcination temperature of hydroxyapatite, and type of pore-forming agent, was studied.

Materials and Methods

Synthesis of hydroxyapatite

Hydroxyapatite was synthesized by the wet precipitation method (Verwilghen et al., 2007). One liter of 0.3 M ammonium phosphate solution at pH 10.3 was slowly added to 1 L of 0.5 M solution of calcium nitrate at pH 10.7, while stirring at 300 rpm at 40 ^{o}C. A 5 M solution of ammonium hydroxide was used to raise the pH of the individual solutions before mixing. All chemicals were purchased from Sigma-Aldrich Corporation, USA. After preparation, the mixture was allowed to age for 60 hours at 40 ^{o}C and then washed with deionized water to remove ammonium salts. Finally, the resulting solids were air-dried at room temperature. The literature reports a specific surface area (SSA) value of 140 m^2/g for hydroxyapatite prepared using this method (Verwilghen et al., 2007). The synthesized hydroxyapatite was sieved and the particle fraction between 40 to 80 mesh (0.420 mm to 0.177 mm) was retained and calcined at 250, 400, 500, 600, 750, or 900 ^{o}C for 6 hours.

Preparation of ceramics

In order to create a porous ceramic material, the calcined hydroxyapatite powder was mixed with soluble starch (hydrolyzed potato starch) and either insoluble starch or cellulose (all purchased from Sigma-Aldrich Corporation, USA) in different ratios. Cellulose and three different types of

insoluble starch – rice, corn and wheat – were used because they varied in size (from 2 to 50 μm) and shape (Figure S2.1). These pore forming agents were also selected for their low ash content (< 0.6%) (Product Specification sheet, sigmaaldrich.com) and ready availability in low-income countries.

Ceramic materials were named according to the following rule: volume of hydroxyapatite – percent volume of insoluble starch or cellulose – percent volume of soluble starch. For example, "50-15-35" refers to a ceramic made with 50% by volume hydroxyapatite, 15% by volume insoluble starch, and 35% by volume soluble starch. All ceramics were made using rice starch as the insoluble component, except where otherwise noted. Furthermore, all results shown are for hydroxyapatite calcined at 500 ^{o}C, unless a different temperature precedes the abbreviation. Rice starch was chosen for the majority of experiments because it was reported to have the smallest granule size (~2 μm) of the four insoluble pore-forming materials (Jane et al., 1994).

Calcined hydroxyapatite, insoluble starch or cellulose, and soluble starch solution (1.5 g/10 mL of deionized water) were mixed in different volume ratios for one minute with a stainless steel spatula, then pressed into a galvanized steel cylindrical mold of length 30 mm and diameter 15 mm (Scott Fetzer Co., USA) at 10 MPa for 120 seconds using a manual hydraulic press (Dake Corporation, USA) to form a compacted composite. The compacted material was then demolded and shaped into beads of approximately 5 mm diameter by hand. Finally, the beads were fired in an electric kiln (Paragon Calderon Kiln, Paragon Industries, L.P.) at a rate of 5 ^{o}C/min and held at 1200 ^{o}C for 2 hours to make a porous ceramic material.

Batch studies

Batch tests were conducted to determine the fluoride removal capacity of the prepared ceramics. Ten grams of ceramic per liter of fluoride solution were used, with initial fluoride concentrations ranging from 5 to 100 parts per million (ppm). Fluoride solutions were prepared by diluting 1000 ppm NaF solution with a solution of 4-(2-hydroxythyl)-1-piperazineethanesulfonic acid (HEPES) buffer to yield a final HEPES concentration of 50 mM and a pH of 7.0. The buffer solution, without fluoride, was used as a blank to ensure fluoride measurement free of contamination. After preparation, samples, in duplicate, were equilibrated on a reciprocal shaker at 30 rpm for 24 hours. After equilibration, the samples were filtered (Whatman, Qualitative filter paper, 150 mm diameter) and the equilibrium fluoride concentration was determined using an ion selective electrode (ElectrodesDirect, Canada). A three-point calibration curve was prepared with standard fluoride concentrations (1, 10 and 100 mg/L). Prior to analysis, samples, blanks, and standards were diluted with total ionic strength adjustment buffer (TISAB) in a 1:1 ratio to maintain a constant pH and ionic strength. The undiluted TISAB contained 60 g/L acetic acid, 58.5 g/L NaCl, and 4 g/L 1, 2–cyclohexylenedinitrilotetraacetic acid (CDTA).

Experimental data were fitted to a Langmuir isotherm by non-linear regression using Sigma Plot 13 (Systat Software, Chicago, Il) to obtain estimates of maximum adsorption capacity, Q_{max}, in mg/g and K (affinity of adsorbent for fluoride) in L/mg. C_e is the equilibrium fluoride concentration in mg/L. The $Q_{1.5}$ (mg/g) value (Q at C_e = 1.5 mg/L) was calculated from the fitted parameters.

Estimates of the sample standard deviations of duplicate C_e and Q_e measurements were calculated using Microsoft Excel 2013 and are depicted as error bars in the isotherms. Uncertainties in Q_{max}

and $Q_{1.5}$ represent standard errors determined from nonlinear regression using SigmaPlot 13 (Q_{max}) and error propagation ($Q_{1.5}$).

Material characterization

The specific surface area (SSA) of the ceramics was determined by the BET method using a Quantochrome Autosorb Automated Gas Sorption System with a Beckman Coulter SA-3100 Surface Area Analyzer and N_2 adsorption.

X-ray diffraction (XRD) analysis of hydroxyapatite powders and powdered ceramic beads was conducted with a Rigaku Ultima IV powder X-ray diffractometer with Cu Kα radiation and Bragg–Brentano optics. Jade 5.0 (Materials Data, Livermore, CA) was used for data analysis. XRD patterns were compared to the powder diffraction file (PDF) of the International Center for Diffraction Data to identify the phase. The pore structure of ceramic materials was characterized by scanning electron microscopy (SEM) using a JEOL JSM-840 microscope operating at 15 kV after sputter coating with gold and palladium. Prior to sputtering, the ceramic beads were cleaved with a double edge stainless steel blade (Proctor & Gamble Co., USA) to obtain images of the internal cross-section.

Density and open porosity of different ceramic materials was measured by ASTM C373-14a (ASTM, 2014). Open porosity is the volume fraction of all interconnected pores and voids that can be measured by gas or liquid penetration (ASTM, 2015). The 10 Ball-Pan Hardness test (ASTM, 2010) was done to estimate the in-service resistance to abrasion and degradation of these ceramic materials. While this test does not exactly mimic water treatment conditions, it is able to compare the hardness and abrasion resistance of different ceramic materials relative to each other, and the

results of the test seemed to correlate with the material's ability to undergo adsorption isotherm experiments without falling apart.

Results and Discussion

Composition and crystallinity of ceramics

X-ray diffraction (XRD) patterns of hydroxyapatite powder (Figure 2.1a) and hydroxyapatite ceramics (Figure 2.1b) showed that both consisted of a pure hydroxyapatite phase. There was also an increase in crystallinity upon sintering at 1200 ^{o}C, evidenced by the increase in intensity of peaks in Figure 2.1b (sintered) compared to Figure 2.1a (unsintered). No thermal decomposition or phase change of hydroxyapatite was observed upon sintering.

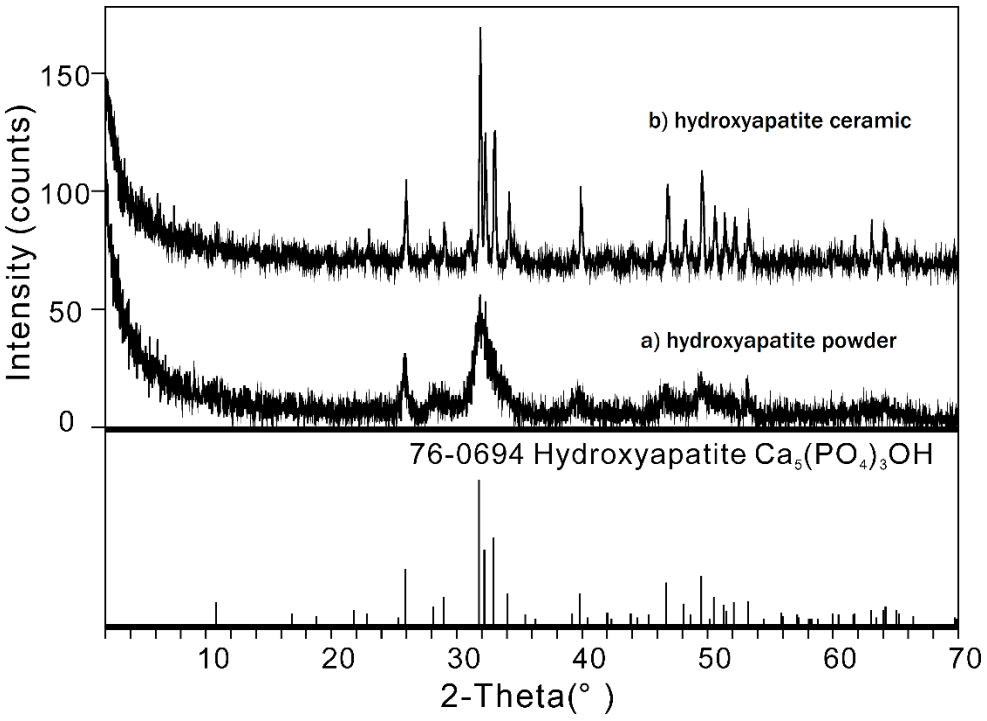

Figure 2.1 XRD pattern of a) hydroxyapatite powder and b) hydroxyapatite ceramic

Adsorption of fluoride

Batch tests were used to determine the fluoride removal capacity of hydroxyapatite ceramics and to study the effect of starch content, calcination temperature and type of pore forming agents on the fluoride removal. The maximum fluoride adsorption capacity (Q_{max}) of hydroxyapatite ceramics, based on a fit to the Langmuir isotherm, was between 7 and 12 mg/g (Figures 2.2 a-d, Table 2.1). This is higher than literature reported maximum adsorption capacities of activated alumina (4.1 mg/g) and bone char (6.1 mg/g) (Brunson and Sabatini, 2014), and is comparable to reported adsorption capacities of hydroxyapatite powder (4.7 to 14.3 mg/g) (Joschek et al., 2000; Jiminéz-Ryes and Sloache-Rios, 2010; Sternitzke et al., 2012).

Effect of starch content

Ceramic materials formed with hydroxyapatite and only insoluble rice starch in different ratios showed limited strength and crumbled easily, so no adsorption experiments were conducted with these materials. Soluble starch was found to be essential for the formation of cohesive ceramic bodies. Soluble starch granules gelatinized in water and acted as a binder, allowing formation of compacted shapes prior to sintering (Lyckfeldt and Ferreira, 1998).

In the absence of insoluble starch, an increase in soluble starch content from 40 to 70%, with a corresponding decrease in hydroxyapatite content, did not have a statistically significant effect on the maximum adsorption capacities of hydroxyapatite ceramics (Table 2.1). However, the addition of insoluble starch to hydroxyapatite/soluble starch mixtures significantly increased the adsorption capacity of the resulting ceramic. In particular, addition of 25% by volume insoluble starch (50-25-25) resulted in a three-fold increase in $Q_{1.5}$ compared to the ceramic with no insoluble starch (50-0-50) (Figure 2.2a, Table 2.1). A series of adsorption experiments using ceramic adsorbents

with different ratios of hydroxyapatite, insoluble starch, and soluble starch, showed that the 50-25-25 ceramic was found to have the highest fluoride adsorption capacity (Figure 2.2b, Table 2.1). At a solid to liquid ratio of 10 g/L, this ceramic adsorbent was able to lower the fluoride concentration from 10 to 0.2 ppm (a 98% decrease). This is well below 1.5 ppm, the WHO limit for fluoride in drinking water.

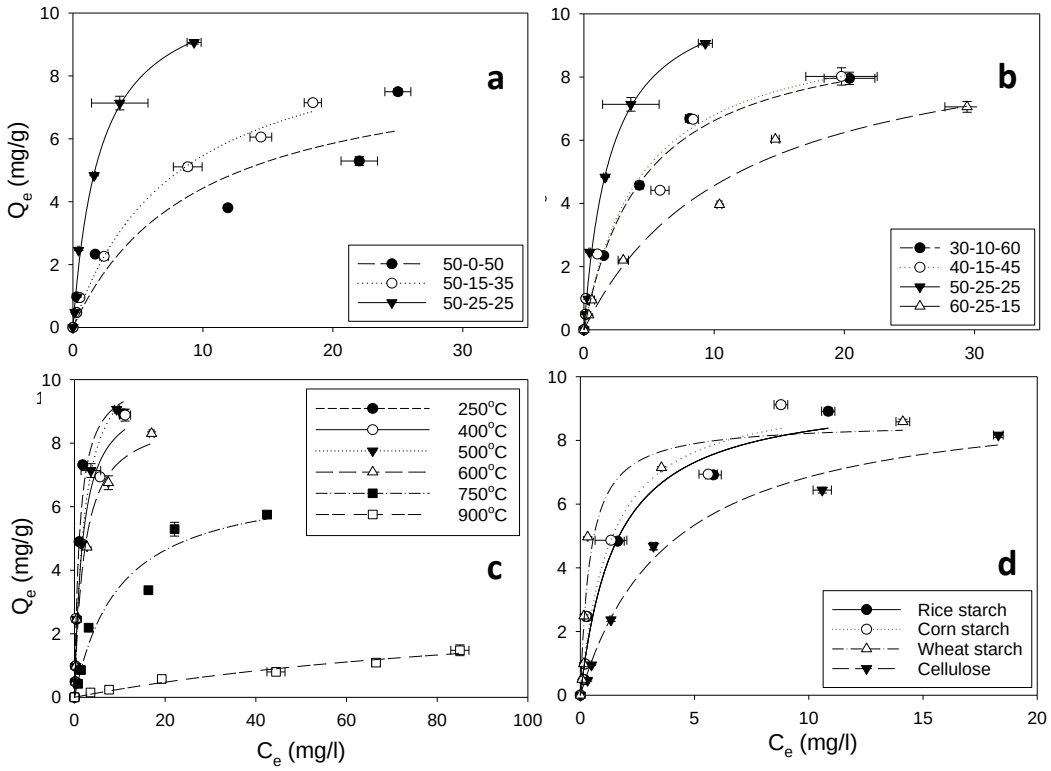

Figure 2.2 Fluoride adsorption to a) ceramics made with 50% hydroxyapatite (calcined at 500 ^{o}C) and varying ratios of insoluble rice starch and soluble starch, b) ceramics made with varying contents of hydroxyapatite (calcined at 500 ^{o}C), insoluble rice and soluble starch, c) 50-25-25 ceramics calcined at different temperatures, and d) 50-25-25 ceramics made with hydroxyapatite calcined at 500 ^{o}C and different types of insoluble starch and cellulose, all with Langmuir isotherm fits.

Table 2.1 Adsorption capacity of ceramic materials with varying fractions of hydroxyapatite and insoluble rice starch and soluble starch, and calcined at 500 ^{o}C

Adsorbent	**Q_{max} (mg/g)**	**$Q_{1.5}$ (mg/g)**	**K (L/mg)**
Ceramics without insoluble rice starch			
60-0-40	7.4 ± 0.8	1.5 ± 0.6	0.2 ± 0.1
50-0-50	7.9 ± 0.6	2.1 ± 0.7	0.3 ± 0.1
40-0-60	8.5 ± 1.2	2.5 ± 0.8	0.3 ± 0.1
30-0-70	8.6 ± 0.9	2.2 ± 1.1	0.3 ± 0.2
Ceramics with 50% hydroxyapatite and varying insoluble rice and soluble starch content			
50-0-50	7.9 ± 0.6	2.1 ± 0.7	0.3 ± 0.1
50-15-35	9.6 ± 1.4	2.4 ± 0.6	0.03 ± 0.01
50-25-25	12.4 ± 0.8	5.8 ± 1.1	0.8 ± 0.2
Ceramics with different ratios of hydroxyapatite, insoluble rice and soluble starch			
30-10-60	9.6 ± 0.7	2.5 ± 0.3	0.2 ± 0.1
40-15-35	9.7 ± 0.9	2.2 ± 0.6	0.2 ± 0.1
50-25-25	12.4 ± 0.8	5.8 ± 1.1	0.8 ± 0.2
60-25-15	9.4 ± 1.4	1.8 ± 0.5	0.1 ± 0.03

Addition of greater than 25% insoluble starch caused ceramics to disintegrate during handling. This may have been due to the fact that at a higher insoluble starch content, there was insufficient hydroxyapatite to enclose the pores and form a solid matrix.

The role of insoluble starch can be explained by its impact on the resulting ceramic pore structure. Adsorbents with 50% hydroxyapatite, 50% by volume soluble starch, and no insoluble starch (50-0-50) had pores that were much smaller than 5 μm (Figure 2.3a), whereas ceramics with 25% each of insoluble and soluble starch (50-25-25) had interconnected pore spaces that were larger than 5 μm (Figure 2.3b). (Pore sizes were estimated from SEM images.) The difference in pore structures of 50-0-50 and 50-25-25 ceramics can be explained by the difference in pore forming mechanisms of insoluble and soluble starch. Yang et al. (2005) reported that soluble starch adsorbs on the hydroxyapatite powders, acting as a binder between hydroxyapatite and insoluble starch. This results in formation of small pores enclosed by hydroxyapatite granules (as in Figure 2.3a). In contrast, insoluble starch particles aggregate in water at higher temperatures and form large, interconnected pores on burning (Figure 2.3b).

The difference in pore forming mechanisms is also evident from measurements of open porosity (Table 2.2). Ceramics made with 30% hydroxyapatite, 0% insoluble starch and 70% soluble starch resulted in an open porosity of only 37%. In contrast, increasing the content of insoluble starch from 0 to 25%, with a corresponding decrease in soluble starch content for 50% hydroxyapatite ceramics (from 50-0-50 to 50-25-25), increased open porosity from 31 to 45% (Table 2.2). The increase in open porosity upon raising the insoluble starch content from 0-25% for the 50% hydroxyapatite ceramics also resulted in an increase in fluoride adsorption (Figure 2.2a, Table 2.1) and SSA (Figure 2.4a). Specifically, increasing the insoluble starch content from 0 to 25% caused both the $Q_{1.5}$ (Table 2.1, Figure 2.4a) and SSA values (1.29 m^2/g for 50-0-50 to 4.02 m^2/g for 50-25-25 (Figure 2.4a)) to increase by a factor of about three. This suggests that $Q_{1.5}$ is a function of surface area. The SSA results are an order of magnitude higher than the surface area reported by Joschek et al. (2000) (0.1 m^2/g) for porous hydroxyapatite ceramics made from natural bone.

Compared to open porosity, the density of ceramic materials was less sensitive to an increase in the volume of insoluble starch. Rather, it depended more on the combined volume of both soluble and insoluble starches. For example, upon increasing the volume of soluble starch from 40 to 70%, the density decreased 28%, from 1.52 to 1.10 g/cm^3 (Table 2.2). However, on increasing the ratio of insoluble to soluble starch while keeping the total starch volume constant for ceramics with 50% hydroxyapatite (i.e., changing from 50-0-50 to 50-25-25), the density decreased only 5%, from 1.42 to 1.35 g/cm^3. This suggests that both open pores (resulting from large pores formed by insoluble starch) and closed pores (resulting from small pores enclosed by hydroxyapatite granules formed by soluble starch) contribute to a decrease in density.

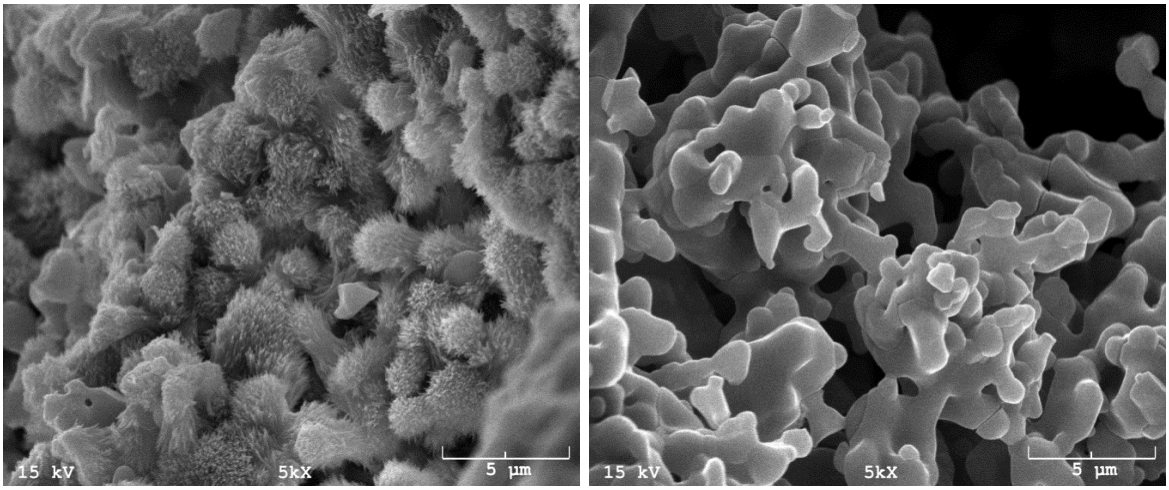

a) b)

Figure 2.3 SEM images of a) hydroxyapatite ceramic without insoluble starch (50-0-50) and b) hydroxyapatite ceramic with insoluble rice starch (50-25-25) both calcined at 500 ºC

Table 2.2 Density and open porosity of ceramic materials with varying hydroxyapatite and starch content. Calcination temperature of hydroxyapatite was 500 ^{o}C unless otherwise specified.

Adsorbent	**Density (g/cm^3)**	**Open Porosity (%)**	**SSA (m^2/g)**
Effect of soluble starch			
60-0-40	1.52	25	nd
50-0-50	1.42	31	1.3
40-0-60	1.34	35	nd
30-0-70	1.10	37	nd
Effect of insoluble rice starch			
50-0-50	1.42	31	1.3
50-15-35	1.34	41	2.0
50-25-25	1.35	45	4.0
Effect of calcination temperature			
250 ºC 50-25-25	not measured*		nd
400 ºC 50-25-25	1.32	43	nd
500 ºC 50-25-25	1.35	45	4.0
600 ºC 50-25-25	1.88	42	nd
750 ºC 50-25-25	2.55	49	0.8
900 ºC 50-25-25	2.81	47	0.3

* Density and open porosity could not be measured because the material disintegrated during handling; SSA only measured and reported for select adsorbents; nd: SSA not determined.

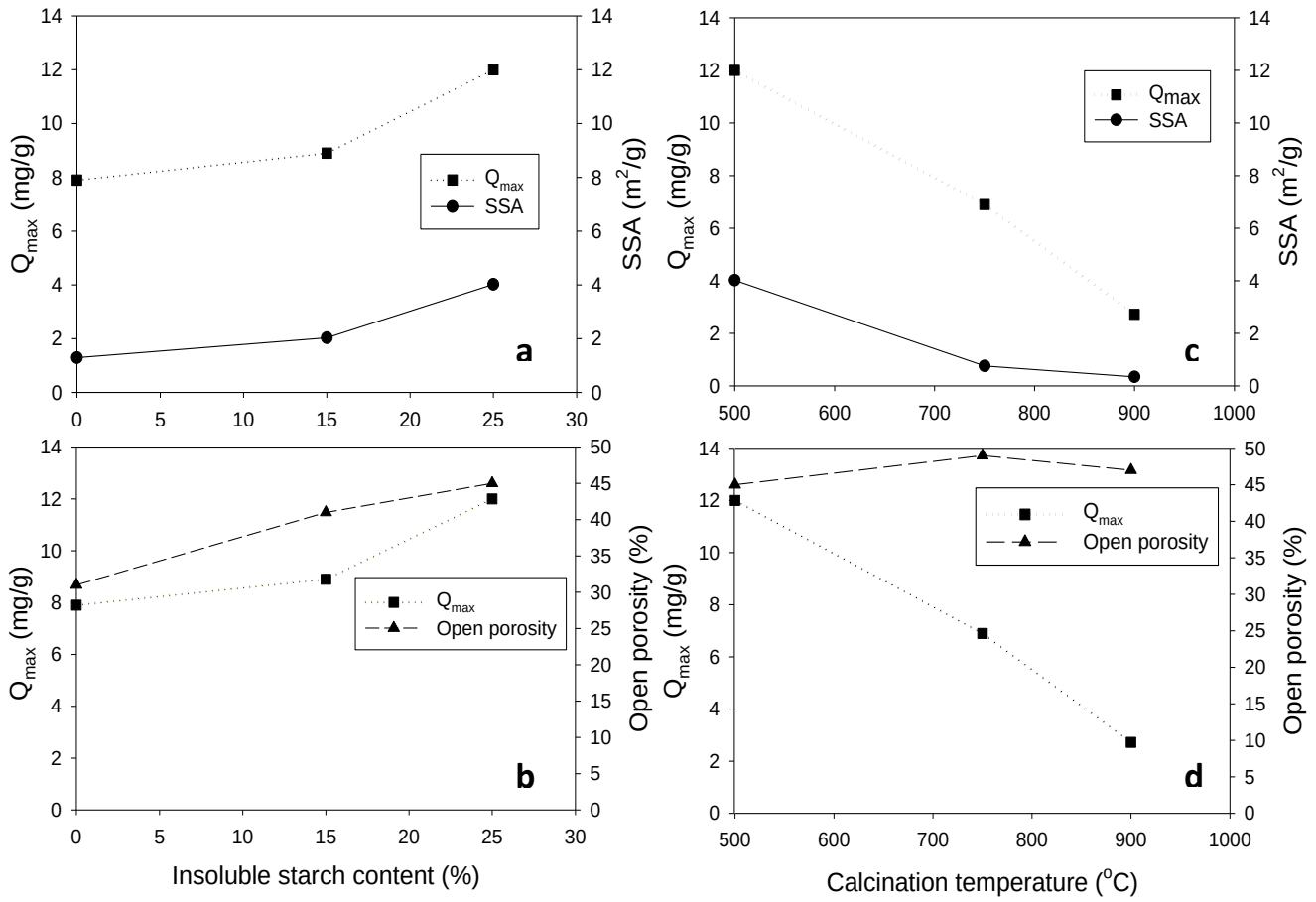

Figure 2.4 Effect of insoluble starch content on a) Qmax and SSA and b) Qmax and open porosity of ceramics with 50% hydroxyapatite calcined at 500 oC and effect of hydroxyapatite calcination temperature on c) Qmax and SSA, and d) Qmax and open porosity of 50-25-25 ceramics

Since the ceramic made with 25% insoluble rice starch and 25% soluble starch (500 ºC 50-25-25) sintered at 1200 ºC achieved the highest fluoride adsorption (Figure 2.2b), subsequent experiments used this basic formula, but varied the type of insoluble component and the hydroxyapatite calcination temperature.

Effect of calcination temperature

Cohesive ceramic materials could not be formed from uncalcined hydroxyapatite powders under the fabrication conditions given in the materials and methods section, and calcination at 250 ^{o}C resulted in ceramics that were fragile and crumbled during characterization tests. Calcination at 400 ^{o}C and above, on the other hand, resulted in formation of ceramic materials with sufficient strength to withstand operation and handling. This can be attributed to improved densification of larger grains, formed upon calcination, during sintering (Exter et al., 1994; Landi et al., 2000). There was a sharp increase in abrasion resistance of ceramic materials when the calcination temperature was increased from 250 ^{o}C to 400 ^{o}C, as is evident by the corresponding increase in hardness number (Figure 2.5). However, the hardness number remained nearly constant with further increases in calcination temperatures. Specifically, materials with hardness number above approximately 70 (made with hydroxyapatite calcined at 400 ^{o}C) could withstand operation and handling and are, therefore, suitable for use as fluoride adsorbents.

The maximum adsorption capacity (Q_{max}) of 50-25-25 ceramic materials decreased by a factor of four when the calcination temperature increased from 500 ^{o}C to 900 ^{o}C (Figure 2.2c, Table 2.3). This increase in calcination temperature from 500 ^{o}C to 900 ^{o}C resulted in ceramics with higher densities (Table 2.2) and fewer micrometer-sized pores (compare Figures 2.3b and 2.6), as well as an order of magnitude decrease in surface area from 4.2 m^2/g to 0.43 m^2/g (Figure 2.4b).

Table 2.3 Adsorption capacity of ceramic materials calcined at different temperatures

Adsorbent	**Q_{max} (mg/g)**	**$Q_{1.5}$ (mg/g)**	**K (L/mg)**
250 ºC 50-25-25	10.3 ± 0.8	5.9 ± 0.9	0.9 ± 0.3
400 ºC 50-25-25	10.3 ± 0.7	4.5 ± 1.2	0.5 ± 0.1
500 ºC 50-25-25	12.4 ± 0.8	5.8 ± 1.1	0.8 ± 0.2
600 ºC 50-25-25	9.0 ± 0.6	3.8 ± 0.8	0.4 ± 0.1
750 ºC 50-25-25	6.9 ± 1.0	0.9 ± 0.5	0.1 ± 0.05
900 ºC 50-25-25	2.7 ± 1.8	0.3 ± 0.2	0.1 ± 0.02

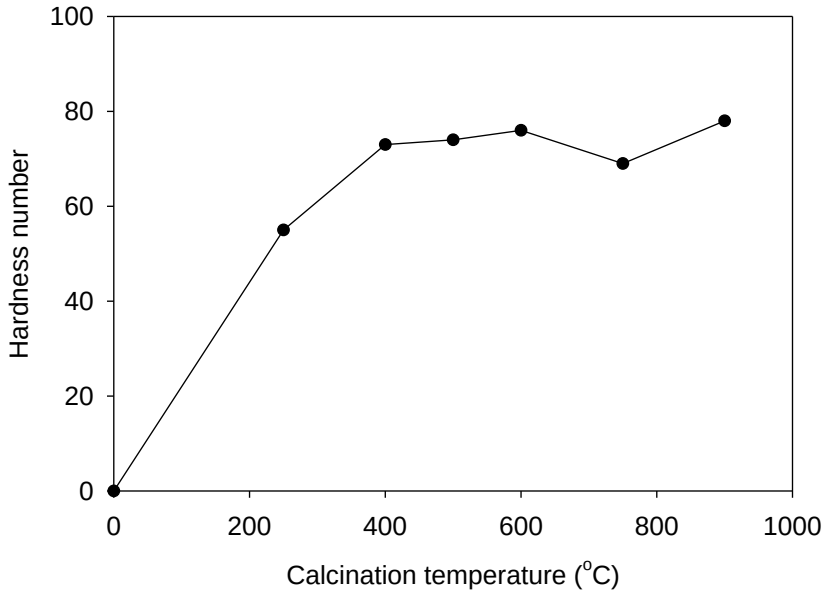

Figure 2.5 Increase in abrasion resistance of ceramics with increasing calcination temperature of 50-25-25 ceramics

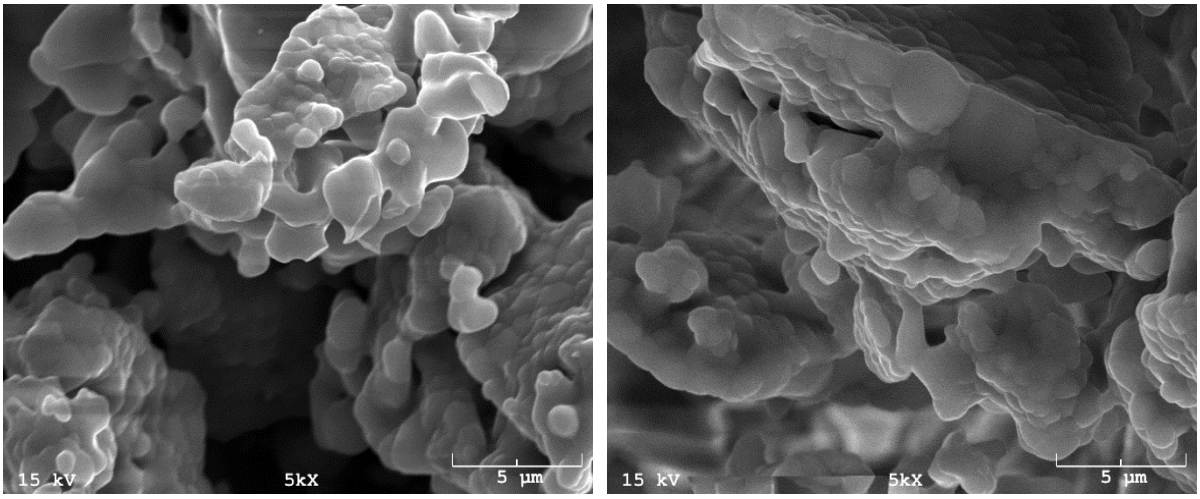

a) b)

Figure 2.6 SEM of 50-25-25 ceramic calcined at a) 750 ^{o}C and b) 900 ^{o}C. See also see Figure 2.3b, which shows the 50-25-25 ceramic calcined at 500 ^{o}C.

Effect of type of pore-forming agents

Changing the type of insoluble starch (i.e., substituting wheat or corn for rice) did not have a significant effect on the fluoride adsorption isotherms of the 500 ^{o}C 50-25-25 ceramics (Figure 2.2d), nor a statistically significant effect on their fluoride adsorption capacities ($Q_{1.5}$ values (Table 2.5)). This is to be expected since the starch granules are all smaller than 10 µm (Supplementary Information, Figure S2.1 a-d). The pores in ceramics made with rice starch (Figure 2.3b), wheat starch (Figure S2.2 a) and corn starch (Figure S2.2 b) are orders of magnitude larger than a fluoride ion (ionic radius of 1.36 Å) (Pauling, 1927) and thus would not hinder rates of fluoride diffusion into the porous matrix. However, the 500 ^{o}C 50-25-25 ceramic made with cellulose as the insoluble component had a significantly lower $Q_{1.5}$ value than did those made with rice, corn, or wheat (Table 2.4). SEM image of this ceramic (Figure S2.2 c) showed fewer open voids compared to ceramics made with the other three types of insoluble starches, which is postulated to negatively impact fluoride adsorption. It is speculated that burn off of larger sized cellulose particles led to less pore

space, possibly due to partial collapse of pore walls, causing a decrease in adsorption capacity (Table 2.4).

Table 2.4 Adsorption capacity of ceramic materials (500 ^{o}C 50-25-25) prepared with different types of insoluble starch and cellulose

Adsorbent	**Q_{max} (mg/g)**	**$Q_{1.5}$ (mg/g)**	**K (L/mg)**
Rice starch ceramic	12.4 ± 0.8	5.8 ± 1.1	0.8 ± 0.2
Corn starch ceramic	9.6 ± 0.9	5.2 ± 1.2	0.8 ± 0.3
Wheat starch ceramic	8.6 ± 0.8	6.7 ± 1.0	2.4 ± 0.8
Cellulose ceramic	9.6 ± 0.6	2.6 ± 0.5	0.3 ± 0.1

Conclusions

Macroporous ceramic beads were formed upon firing compacted hydroxyapatite and plant-based pore forming agents at 1200 ^{o}C. The ceramic beads did not disintegrate or undergo resuspension when submerged in water. This may eliminate the need for filtration of the adsorbent from the treated water and will be useful in maintaining a low pressure drop in a continuous-flow column.

The maximum adsorption capacity of these ceramics was between 7 and 12 mg/g, depending on the volume ratios of hydroxyapatite, insoluble starch, and soluble starch, which is higher than activated alumina and bone char results reported in the literature (4 to 6 mg/g). The binding effect of soluble starch was essential for ceramic formation, and the addition of insoluble starch resulted in formation of interconnected pores. Addition of insoluble starch led to an increase in $Q_{1.5}$, open porosity and SSA of 50% hydroxyapatite ceramics. Ceramic materials with 50% hydroxyapatite and 25% each of insoluble and soluble starch content had the highest fluoride adsorption. Three

types of insoluble starch – rice, corn and wheat – and insoluble cellulose were evaluated for their impact on macroporous ceramic formation and fluoride adsorption. No statistically significant difference was found in the adsorption capacity ($Q_{1.5}$) of ceramics prepared with the three starches. However, ceramics prepared using cellulose showed lower adsorption. This may be due to a collapsed pore structure caused by the large size of cellulose particles relative to the synthesized hydroxyapatite grains. This explanation is supported by SEM images that show less open pore space in ceramics made with cellulose compared to the other ceramics.

Calcination of hydroxyapatite powders prior to sintering was found to be critical for formation of ceramics with sufficient strength and abrasion resistance to withstand operation and handling. Calcination temperatures of 400 ^{o}C and higher led to denser ceramics with adequate abrasion resistance. Calcining beyond 600 ^{o}C, however, dramatically lowered the SSA and fluoride adsorption capacity of these materials.

Hydroxyapatite ceramic beads made with starches as pore-forming agents have potential applications in community- or household-level fluoride removal. They can be fabricated from cheap raw materials using simple equipment (e.g., a hydraulic press and a kiln) that is easy to operate, and that can be procured in developing countries. Both starch and hydroxyapatite are non-toxic and have no known health hazards. Further research will explore the regeneration potential and performance of hydroxyapatite ceramics in continuous flow column studies.

Acknowledgements

This work in an outgrowth of discussions with Dr. James Smith at the University of Virginia. This research was partially funded by the National Science Foundation (NSF) (CBET - 1066425), the University of Oklahoma WaTER Center, the Sun Oil Company Endowed Chair, and University of

Oklahoma Graduate College Robberson Research Grant. We thank Dr. Preston Larson, Ms. Brittany Pritchett, and Dr. Junyi Du for their help with SEM, XRD, and BET analyses.

References

1. Amini, M., Mueller, K., Abbaspour, K. C., Rosenberg, T., Afyuni, M., Møller, K. N., ... & Johnson, C. A. (2008). Statistical modeling of global geogenic fluoride contamination in groundwaters. Environmental science & technology, 42(10), 3662-3668.
2. Ashby, M. F. (1974). A first report on sintering diagrams. *Acta Metallurgica*, *22*(3), 275-289.
3. ASTM (2015). ASTM52900-15 Standard Terminology for Additive Manufacturing—General Principles—Terminology. *ASTM International, West Conshohocken, PA*.
4. ASTM (2014). C373-Standard Test Method for Water Absorption. Bulk Density, Apparent Porosity, and Apparent Specific Gravity of Fired Whiteware Products, Ceramic Tiles, and Glass Tiles. *ASTM International, West Conshohocken, PA*.
5. ASTM (2010) D3802-10 Standard Test Method for Ball-Pan Hardness of Activated Carbon. *ASTM International, West Conshohocken, PA*.
6. Bhatnagar, A., Kumar, E., & Sillanpää, M. (2011). Fluoride removal from water by adsorption—a review. *Chemical Engineering Journal*, *171*(3), 811-840.
7. Bhattacharjee, S., Besra, L., & Singh, B. P. (2007). Effect of additives on the microstructure of porous alumina. *Journal of the European Ceramic Society*, *27*(1), 47-52.
8. Brindha, K., Rajesh, R., Murugan, R., & Elango, L. (2011). Fluoride contamination in groundwater in parts of Nalgonda District, Andhra Pradesh, India. *Environmental Monitoring and Assessment*, *172*(1-4), 481-492.

9. Brunson, L. R., & Sabatini, D. A. (2014). Practical considerations, column studies and natural organic material competition for fluoride removal with bone char and aluminum amended materials in the Main Ethiopian Rift Valley. *Science of the Total Environment*, *488*, 580-587.

10. Chen, L., Zhang, K. S., He, J. Y., Xu, W. H., Huang, X. J., & Liu, J. H. (2016). Enhanced fluoride removal from water by sulfate-doped hydroxyapatite hierarchical hollow microspheres. *Chemical Engineering Journal*, *285*, 616-624.

11. Chen, N., Zhang, Z., Feng, C., Sugiura, N., Li, M., & Chen, R. (2010). Fluoride removal from water by granular ceramic adsorption. Journal of colloid and interface science, 348(2), 579-584.

12. den Exter, P., Winnubst, L., Leuwerink, T. H., & Burggraaf, A. J. (1994). Effect of Calcination on the Sintering of Gel-Derived, Zirconia-Toughened Alumina. *Journal of the American Ceramic Society*, *77*(9), 2376-2380.

13. Fawell, J., Bailey, K., Chilton, J., Dahi, E., & Magara, Y. (2006). *Fluoride in drinking-water*. IWA publishing.

14. Fewtrell, L., Smith, S., Kay, D., & Bartram, J. (2006). An attempt to estimate the global burden of disease due to fluoride in drinking water. *Journal of Water and Health*, *4*(4), 533-542.

15. Hammari, L. E. L., Laghzizil, A., Barboux, P., Lahlil, K., & Saoiabi, A. (2004). Retention of fluoride ions from aqueous solution using porous hydroxyapatite: structure and conduction properties. *Journal of Hazardous Materials*, *114*(1-3), 41-44.

16. Hendrickson, K., & Vik, E. A. (1984). Adsorption in water treatment: fluoride removal. In *Rapport* (Vol. 6). Norwegian Institute for Water Research.

17. Herring, C. (1999). Surface tension as a motivation for sintering. In *Fundamental Contributions to the Continuum Theory of Evolving Phase Interfaces in Solids* (pp. 33-69). Springer, Berlin, Heidelberg.

18. Huang, C. J., & Liu, J. C. (1999). Precipitate flotation of fluoride-containing wastewater from a semiconductor manufacturer. *Water Research, 33*(16), 3403-3412.

19. IUPAC (2006) Compendium of Chemical Terminology, 2nd ed. (the "Gold Book"). Compiled by A. D. McNaught and A. Wilkinson. Blackwell Scientific Publications, Oxford (1997). XML on-line corrected version: http://goldbook.iupac.org (2006-) created by M. Nic, J. Jirat, B. Kosata; updates compiled by A. Jenkins. ISBN 0-9678550-9-8.

20. Jane, J. L., Kasemsuwan, T., Leas, S., Zobel, H., & Robyt, J. F. (1994). Anthology of starch granule morphology by scanning electron microscopy. *Starch-Stärke, 46*(4), 121-129.

21. Jiménez-Reyes, M., & Solache-Ríos, M. (2010). Sorption behavior of fluoride ions from aqueous solutions by hydroxyapatite. *Journal of Hazardous Materials, 180*(1-3), 297-302.

22. Joschek, S., Nies, B., Krotz, R., & Göpferich, A. (2000). Chemical and physicochemical characterization of porous hydroxyapatite ceramics made of natural bone. *Biomaterials, 21*(16), 1645-1658.

23. Juang, H. Y., & Hon, M. H. (1996). Effect of calcination on sintering of hydroxyapatite. *Biomaterials, 17*(21), 2059-2064.

24. Kaseva, M. E. (2006). Optimization of regenerated bone char for fluoride removal in drinking water: a case study in Tanzania. *Journal of Water and Health, 4*(1), 139-147.

25. Komlev, V. S., Barinov, S. M., Orlovskii, V. P., & Kurdyumov, S. G. (2001). Porous ceramic granules of hydroxyapatite. *Refractories and industrial ceramics*, *42*(5-6), 195-197.

26. Landi, E., Tampieri, A., Celotti, G., & Sprio, S. (2000). Densification behaviour and mechanisms of synthetic hydroxyapatites. *Journal of the European Ceramic Society, 20*(14-15), 2377-2387.

27. Lin, J., Raghavan, S., & Fuerstenau, D. W. (1981). The adsorption of fluoride ions by hydroxyapatite from aqueous solution. *Colloids and Surfaces, 3*(4), 357-370.

28. Lyckfeldt, O., & Ferreira, J. M. F. (1998). Processing of porous ceramics by 'starch consolidation'. *Journal of the European Ceramic Society, 18*(2), 131-140.

29. McCann, H. G. (1953). Reactions of fluoride ion with hydroxyapatite. *J Biol Chem, 201*(1), 247-59.

30. Meenakshi and Maheshwari, R. C. (2006). Fluoride in drinking water and its removal. *Journal of Hazardous Materials, 137*(1), 456-463.

31. Moges, G., Zewge, F., & Socher, M. (1996). Preliminary investigations on the defluoridation of water using fired clay chips. *Journal of African Earth Sciences*, *22*(4), 479-482.

32. Odiyo, J. O., & Makungo, R. (2012). Fluoride concentrations in groundwater and impact on human health in Siloam Village, Limpopo Province, South Africa. *Water SA, 38*(5), 731-736.

33. Pask, J.A. (1979). Ceramic Processing – A Ceramic Science. *Am Ceram Soc Bull 58* (12), 1163-1166.

34. Pauling L. (1927). The sizes of ions and the structure of ionic crystals. *J Am Chem Soc 49*(3),765-790.

35. Reed, J. S. (1995). Principles of Ceramic Processing 2nd edn (New York: Wiley)

36. Scalera, F., Gervaso, F., Sanosh, K. P., Sannino, A., & Licciulli, A. (2013). Influence of the calcination temperature on morphological and mechanical properties of highly porous hydroxyapatite scaffolds. *Ceramics International, 39*(5), 4839-4846.

37. Ślósarczyk, A., Stobierska, E., & Paszkiewicz, Z. (1999). Porous hydroxyapatite ceramics. *Journal of Materials Science Letters, 18*(14), 1163-1165.

38. Spinelli, M. A., Brudevold, F., & Moreno, E. C. (1971). Mechanism of fluoride uptake by hydroxyapatite. *Archives of Oral Biology, 16*(2), 187-203.

39. Sternitzke, V., Kaegi, R., Audinot, J. N., Lewin, E., Hering, J. G., & Johnson, C. A. (2012). Uptake of fluoride from aqueous solution on nano-sized hydroxyapatite: examination of a fluoridated surface layer. *Environmental Science & Technology, 46*(2), 802-809.

40. Sundaram, C. S., Viswanathan, N., & Meenakshi, S. (2008). Defluoridation chemistry of synthetic hydroxyapatite at nano scale: equilibrium and kinetic studies. *Journal of Hazardous Materials*, *155*(1-2), 206-215.

41. Tang, Y., Tang, Y., Lv, C., & Zhou, Z. (2008). Preparation of uniform porous hydroxyapatite biomaterials by a new method. *Applied Surface Science, 254*(17), 5359-5362.

42. Verwilghen, C., Rio, S., Nzihou, A., Gauthier, D., Flamant, G., & Sharrock, P. J. (2007). Preparation of high specific surface area hydroxyapatite for environmental applications. *Journal of Materials Science, 42*(15), 6062-6066.

43. Wang, P., Li, Y., & Lu, Y. (2011). Enhanced piezoelectric properties of (Ba0. 85Ca0. 15)(Ti0. 9Zr0. 1) O3 lead-free ceramics by optimizing calcination and sintering temperature. *Journal of the European Ceramic Society, 31*(11), 2005-2012.

44. WHO. (2011). Guidelines for drinking-water quality. *World Health Organization*, *216*, 303-4.

45. Yakub, I., & Soboyejo, W. (2013). Adsorption of fluoride from water using sintered clay-hydroxyapatite composites. *Journal of Environmental Engineering, 139*(7), 995-1003.

46. Yang, L., Ning, X.S., Chen, K.X., Xiao, Q.F. & Zhou, H.P. (2005). Preparation of porous hydroxyapatite ceramics with starch additives. *Transactions of Nonferrous Metals Society of China 15*, 257-260.

47. Yang, L., Ning, X., Xiao, Q., Chen, K., & Zhou, H. (2007). Development and characterization of porous silver-incorporated hydroxyapatite ceramic for separation and elimination of microorganisms. *Journal of Biomedical Materials Research Part B, 81*(1), 50-56.

48. Zhang, W., & Gladwell, I. (1998). Sintering of two particles by surface and grain boundary diffusion–a three-dimensional model and a numerical study. *Computational Materials Science*, *12*(2), 84-104.

Supplementary Information

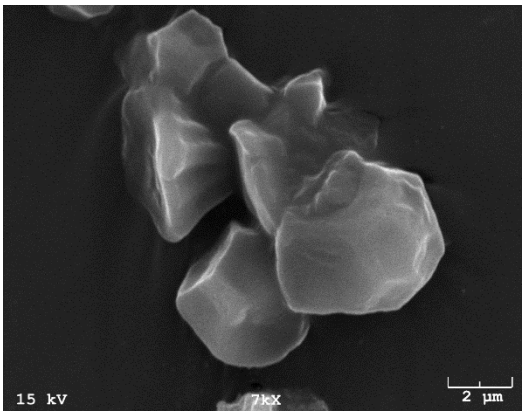

a)

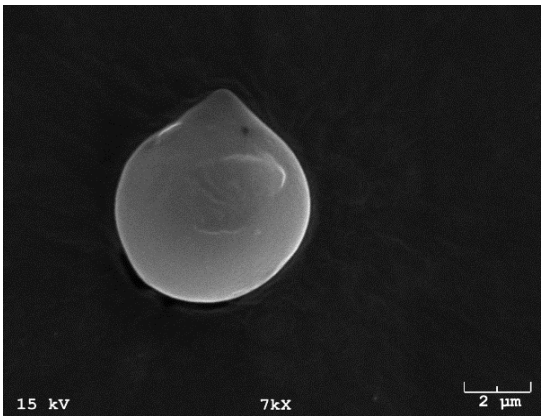

b)

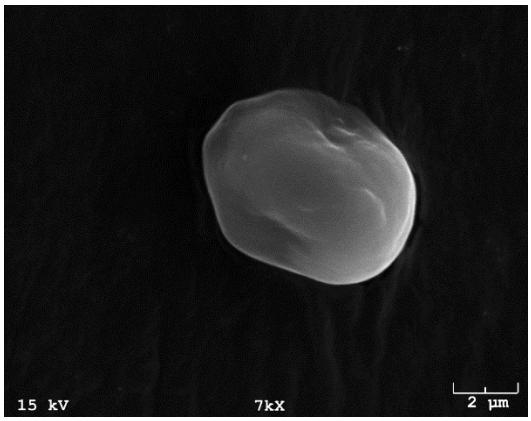

c)

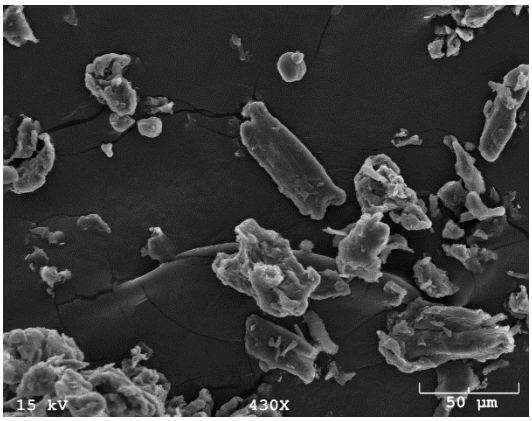

d)

Figure S2.1 SEM images of particles of a) rice starch, b) wheat starch, c) corn starch and d) cellulose

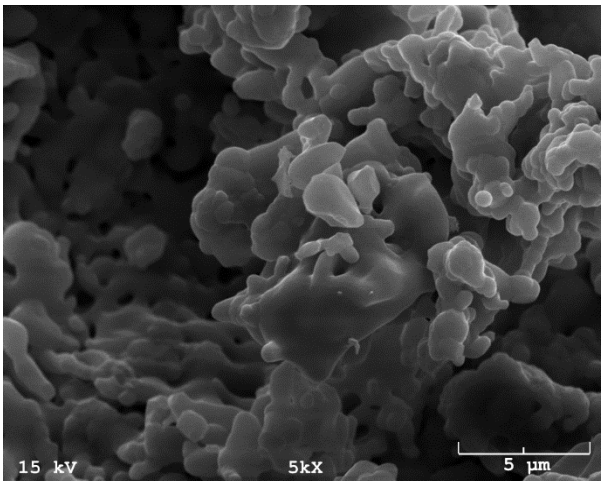

a)

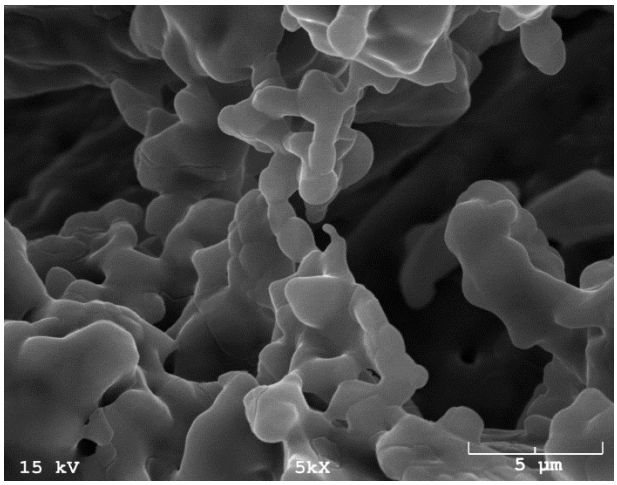

b)

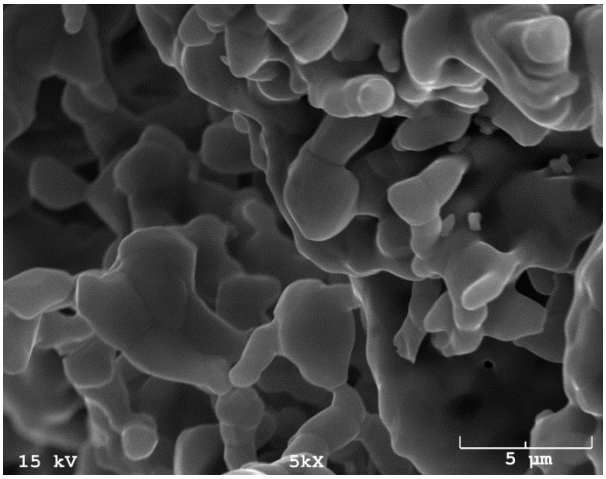

c)

Figure S2.2 SEM images of 500 ºC 50-25-25 ceramic prepared with a) wheat starch, b) corn starch, and c) cellulose. See Figure 2.3b for the 500 ºC 50-25-25 ceramic prepared with rice starch

Chapter 3 Hydroxyapatite ceramic adsorbents: effect of pore size, regeneration, and selectivity for fluoride[2]

Abstract

Fluoride uptake by porous hydroxyapatite ceramics was investigated through batch adsorption studies to determine the effect of varying the size of hydroxyapatite grains and pore size. It was found that ceramics made from fine hydroxyapatite (d_{50} of 100 μm) had higher fluoride uptake and smaller pores compared to coarse (d_{50} of 240 μm) hydroxyapatite (18.2 mg/g versus 12.4 mg/g, respectively). Fewer processing steps were also required for ceramics made from fine hydroxyapatite. This ceramic showed high selectivity for fluoride relative to anions commonly found in groundwater and natural organic matter (NOM) and could be regenerated for up to five adsorption cycles using 0.05 M and 0.1 M sodium hydroxide.

Introduction

Nearly 200 million people worldwide are exposed to drinking water with elevated levels of naturally occurring fluoride (Fewtrell et al., 2006). The World Health Organization recommends a maximum fluoride concentration of 1.5 mg/L in drinking water (WHO 2011) above which it can cause dental fluorosis (between 1.5 and 4 mg/L) and skeletal fluorosis (> 4mg/L) (Fawell et al., 2006). Several fluoride-removal technologies have been optimized for field applications, but they often suffer from certain limitations – activated alumina and bone char show limited fluoride removal at neutral pH (Fawell et al., 2006), while electrocoagulation and co-precipitation methods

[2] Nijhawan, A., Butler, E. C., & Sabatini, D. A. (2018). Hydroxyapatite Ceramic Adsorbents: Effect of Pore Size, Regeneration, and Selectivity for Fluoride. *Journal of Environmental Engineering*, *144*(11), 04018117.

generate fluoride-rich sludge that requires safe disposal (Meenakshi and Maheshwari, 2006; Ayoob et al., 2008). Chen et al. (2010) observed that powdered adsorbents dispersed in water cause clogging and an increase in head loss in a continuous-flow column. Hydroxyapatite powders turn into gel in the presence of water while activated alumina dissolves in alkaline solutions (Padungthon et al., 2014). Granular adsorbents such as porous ceramics, on the other hand, offer the advantage of better hydraulic performance in flow-through columns and eliminate the need for a separate filtration step.

Recently, Nijhawan et al. (2017) developed porous hydroxyapatite ceramics capable of removing fluoride from drinking water with a maximum fluoride adsorption capacity of 12.4 mg/g. Ceramics made with 50% by volume of hydroxyapatite and 25% each of rice starch and soluble starch had the highest fluoride uptake. Use of larger pore forming materials such as cellulose fibers led to a diminished adsorption capacity (Nijhawan et al., 2017). Hydroxyapatite was chosen as the ceramic based on its affinity for fluoride (McCann, 1953; Spinelli et al., 1971; Lin et al., 1981), its potential for regeneration at high pH without dissolution (Kamieniak et al., 2017), and the fact that it does not undergo phase changes at high temperatures as do aluminum and zirconium hydr(oxides) (Sato et al., 1979; Chen et al., 1989; Mostafa, 2005).

Pore size can be controlled by varying the size of the starting powders used to make the ceramics. Ceramic filters made from finer clay fractions were found to have a smaller average pore diameter (Oyanedel-Craver and Smith, 2007), while Parkhomey et al. (2016) reported a decrease in pore size of hydroxyapatite-glass composite ceramics with decreasing particle size of hydroxyapatite.

In this research, the first objective was to study the effect of varying the size of hydroxyapatite grains on fluoride uptake. It was hypothesized that ceramics with smaller hydroxyapatite grains should show higher fluoride uptake by forming smaller pores.

Before application in the field, it is essential to consider the regeneration potential of adsorbents. Regenerability is a key feature that impacts the cost-effectiveness of adsorbents in resource-limited settings. Fluoride adsorbents are most commonly regenerated using NaOH (Bhatnagar et al., 2011) but $NaAlO_2$ (Zhao et al., 2010), $AlCl_3$ (Bansiwal et al., 2009), and alum (Jagtap et al., 2009) have also been used. Thus, the second objective of the study was to determine the regeneration potential of the ceramic adsorbents by subjecting the adsorbents to repeated adsorption – desorption cycles.

The third objective of the study was to determine the effect of other ground water anions on the adsorption of fluoride. Phosphate, sulfate, chloride, nitrate, and bicarbonate have all been shown to compete with fluoride for surface sites (Habuda-Stanić et al., 2014), but limited studies have evaluated the competitive fluoride uptake on hydroxyapatite (Garg and Chaudhari, 2012; Yu et al., 2013). Natural organic matter (NOM) was also considered because it is negatively charged at neutral pH (Macalady and Ranville, 1998) and can reduce fluoride uptake (Mouelhi, 2016). NOM is a mixture of humic and fulvic acids and is generally found in groundwaters at concentrations between 1 and 50 mg C/L (Redman et al., 2002).

Materials and methods

Ceramic preparation

Porous ceramic beads were fabricated from hydroxyapatite powders with starch as the pore-forming agent. Hydroxyapatite was synthesized according to Verwilghen et al. (2007) as modified in Nijhawan et al. (2017). A 1 L solution of 0.3 M ammonium phosphate at pH 10.3 was slowly

poured into 1 L of 0.5 M calcium nitrate solution at a pH of 10.7. A 5 M ammonium hydroxide solution was used to raise the pH. All chemicals were purchased from Sigma Aldrich Corp, USA. The resulting precipitate was matured for 60 hours at 40 ^{o}C and subsequently washed with DI water and air dried. The dried powder was sieved between no. 40 and 80 mesh sieves (0.420 mm and 0.177 mm; coarse hydroxyapatite) or between no. 120 and 325 mesh sieves (0.125 mm and 0.044 mm; fine hydroxyapatite).

The coarse hydroxyapatite powder required calcination at 500 ^{o}C for 6 hours before formation of a ceramic with sufficient cohesion (Nijhawan et al. 2017). The calcined powder was hand-mixed with different volumes of pore-forming materials (insoluble rice starch and soluble starch) and molded using a cylindrical stainless-steel mold of diameter 15 mm and length 30 mm (Scott Fetzer Co. USA), and compacted at 10 MPa using a manual hydraulic press (Dake Corporation USA). The compacted mixture was then shaped into beads of approximately 4 mm diameter by hand.

The fine hydroxyapatite required fewer steps to form ceramics. Uncalcined powder was mixed with pore-forming materials as described above and shaped into beads of approximately 4 mm without calcining or compaction. All beads were fired in an electric kiln (Paragon Calderon Kiln, Paragon Industries, L.P.) at 1200 ^{o}C for 2 hours.

Adsorption studies

Batch adsorption studies were carried out using ceramic beads with a solid to liquid ratio of 5 g adsorbent/L fluoride solution. Fluoride solutions with concentrations ranging from 5 to 150 mg/L were prepared by diluting a 1000 mg/L NaF solution in 50 mM HEPES (4-(2-hydroxyethyl)-1-piperazineethanesulfonic acid) buffer solution, and then used in the batch tests, along with a blank. Duplicate samples were kept on a reciprocating shaker for 24 hours at 30 rpm. The equilibrium

fluoride concentration was measured using an ion-selective electrode (Thermo Fisher Scientific, USA). A three-point calibration curve was prepared using 1 mg/L, 10 mg/L and 100 mg/L fluoride solutions. Standards, samples and blanks were all mixed with a total ionic strength adjustment buffer (TISAB) in a 1:1 ratio before analysis to decomplex dissolved fluoride complexes (Adriano and Doner, 1982).

Batch study results were fitted to the Langmuir isotherm to obtain an estimate of the adsorption parameters – maximum adsorption capacity (Q_{max}) in mg/g and K (affinity of adsorbent to fluoride) in L/mg. Sigma Plot 13 (Systat Software, USA) was used for the non-linear regression. The value of $Q_{1.5}$ (Q at an equilibrium fluoride concentration, C_e, of 1.5 mg/L, the WHO recommended level) was calculated from these parameters. The standard deviations of triplicate C_e and Q_e measurements were calculated using Microsoft Excel 2016 (Microsoft Corporation, USA) and are depicted as error bars in the figures. Standard errors in estimating Q_{max}, K and $Q_{1.5}$ were also calculated using Sigma Plot 13. The best performing adsorbents were selected for competition and regeneration studies.

Competition studies

Standard solutions of phosphate, chloride, sulfate, nitrate, and bicarbonate (1 mM, 2 mM, and 5 mM) were prepared and added to 20 mg/L fluoride solutions to determine the effect of competing ions on fluoride adsorption. The concentration of these ions was within the range commonly found in fluoride–rich groundwaters (Kundu et al. 2001; Ayenew, 2005). A sodium salt of humic acid (CAS Number 68131-04-4, 226.14 g/mole, 108 g C/mole) was used as a surrogate for NOM. Four different concentrations of this salt (NOM, 1 to 30 mg/L) were added to 20 mg/L fluoride solutions to determine competition.

Regeneration studies

Six adsorption-desorption cycles were conducted on the ceramic beads to evaluate the regeneration potential. Beads were allowed to equilibrate with 10 mg/L fluoride solution at a solid to liquid ratio of 3.33 g/L for 24 hours at 30 rpm on a rotational shaker. Regeneration experiments were conducted using a lower solid to liquid ratio (3.33 g/L) than the adsorption tests (10 g/L) to ensure higher fluoride loading onto the ceramic. With a solid to liquid ratio of 10g/L, there was little difference in equilibrium dissolved fluoride between the regenerated and control materials. Desorption was carried out with 0.05 M and 0.1 M NaOH solutions at a solid to liquid ratio of 10 g/L at the same conditions as the adsorption experiment.

Material characterization

The hydroxyapatite powders used to make the ceramics, or starting powders, were imaged using a Zeiss NEON High Resolution Scanning Electron Microscope (SEM) at 5 kV operating voltage after sputter coating with iridium. The pore structures of the ceramic beads were characterized by examining a cross-section under a JEOL JSM-840a SEM operating at 15 kV after sputter coating with gold and palladium. A stainless-steel blade (Procter and Gamble, USA) was used to cleave the beads and obtain a flat cross-section. The median particle size of starting powders (d_{50}) was determined through sieve analysis by standard method ASTM C136 (ASTM, 2014) and ceramic pore sizes were estimated from SEM micrographs, using Image J (Schneider et al. 2012). Density and open porosity were measured according to ASTM C373-14a (ASTM, 2014). Open porosity is the ratio of the volume of all pores connected to the surface of the bead (thus available for gas or liquid penetration) to its total volume (ASTM, 2015).

Results and discussion

Effect of hydroxyapatite grain size on fluoride adsorption

Ceramics made with fine hydroxyapatite (d_{50}: 100 µm; uniformity coefficient: 1.75)) had a 50% higher maximum fluoride adsorption (Q_{max}) than those made with coarse hydroxyapatite (d_{50}:240 µm; uniformity coefficient: 1.86) although the difference in $Q_{1.5}$ was not statistically significant (Figure 3.1, Table 3.1), perhaps due to the very high affinity shown by both ceramics at low C_e values. Q_{max} values are higher than those reported for activated alumina – 4.1 mg/g (Bhatnagar et al. 2011) and bone char – 6.1 mg/g (Brunson and Sabatini, 2009), and are comparable to aluminum amended chars – 18.8 mg/g (Brunson and Sabatini, 2014) and modified chitosan beads – 11.4 to 22.4 mg/g (Ma et al. 2007; Yao et al. 2009).

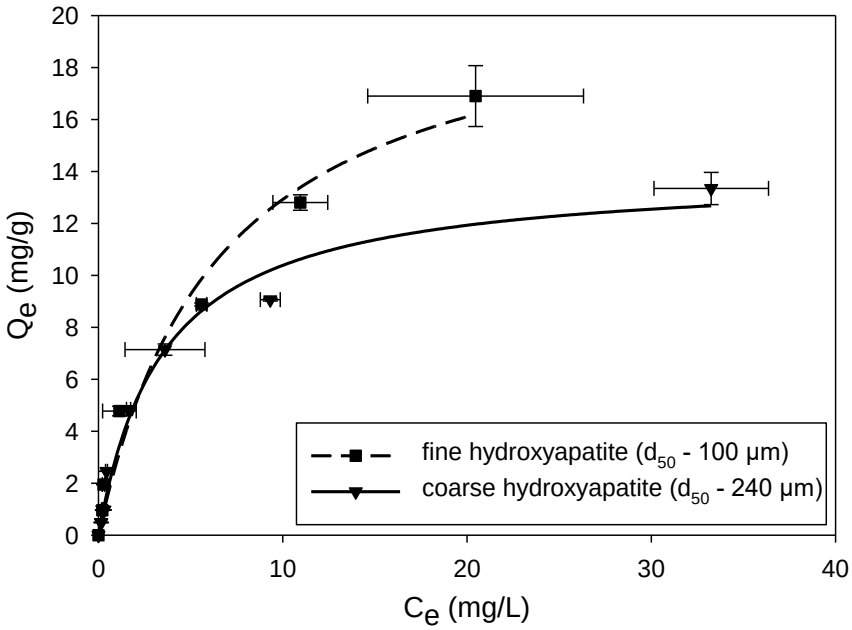

Figure 3.1 Fluoride adsorption by ceramics made with 50% by volume of fine and coarse hydroxyapatite and 25% each by volume of rice starch and soluble starch (Langmuir isotherm fits shown)

Table 3.1 Physical properties and Langmuir isotherm parameters of ceramic adsorbents made from coarse and fine hydroxyapatite

Material used to form ceramic	**Median pore size (d_{50}) and range (µm)**	**Open porosity (%)**	**Density (g/cm^3)**	**Q_{max} (mg/g)**	**K (L/mg)**	**$Q_{1.5}$ (mg/g)**	**Reference**
Coarse hydroxyapatite (d_{50} of 240 µm)	0.29 (0.11 – 6.9)	45	1.35	12.4 ± 0.8	0.8 ± 0.2	5.8 ± 1.1	Nijhawan et al. (2017)
Fine hydroxyapatite (d_{50} of 100 µm)	0.22 (0.11 – 2.6)	42	1.33	18.2 ± 1.6	0.3 ± 0.1	6.0 ± 0.9	This study

Note: (Uncertainties represent standard error calculated from non-linear regression using Sigma Plot 13 (Q_{max}) and error propagation ($Q_{1.5}$)).

The median grain size (d_{50}) of coarse and fine hydroxyapatite (240 µm and 100 µm) was directly correlated with the maximum pore diameters of the resulting ceramics (6.9 µm and 2.6 µm, respectively) (Table 3.1). Ceramics made from fine hydroxyapatite had pore sizes ranging from 0.11 to 2.60 µm. The median pore size of these ceramics was 0.22 µm and 55% of the pores were between 0.1 and 0.25 µm (Figure 3.2). As hypothesized, ceramics made with coarse hydroxyapatite had larger pores in the range of 0.11 to 6.9 µm, with a median pore size 0.29 µm.

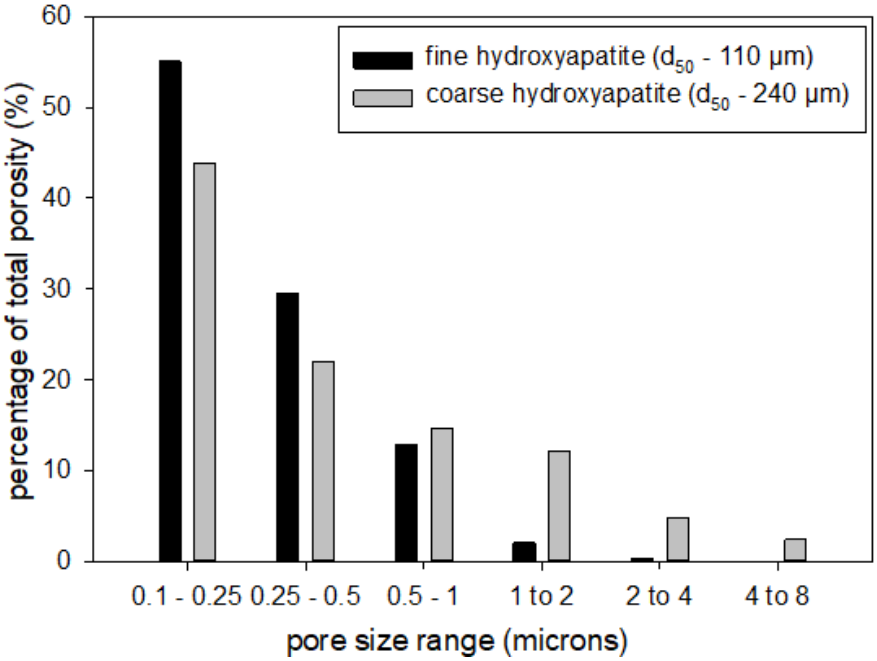

Figure 3.2 Pore size distribution of ceramics made from fine and coarse hydroxyapatite

Changing the grain size of hydroxyapatite did not significantly impact the open porosity or density of the resulting ceramics (Table 3.1). Ceramics made from fine hydroxyapatite had a 50% higher maximum fluoride adsorption capacity (Q_{max}) than ceramics made from coarse hydroxyapatite, even though their open porosity values are similar (Table 3.1). This can be explained by the fact that open porosity simply refers to the percent by volume of surface-accessible pores, without giving any information about their size or internal surface area. For cylindrical pores, a single pore with diameter *d* will have half the internal surface area or "wall area" compared to two pores with diameter *d/2*, even though the volume of the larger pore is equal to the sum of volumes of each of the smaller pores, as illustrated in Figure 3.3.

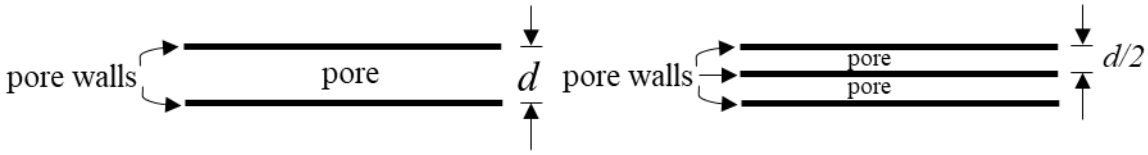

Figure 3.3 Increase in internal surface area of cylindrical pores on decreasing pore size

The effect of pore size on surface area and adsorption capacity can be explained mathematically by estimating the surface area of a sphere with cylindrical pores. This geometry seemed to best approximate the shape and pore structure of the ceramics, which were spherical (not shown) and had pores that could be approximated by cylinders (Figures 3.3 c and d). Cama et al. (2009) developed an expression for the theoretical surface area of a sphere with cylindrical pores:

$$A_{TOT} = A_s + f_p V_s\left(\frac{Ap}{Vp}\right) = 4\pi r_s^2 + f_p \times \frac{4}{3}\pi r_s^3\left(\frac{2\pi r_p h}{\pi r_p^2 h}\right) \qquad (3.1)$$

where A_{TOT} is the total surface area of a spherical ceramic bead, A_s and V_s are the external surface area and total volume of the bead, f_p is the volume fraction of open pores (or open porosity), A_p and V_p are the area and volume of a cylindrical pore, r_s and r_p are the radii of the ceramic bead and the pore, respectively, and h is the length of a cylindrical pore.

The specific surface areas (SSA) of each ceramic were estimated by dividing the total surface area (A_{TOT}) by its density (Table 3.1) and volume (calculated for a sphere of radius 2 mm). The values of SSA were 5.2 and 4.6 m^2/g for fine and coarse hydroxyapatite ceramics, respectively. This is consistent with our previously reported value of SSA_{BET} for ceramics (4.02 m^2/g) measured by N_2 adsorption (Nijhawan et al., 2017). The ratio of SSA for ceramics made from fine and coarse hydroxyapatite is 1.12, while the ratio of their Q_{max} values is 1.47. Values of pore radii (r_p) and the percent contribution of each to the overall porosity were determined from Figure 3.2.

A_{TOT} for different pore radii (r_p) and pore fractions (f_p) were calculated using Equation 3.1 and corresponding SSA values were plotted to show the effect of decreasing pore size (Figure 3.4). A sharp increase in SSA is observed as the value of pore radius drops below 0.2 µm. This validated the effort to make ceramics with smaller pores to increase their surface area and fluoride

adsorption. The effect of pore fraction (or porosity) also became more significant at smaller pore radii.

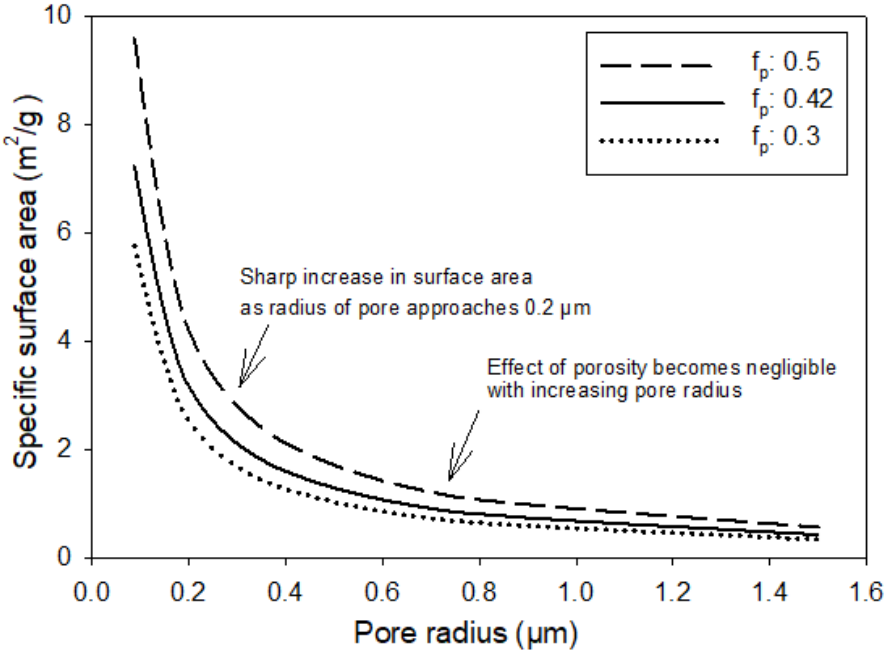

Figure 3.4 Specific surface area of porous spherical ceramics with cylindrical pores as a function of pore radius (f_p: pore fraction, or porosity)

SEM micrographs confirmed the difference in particle sizes of coarse and fine hydroxyapatite (Figures 3.5 a and b, respectively) and the pore sizes of the resulting ceramics (Figures 3.5 c and d). Fine hydroxyapatite grains resulted in ceramics with narrower pores and smaller sintered grains (Figure 3.5 c) compared to ceramics made from coarse hydroxyapatite (Figure 3.5 d). This is consistent with the findings of Yan et al. (2013) and Parkhomey et al. (2016) who reported a decrease in pore size, but similar pore volumes, of porous composites when the particle size of starting powders were decreased. After the starch burns off, finer hydroxyapatite grains have better packing density and smaller void spaces between them, resulting in smaller pores.

Since the ceramic made from fine hydroxyapatite performed the best, it was selected for further experiments to determine its selectivity towards fluoride in the presence of competing ions and its potential for regeneration.

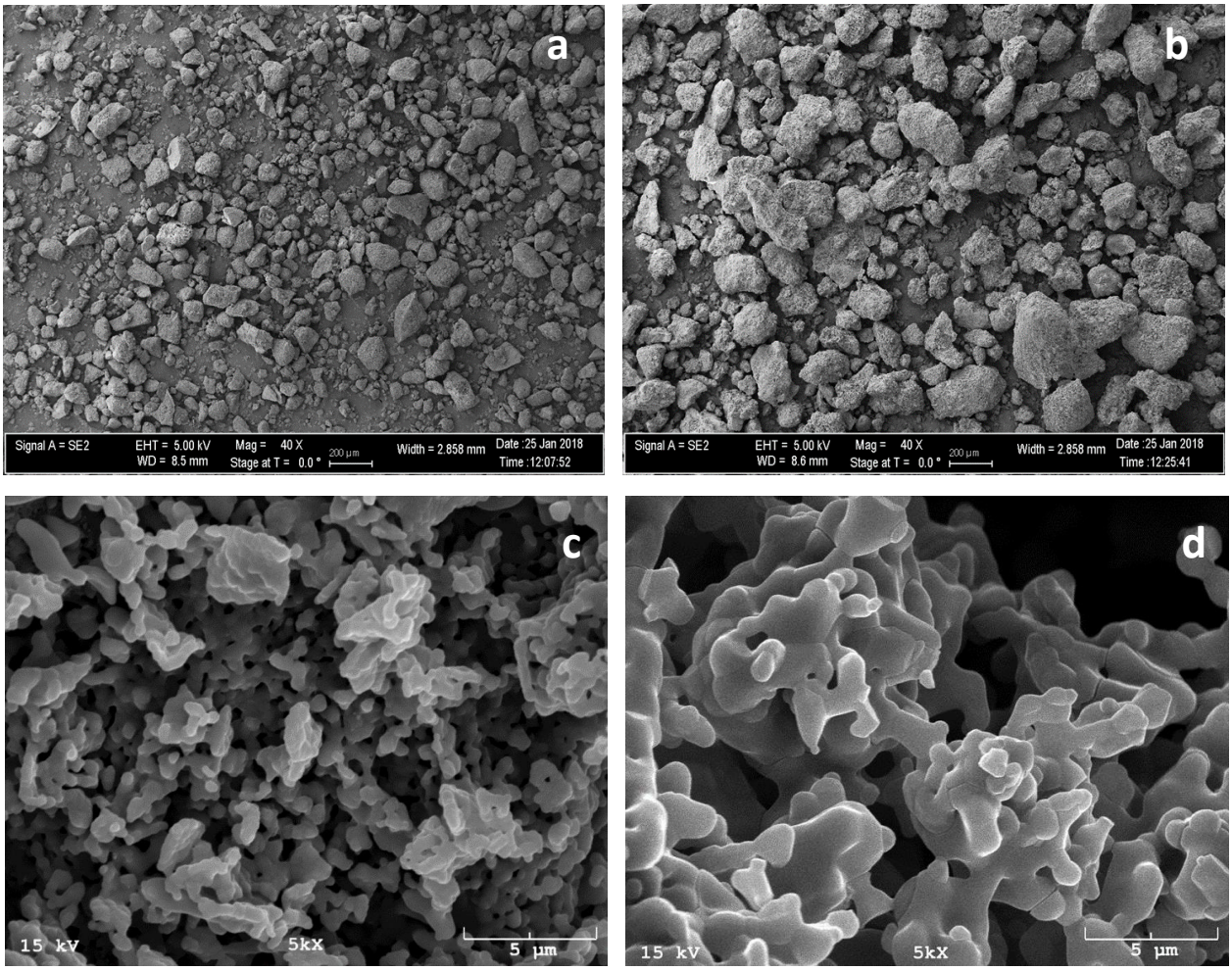

Figure 3.5 SEM micrographs of a) coarse hydroxyapatite, b) fine hydroxyapatite and ceramics made from c) coarse hydroxyapatite* and d) fine hydroxyapatite (*Image reprinted with permission from Nijhawan et al., 2017)

Effect of competing ions and natural organic matter

The results of batch adsorption studies in the presence of other anions and NOM are presented in Figures 3.6 a and b, respectively. Except for chloride, none of the anions competed significantly with fluoride at concentrations commonly found in groundwater (Figure 3.6 a) and even then, only when the chloride to fluoride molar ratio was much greater than 1. The affinity of hydroxyapatite for chloride ions comes from the fact that they can replace hydroxide ions in the apatite crystal to form chlorapatite, one of the three naturally occurring forms of apatite (Mackie et al., 1972). Similar competition by chloride for adsorption was reported for modified chitosan beads (Bansiwal et al., 2009; Jagtap et al., 2009) and nano-goethite (Mohapatra et al., 2010).

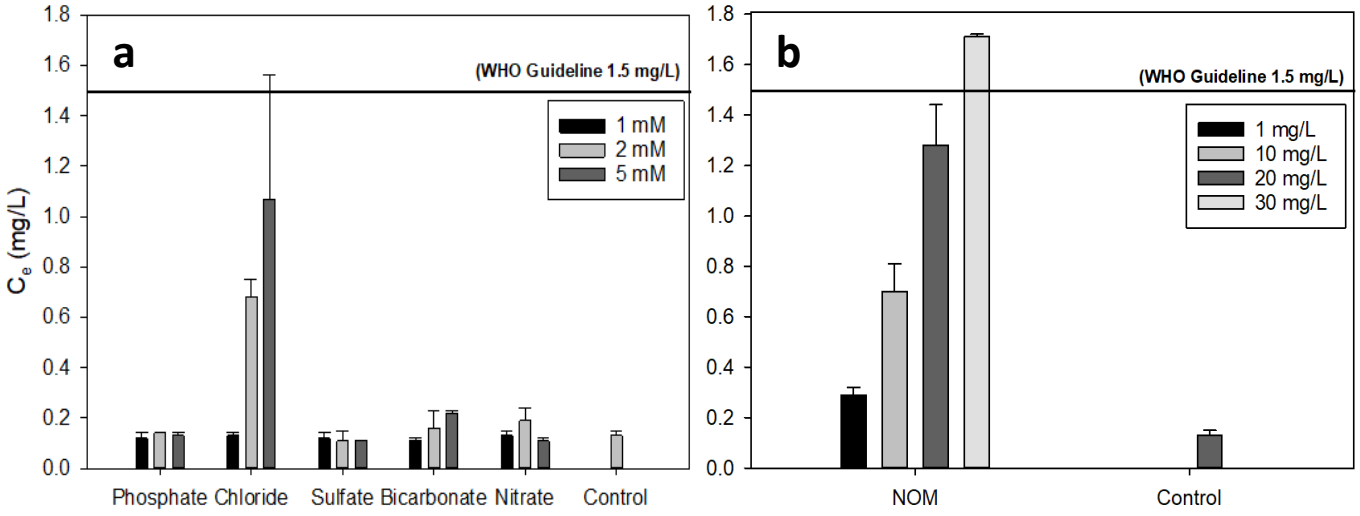

Figure 3.6 Results of batch adsorption tests in the presence of a) competing anions and b) NOM

NOM competed strongly with fluoride at concentrations above 10 mg/L (Figure 3.6 b), or 4.8 mg C/L. This lies within the range of NOM concentrations reported in groundwater - 1 to 50 mg C/L, as reported by Redman et al. (2002), implying that, at these elevated levels, NOM has the potential to reduce the fluoride uptake of these ceramics. This can either be a result of competition for adsorption sites or a result of accumulation of NOM in the pores which can hinder pore and surface

diffusion of fluoride ions (Worch, 2012). Alfredo (2012) observed reduced fluoride uptake by alum in the presence of NOM surrogates, likely due to the latter imparting a negative charge onto aluminum hydroxide precipitates. Similarly, Mouelhi (2016) found lower adsorption of fluoride onto porous activated alumina in the presence of NOM.

Regeneration potential

Figure 3.7 shows the results of the regeneration experiments done with 0.05 M and 0.1 M sodium hydroxide solutions. The ceramics retained approximately 70% of their adsorption capacity after five adsorption cycles (e.g., the adsorption capacity was reduced from 2.5 mg/g in the first cycle to 1.75 mg/g after 5 adsorption cycles when 0.1 M sodium hydroxide was used for regeneration, and very similar results were obtained for regeneration with 0.05 M sodium hydroxide (Figure 3.7)).

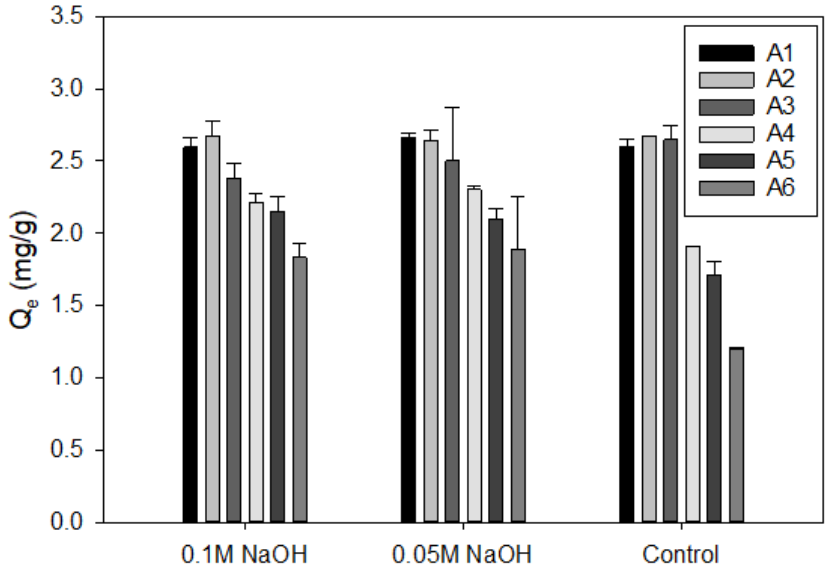

Figure 3.7 Results of regeneration studies with 0.1 M and 0.05 M NaOH (C_0 = 10 mg F-/L) (A1, A2… refer to consecutive adsorption cycles)

There was no significant difference in the equilibrium fluoride concentration (C_e) between the regenerated and control (no regeneration) ceramics for up to three adsorption cycles under the experimental conditions (Figure 3.7). However, the adsorption capacity of the control materials decreased drastically in the fourth adsorption cycle, indicating that the ceramic was saturated with fluoride (Figure 3.7). The ceramics did not dissolve even at pH values higher than 12 after repeated adsorption–desorption cycles, unlike aluminum–based adsorbents (Du et al., 2016) which can form soluble alumino–fluoro complexes at alkaline pH (Hao and Huang, 1986).

In contrast to regeneration with 0.1 M NaOH, only 9% of the initial adsorption capacity was recovered when low concentrations of sodium hydroxide (0.001 M and 0.01M) were used to regenerate the ceramics (data not shown). This is consistent with studies that reported limited desorption with 0.001 N NaOH (Zhang et al., 2012). The difficulty in desorbing fluoride from the hydroxyapatite ceramics using low concentrations of sodium hydroxide points to the possibility that physical adsorption may not be the only mechanism of fluoride removal.

Zhang et al. (2012) reported an increase in pH during batch studies from 6.75 to 8.2 indicating an exchange of fluoride and hydroxide ions and the release of the latter in a non-buffered system. de Leeuw (2004) proposed the presence of a superficial layer of fluorapatite of thickness 10 Å on fluoride – treated hydroxyapatite, through simulations. They also postulated that fluoride ions, once incorporated into the apatite crystal lattice, do not dissolve in water like hydroxide, making them less susceptible to desorption.

Conclusions

Use of fine hydroxyapatite (d_{50} of 100 µm) led to a 50% improvement in the maximum fluoride adsorption capacity (Q_{max}) from 12.4 to 18.2 mg/g compared to ceramics prepared with coarse

hydroxyapatite (d_{50} of 240 µm). This maximum adsorption is higher than the fluoride adsorption capacities for activated alumina and bone char (4 to 6 mg/g) and comparable to modified chars and chitosan-based adsorbents reported in literature (17 to 22 mg/g). Micrographs revealed smaller pores in ceramics made from fine hydroxyapatite, which provide more surface area for adsorption. This was mathematically validated by the fact that the ratio of estimates of SSA of fine and coarse hydroxyapatite ceramics was similar to the ratio of Q_{max}. The non-linear relationship between specific surface area (SSA) and pore radii for a sphere with cylindrical pores also justified our effort to decrease pore size to increase fluoride uptake. The impact of increasing porosity was also more significant at smaller pore radii. Therefore, future work should focus on developing porous ceramic adsorbents with pore radii lower than 0.2 µm. Fine hydroxyapatite with a higher surface area has a higher driving force for sintering precluding the need for calcination and compaction. This could result in significant cost savings in terms of equipment and energy needs.

The fluoride selectivity and regeneration potential were investigated through batch adsorption studies. At concentrations found in groundwater, only chloride and NOM competed with fluoride. Chloride ions can be incorporated into the apatite structure, leading to reduced fluoride uptake while the decreased fluoride uptake in the presence of NOM may be attributed to blocking of pores of the ceramics or modification of surface charge of the ceramic by negatively charged NOM particles.

The ceramic beads could be regenerated for up to five adsorption cycles with only a 30% loss in adsorption capacity. Strong concentrations of sodium hydroxide (0.05 M and 0.1 M) were needed to remove fluoride ions which can be associated with hydroxyapatite by adsorption, hydrogen

bonding or ion exchange. Future studies will focus on testing the performance of ceramic adsorbents in continuous-flow column systems and scale up to field applications.

Acknowledgements

This research was partially funded by the University of Oklahoma WaTER Center, the Sun Oil Company Endowed Chair, and University of Oklahoma Graduate College Robberson Research Grant. We thank Dr. Preston Larson for his help with SEM.

References

1. Adriano, O. C. and Doner, H. E. (1982). in *Methods of Soil Analysis. Part 2 – Chemical and Microbiological Properties*. Page, A. L., Miller, R. H. and Keeney, D. R. (eds.). Second edition, 449–483, Madison, WI.
2. Alfredo, K. A. (2012). "Drinking water treatment by alum coagulation: competition among fluoride, natural organic matter, and aluminum." Doctoral dissertation, Univ. of Texas at Austin, Austin, TX.
3. ASTM C136 / C136M-14. (2014). "Standard Test Method for Sieve Analysis of Fine and Coarse Aggregates." ASTM International, West Conshohocken, PA. http://dx.doi.org/10.1520/C0136_C0136M-14.
4. ASTM C242-15. (2015). "Standard Terminology of Ceramic Whitewares and Related Products." ASTM International, West Conshohocken, PA. http://dx.doi.org/10.1520/C0242-15.
5. ASTM C373-14a. (2014). "Standard Test Method for Water Absorption, Bulk Density, Apparent Porosity, and Apparent Specific Gravity of Fired Whiteware Products, Ceramic

Tiles, and Glass Tiles." ASTM International, West Conshohocken, PA. http://dx.doi.org/10.1520/C0373-14A.

6. Ayenew, T. (2005). "Major ions composition of the groundwater and surface water systems and their geological and geochemical controls in the Ethiopian volcanic terrain." *SINET: Ethiopian Journal of Science*, 28(2), 171-188.
7. Ayoob, S., Gupta, A. K., and Bhat, V. T. (2008). "A conceptual overview on sustainable technologies for the defluoridation of drinking water." *Crit. Rev. Env. Sci. Technol.*, 38(6), 401-470.
8. Bansiwal, A., Thakre, D., Labhshetwar, N., Meshram, S., and Rayalu, S. (2009). "Fluoride removal using lanthanum incorporated chitosan beads." *Colloids Surf., B*, 74(1), 216-224.
9. Bhatnagar, A., Kumar, E., and Sillanpää, M. (2011). "Fluoride removal from water by adsorption—a review." *Chem. Eng. J.*, 171(3), 811-840.
10. Brunson, L. R., and Sabatini, D. A. (2009). "An evaluation of fish bone char as an appropriate arsenic and fluoride removal technology for emerging regions." *Environ. Eng. Sci.*, 26(12), 1777-1784.
11. Brunson, L. R., and Sabatini, D. A. (2014). "Practical considerations, column studies and natural organic material competition for fluoride removal with bone char and aluminum amended materials in the Main Ethiopian Rift Valley." *Sci. Total Environ.*, 488, 580-587.
12. Cama, G., Barberis, F., Botter, R., Cirillo, P., Capurro, M., Quarto, R., Scaglione, S., Finocchio, E., Mussi, V., and Valbusa, U. (2009). "Preparation and properties of macroporous brushite bone cements." *Acta Biomater.*, 5(6), 2161-2168.
13. Colombo, P., Vakifahmetoglu, C., and Costacurta, S. (2010). "Fabrication of ceramic components with hierarchical porosity." *J. Mater. Sci.*, 45(20), 5425-5455.

14. Chen, I., Hwang, S. K., and Chen, S. (1989). “Chemical kinetics and reaction mechanism of thermal decomposition of aluminum hydroxide and magnesium hydroxide at high temperature (973-1123 K).” *Ind. Eng. Chem. Res.*, 28(6), 738-742.
15. Chen N., Zhang Z., Feng C., Sugiura N., and Chen R. (2010). “Fluoride removal from water by granular ceramic adsorption.” *J. Colloid. Interface Sci.,* 348, 579-584.
16. de Leeuw, N. H. (2004). “A computer modelling study of the uptake and segregation of fluoride ions at the hydrated hydroxyapatite (0001) surface: introducing a Ca 10 (PO 4) 6 (OH) 2 potential model.” *Phys. Chem. Chem. Phys.*, 6(8), 1860-1866.
17. Du, J., Sabatini, D. A., and Butler, E. C. (2016). “Evaluation of aluminum hydroxide-amended zeolites in fluoride removal: Column filtration and regeneration.” *J. Environ. Eng.*, 10.1061/(ASCE)EE.1943-7870.0001182, 04016092.
18. Fawell, J., Bailey, K., Chilton, J. and Dahi, E. (2006). *Fluoride in drinking-water*, World Health Organization, Geneva, Switzerland.
19. Fewtrell, L., Smith, S., Kay, D. and Bartram, J. (2006). “An attempt to estimate the global burden of disease due to fluoride in drinking water.” *J. Water Health,* 4(4), 533–542.
20. Garg, P., and Chaudhari, S. (2012). “Adsorption of fluoride from drinking water on magnesium substituted hydroxyapatite.” *Proc., 2012 International Conference on Future Environment and Energy (ICFEE 2012),* Singapore, 26-28.
21. Habuda-Stanić, M., Ravančić, M. E., and Flanagan, A. (2014). “A review on adsorption of fluoride from aqueous solution.” *Materials*, *7*(9), 6317-6366.
22. Hamedani, H. A., Baradari, H., Karimi, S., Rezaie, H. and Javadpour, J. (2008). “Influence of Sintering Conditions on the Microstructure of Chemically Precipitated Hydroxyapatite Nanopowder” in *Advances in Bioceramics and Porous Ceramics: Ceramic Engineering*

and Science Proceedings. R. Narayan and P. Colombo (eds.) Volume 29, Issue 7, John Wiley & Sons, Inc., Hoboken, NJ, USA.

23. Hao, O. J., and Huang, C. P. (1986). "Adsorption characteristics of fluoride onto hydrous alumina." *J. Environ. Eng.*,10.1061/(ASCE)0733-9372(1986)112:6(1054), 1054-1069.
24. Herring, C. (1950). "Effect of change of scale on sintering phenomena." *J. Appl. Phys.*, 21(4), 301-303.
25. Jagtap, S., Thakre, D., Wanjari, S., Kamble, S., Labhsetwar, N., and Rayalu, S. (2009). "New modified chitosan-based adsorbent for defluoridation of water." *J. Colloid Interface Sci.*, 332(2), 280-290.
26. Kamieniak, J., Kelly, P. J., Banks, C. E., and Doyle, A. M. (2018). "Mechanical, pH and Thermal Stability of Mesoporous Hydroxyapatite." *J. Inorg. Organomet. Polym. Mater.*, 28(1), 84-91.
27. Kundu, N., Panigrahi, M., Tripathy, S., Munshi, S., Powell, M. A., and Hart, B. (2001). "Geochemical appraisal of fluoride contamination of groundwater in the Nayagarh District of Orissa, India." *Environ. Geol.*, 41(3-4), 451-460.
28. Lin, J., Raghavan, S. and Fuerstenau, D.W. (1981). "The adsorption of fluoride ions by hydroxyapatite from aqueous solution." *Colloids Surf.*, 3(4), 357–370.
29. Ma, W., Ya, F. Q., Han, M., and Wang, R. (2007). "Characteristics of equilibrium, kinetics studies for adsorption of fluoride on magnetic-chitosan particle." *J. Hazard. Mater.*, 143(1-2), 296-302.
30. Macalady, D. L., and Ranville, J. F. (1998). *The chemistry and geochemistry of natural organic matter (NOM),* Oxford Press, New York.

31. Mackie, P. E., Elliot, J. C., and Young, R. A. (1972). “Monoclinic structure of synthetic Ca5 (PO4) 3Cl, chlorapatite.” *Acta Crystallogr., Sect. B: Struct. Sci.,* 28(6), 1840-1848.

32. McCann, H.G. (1953). “Reactions of fluoride ion with hydroxyapatite.” *J. Biol. Chem.* 201, 247–259.

33. Meenakshi and Maheshwari R.C. (2006). “Fluoride in drinking water and its removal.” *J. Hazard Mater.,* 137(1), 456–463.

34. Mohapatra, M., Rout, K., Gupta, S. K., Singh, P., Anand, S., and Mishra, B. K. (2010). “Facile synthesis of additive-assisted nano goethite powder and its application for fluoride remediation.” *J. Nanopart. Res.,* 12(2), 681-686.

35. Mouelhi, M., Giraudet, S., Amrane, A., and Hamrouni, B. (2016). “Competitive adsorption of fluoride and natural organic matter onto activated alumina.” *Environ. Technol.,*37(18), 2326-2336.

36. Nijhawan, A., Butler, E. C., and Sabatini, D. A. (2017). “Macroporous hydroxyapatite ceramic beads for fluoride removal from drinking water.” *J Chem Technol Biot,* 92(8), 1868-1875.

37. Oyanedel-Craver, V. A., and Smith, J. A. (2007). “Sustainable colloidal-silver-impregnated ceramic filter for point-of-use water treatment.” *Environ. Sci. Tech.,* 42(3), 927-933.

38. Padungthon, S., Li, J., German, M., and SenGupta, A. K. (2014). “Hybrid anion exchanger with dispersed zirconium oxide nanoparticles: a durable and reusable fluoride-selective sorbent.” *Environ. Eng. Sci.,* 31(7), 360-372.

39. Parkhomey, O., Pinchuk, N., Sych, O., Tomila, T., Kuda, O., Tovstonoh, H., ... and Evych, Y. (2016). “Effect of particle size of starting materials on the structure and properties of biogenic hydroxyapatite/glass composites.” *Process. Appl. Ceram.*, 10(1), 1-8.

40. Redman, A. D., Macalady, D. L., and Ahmann, D. (2002). “Natural organic matter affects arsenic speciation and sorption onto hematite.” *Environ. Sci. Technol.*, 36(13), 2889-2896.

41. Sato, T., Ozawa, F., Nakamura, T., Watanabe, H., and Ikoma, S. (1979). “Thermal decomposition of zirconium hydroxide.” *Thermochim. Acta.*, 34(2), 211-220.

42. Schneider, C.A., Rasband, W.S., and Eliceiri, K.W. (2012). "NIH Image to ImageJ: 25 years of image analysis". *Nat. Methods*, 9, 671-675.

43. Spinelli, M.A., Brudevold, F. and Moreno, E. (1971). “Mechanism of fluoride uptake by hydroxyapatite.” *Arch. Oral Biol.*,16, 187–203.

44. Verwilghen, C., Rio, S., Nzihou, A., Gauthier, D., Flamant, G., and Sharrock, P. J. (2007). “Preparation of high specific surface area hydroxyapatite for environmental applications.” *J. Mater. Sci.*, 42(15), 6062-6066.

45. Worch, E. (2012). *Adsorption technology in water treatment: fundamentals, processes, and modeling.* de Gruyter, Berlin.

46. WHO (World Health Organization). (2011). *Guidelines for Drinking Water Quality*, 4th ed. Geneva.

47. Yan, W., Li, N., Tong, J., Liu, G., and Xu, J. (2013). “Effect of particle size on the pore characterization and strength of porous cordierite-mullite ceramics prepared by a pore-forming in-situ technique.” *Sci. Sinter.*, 45(2), 165-172.

48. Yao, R., Meng, F., Zhang, L., Ma, D., and Wang, M. (2009). Defluoridation of water using neodymium-modified chitosan. *J. Hazard. Mater.*, 165(1-3), 454-460.

49. Yu, X., Tong, S., Ge, M., and Zuo, J. (2013). “Removal of fluoride from drinking water by cellulose@ hydroxyapatite nanocomposites.” *Carbohydr. Polym.*, *92*(1), 269-275.

50. Zhai, Y., and Cui, F. Z. (2006). “Recombinant human-like collagen directed growth of hydroxyapatite nanocrystals.” *J. Cryst. Growth*, 291(1), 202-206.

51. Zhang, D., Luo, H., Zheng, L., Wang, K., Li, H., Wang, Y., and Feng, H. (2012). “Utilization of waste phosphogypsum to prepare hydroxyapatite nanoparticles and its application towards removal of fluoride from aqueous solution.” *J. Hazard. Mater.*, 241, 418-426.

52. Zhao, B., Zhang, Y., Dou, X., Wu, X., and Yang, M. (2012). “Granulation of Fe–Al–Ce trimetal hydroxide as a fluoride adsorbent using the extrusion method.” *Chem. Eng. J.*, 185, 211-218.

Chapter 4 Studying the kinetics of fluoride adsorption on porous hydroxyapatite ceramics

Abstract

Batch kinetic tests and continuous flow column experiments were conducted to study the kinetics of fluoride adsorption on porous hydroxyapatite ceramics. Batch tests demonstrated the time-dependent nature of fluoride uptake, which is expected for ceramics with internal porosity and sorption sites, with intraparticle mass transfer occurring faster for smaller adsorbent particles with shorter diffusion distances. Columns with different flow rates had different breakthrough curves. Fluoride loading on the adsorbent (q) was determined through mass balance for each of the columns. The mass loading at point of exhaustion ($C_{eff} = 0.85\ C_0$) increased with decrease in EBCT while the mass loading at breakthrough ($C_{eff} = 0.15\ C_0$) showed the opposite trend. Interrupting the flow at different points during the run led to a temporary decrease in the effluent fluoride concentration demonstrating that these columns experienced non-equilibrium conditions and that intraparticle diffusion plays a significant role in fluoride uptake. The Rapid Small-Scale Column Test (RSSCT) concept was tested as a scale up approach. Small-scale columns were designed using the constant diffusivity (CD) and proportional diffusivity (PD) RSSCT approaches and the resulting breakthrough curves were compared to a large-scale column, with CD found to be the more suitable approach to predict fluoride breakthrough. Overall, two large columns with an empty bed contact time (EBCT) of 49 minutes and three small columns with EBCTs of 49, 24.5 and 12.3 minutes were run to evaluate the kinetic and scale-up nature of the porous hydroxyapatite ceramics. These results serve to further validate the use of porous hydroxyapatite ceramics for fluoride uptake and provide valuable insights into kinetic considerations in the full-scale column design of such systems.

Introduction

Fluoride is a geogenic ground water contaminant, naturally found in ground water with high pH and low calcium concentrations. It is found in minerals such as fluorite, fluorspar and apatite, in areas with high volcanic activity and igneous and sedimentary rock formations (Fawell et al. 2006). Amini et al. (2008) estimated that nearly 200 million people are exposed to drinking water with elevated levels of fluoride. Nearly 50% of ingested fluoride is retained by the body, depending on stomach pH and presence of calcium in the diet, and drinking-water is a major contributor to overall fluoride intake (Fawell et al. 2006). Over time, this exposure manifests itself as dental fluorosis at concentrations between 1.5 to 4 mg/L and as skeletal fluorosis at higher concentrations (Fewtrell et al. 2006). The World Health Organization recommends 1.5 mg/L of fluoride in drinking water below which the risk of fluorosis is minimal (WHO, 2011).

Among the most widely studied adsorbents for fluoride removal are activated alumina (Ghorai and Pant, 2005; Hao and Huang, 1986; Ku and Chiou, 2002; Levya-Ramos et al. 2008) and bone char (Brunson and Sabatini, 2009; Kloos and Haimanot, 2002; Mlilo et al., 2009). Activated alumina (AA) has a reported maximum fluoride adsorption capacity of 16 mg/g at a pH of 6.0 (Ku and Chiou, 2002). However, it can dissolve in alkaline conditions required for regeneration (Padungthon et al 2014) which limits its regenerability. Bone char (BC) also suffers from similar sensitivity to pH and its maximum fluoride adsorption capacity is between 4 and 6 mg/g at a pH of 7 (Levya-Ramos et al., 2010; Mlilo et al., 2009). Moreover, materials derived from animal bone can be considered culturally inappropriate in parts of the world such as India. These adsorbents, when used in powdered form, can also disperse in water causing an increase in head loss in a continuous-flow column (Chen et al., 2010)

A granular hydroxyapatite adsorbent was developed to simultaneously address the challenges of pH instability, cultural unsuitability and dispersion in aqueous medium. Hydroxyapatite powder, synthesized in the lab, was mixed with insoluble rice starch and soluble starch and fired at 1200^{o}C to form porous ceramics (Nijhawan et al., 2017). Nijhawan et al. (2018) found that porous hydroxyapatite ceramic beads can remove up to 18 mg F^{-}/g at a pH of 7 with little to no interference from most anions common in ground water (with high chloride an exception). The ceramic media could be regenerated for up to four adsorption cycles with a 30% loss in adsorption capacity using 1 M sodium hydroxide (Nijhawan et al. 2018).

While equilibrium adsorption tests give useful information about the maximum adsorption capacity of adsorbents, continuous-flow column tests are needed to predict adsorbent performance in a community-scale or point-of-use (POU) flow-through (column) system. Kinetic tests can give insight into intraparticle mass transfer effects and the effect of non-equilibrium conditions on fluoride adsorption in the column. Moreover, the adsorption capacity of a material is more efficiently utilized in a column experiencing constant loading. Tor et al. (2009) studied fluoride adsorption by granular red mud and reported faster breakthrough and decreased fluoride loading onto the adsorbent until breakthrough with increase in flow rate. To our knowledge, there are no reported studies on the kinetics of fluoride removal by porous hydroxyapatite ceramics, therefore, the first objective of this research was to evaluate the performance of these materials in continuous flow columns and evaluate mass transfer limitations of fluoride removal.

When properly designed, small lab-scale columns can be used to predict the performance of a full-scale column. A simple way to do this is the Rapid Small-Scale Columns Test (RSSCT) approach. The RSSCT approach uses dimensionless mass transport parameters to design small-scale columns

that can be tested in a short time with significantly less consumption of water and adsorbents (Crittenden et al. 1986). The small columns use a smaller adsorbent particle size compared to the larger column. As the size of the adsorbent particle is decreased, the superficial velocity (determined by the flow rate and cross-sectional area of the column) can be increased to maintain similar kinetic and mass transfer limitations. This approach is applicable if the equilibrium adsorption capacity and mechanism of uptake are independent of the size of the adsorbent (Crittenden et al. 1986) and the porous medium is chemically homogenous (as opposed to amended materials). Compared to mathematical modeling, with its inherent complexities, the RSSCT approach has proven to predict the performance of pilot or full-scale columns more accurately so long as mass transfer parameters are scaled correctly. Doing so should result in identical breakthrough curves for the large and small RSSCT columns (Crittenden et al. 1986, 1987a).

The general scaling equations are based on the relationship between the effective diffusivity, *D*, and particle diameter of the adsorbent, *d*, and are given in equations 4.1 and 4.2, where X can be any integer. Effective diffusivity of an ion in a porous media depends on its diffusion coefficient in the liquid filling the pores, porosity of the media and the constrictivity and tortuosity of the pores (Grathwohl, 2012). A relationship between the empty bed contact time (EBCT) and adsorbent diameter is given in equation 4.2 (*SC* and *LC* stand for small column and large column, respectively).

$$D_{SC}/D_{LC} = \left(\frac{d_{SC}}{d_{LC}}\right)^{X} \quad (4.1)$$

$$EBCT_{SC}/EBCT_{LC} = \left(\frac{d_{SC}}{d_{LC}}\right)^{2-X} \quad (4.2)$$

If the effective (pore and surface) diffusivities are independent of adsorbent particle size (X = 0), then the small-scale columns can be designed using the constant diffusivity (CD) approach (Crittenden et al. 1986) and equation 4.2 is reduced to

$$EBCT_{SC}/EBCT_{LC} = \left(\frac{d_{SC}}{d_{LC}}\right)^2 \quad (4.3)$$

This approach assumes that the Reynolds numbers of small and large column stay constant, which gives us the following relationship between superficial velocities, *v*, and adsorbent diameters, *d*.

$$v_{SC}/v_{LC} = \left(\frac{d_{LC}}{d_{SC}}\right) \quad (4.4)$$

Crittenden et al. (1987a) found that the CD approach did not result in similar breakthrough curves for their large and small columns. Instead, the proportional diffusivity (PD) approach was applicable, which assumes that the effective diffusivity increases with increase in adsorbent particle size. For this approach, X=1 and equation 4.2 becomes

$$EBCT_{SC}/EBCT_{LC} = \left(\frac{d_{SC}}{d_{LC}}\right) \quad (4.5)$$

The superficial velocity can be calculated using the $EBCT_{SC}$ (determined from equation 4.5) and the dimensions of the small column.

Once the dimensions of the small column are determined, the superficial velocity of the small column, v_{SC}, can be calculated using the bed volume of the column (BV_{SC}), cross-sectional area of the column A_{SC}, flowrate Q_{SC} and $EBCT_{SC}$ using equations 4.6 and 4.7:

$$Q_{SC} = \left(\frac{BV_{SC}}{EBCT_{SC}}\right) \quad (4.6)$$

$$v_{SC} = \left(\frac{Q_{SC}}{A_{SC}}\right) \quad (4.7)$$

RSSCT columns scaled down using the PD approach typically have a longer empty bed contact time and consequently, longer time to breakthrough compared to the CD RSSCT columns (Westerhoff et al 2005).

The RSSCT approach, initially developed and validated for granular activated carbon (Crittenden et al. 1986, 1987a), has been extensively studied for arsenic removal by granular ferric oxides (Badruzzaman et al. 2004, Westerhoff et al. 2005). It has been applied in a preliminary way to fluoride removal by bone char and amended wood chars (Brunson and Sabatini, 2014). To the best of our knowledge, there are no published studies applying the RSSCT approach to porous ceramics for fluoride removal. It is hypothesized that the RSSCT approach will be valid for these materials because of the fundamental similarities between porous hydroxyapatite ceramics and granular activated carbon (GAC) – they are both chemically homogeneous (as opposed to metal amended chars or resins) and have accessible internal pores that contribute most of the available surface sites while also introducing kinetic limitations due to intraparticle diffusion.

Materials and methods

Preparation of ceramics

Hydroxyapatite powder was synthesized in the lab according to the procedure described in Nijhawan et al. (2018). Briefly, calcium nitrate tetrahydrate and ammonium phosphate salts were mixed at a pH of 10.6 and the precipitated crystals were matured at 40^{o}C for 60 hours (Verwilghen et al., 2007). After drying, the precipitate was crushed and sieved through numbers 120 (pore size 125 µm) and 325 mesh (pore size 44 µm) to obtain a uniform particle size. The powdered hydroxyapatite was then mixed with rice starch and soluble potato starch in a volumetric ratio of

50%, 25% and 25% each. During batch adsorption experiments, this volumetric ratio was found to have the highest fluoride adsorption capacity of 18 mg/g (Nijhawan et al. 2018).

The mixture of powdered hydroxyapatite and the two types of starches was packed into a BD 5 mL syringe with a Luer-Lok tip (Bector, Dickinson and Company, NJ) and pushed out to form thin strings. These were then allowed to dry and cut into cylindrical pellets. Pellets of approximate diameter 2 mm and length 3 to 4 mm were used for the small columns (diameter 2.5 cm) and pellets of 4 mm in diameter and 6 to 8 mm in length were used for the larger column (diameter 5 cm). Usually, a column diameter to pellet diameter ratio of at least 10 to 1 is recommended to avoid channeling (Rase, 1977), however, a ratio of 7 to 1 has also been found satisfactory (Arbuckle and Ho, 1990). Finally, these pellets were fired in a kiln at 1200^{o}C for 6 hours to obtain the porous ceramic. The actual porosity of the packed bed was determined gravimetrically by measuring the weight of water needed to saturate the bed. The porosity of the porous ceramic along with the inter-pellet porosity contribute to the overall porosity of the packed bed.

Batch kinetic test

A batch kinetic test was done to (1) assess the kinetics of fluoride uptake and (2) to evaluate the effect of pellet size on rate of fluoride adsorption and equilibrium fluoride concentration, which would guide the application of the RSSCT approach. A 10 mg/L fluoride solution was prepared by diluting a 1000 mg/L NaF solution in 50 mM HEPES (4-(2-hydroxyethyl)-1-piperazineethanesulfonic acid) buffer solution. Ceramic pellets were added to this solution in a solid to liquid ratio of 5 g/L in 100-mL Nalgene high density polyethylene bottles and kept on a reciprocating shaker at 30 rpm. Samples were collected for fluoride measurement every 30 minutes for the first 5 hours and then every hour until hour 48.

Column adsorption tests

Small-scale column tests were done in a glass column with inner diameter of 2.5 cm and bed depth of 10 cm (bed volume of 49 mL). Two flow rates were tested – 1 and 2 mg/L – corresponding to EBCTs of 49 and 24.5 minutes respectively. A 10 mg/L fluoride solution was pumped from the influent storage to the inlet of the column using a peristaltic pump (Cole-Palmer Masterflex, Vernon Hills, Illinois) to maintain a constant flow rate. A pressure gauge was connected between the pump and inlet of the column to record the inlet pressure (Figure 4.1, P1). The column was setup as an up-flow column to prevent flow by gravity. Glass wool was placed near the inlet and outlet of the column to support the adsorbent bed. Glass beads were placed at both ends of the bed to allow dispersion of the water. The 10 mg/L fluoride solution was prepared according to the method described in the previous section. An outlet pressure gauge (Figure 4.1, P2) was placed between the column outlet and the automatic fraction collector (Pharmacia LKB-Frac-100, New York City, New York), to measure the pressure drop across the column. P1 and P2 were placed at the same height to avoid a difference in potential energy at the two points. Silicone tubing was used to connect each part of the column setup.

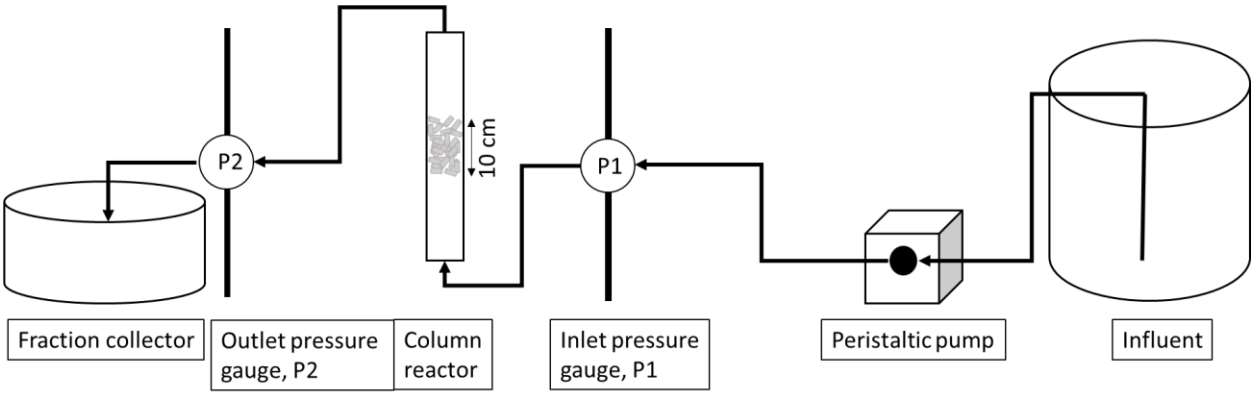

Figure 4.1 Lab-scale continuous-flow column set up (Influent fluoride concentration, C_0 = 10 mg/L)

Large-scale column studies were done in a glass column with an inner diameter of 5 cm and bed depths of 12 and 18 cm with a flow rate of 4.8 mL/min and 7.2 mL/min (both with an EBCT of 49 minutes), respectively.

For the RSSCT design, $EBCT_{SC}$ and v_{SC} were calculated from equations 4.3 and 4.4 whereas $EBCT_{LC}$ and v_{LC} were determined from equations 4.5 and 4.7.

Fluoride Analysis

Fluoride concentrations for the batch kinetic study and the column studies were measured using an ion selective electrode (Thermo-Scientific Orion, Waltham, Massachusetts) that was calibrated using 0.025, 0.5, 1, 10 and 100 mg F^-/L standards. Total ionic strength adjustment buffer (TISAB) was used to dilute samples, standards and blanks in a 1:1 ratio to maintain a constant ionic strength and to decomplex dissolved fluoride complexes (Adriano and Doner, 1982).

Breakthrough analysis

Fluoride loading in the column was measured by doing a mass balance. The WHO Guideline for safe intake of drinking-water containing fluoride, 1.5 mg/L, was chosen as the point of 'breakthrough', while 85% of influent concentration, (C_0 =10 mg/L), 8.5 mg/L was chosen as point of exhaustion. These values were expressed as q_b and q_e, respectively and refer to the mass of fluoride (mg) loaded per gram of the adsorbent in the column bed.

Results and Discussion

Batch kinetic study

The applicability of the RSSCT approach was tested through batch kinetic studies which showed similar equilibrium fluoride concentrations for the small and large pellets (Figure 4.2). The smaller

pellets showed a higher rate of fluoride removal initially, but the two curves converged around t = 24 hours (see inset) and eventually reached an equilibrium concentration of 0.03 ± 0.003 mg/L at t = 26 hours. The initial rate of fluoride removal was higher for both pellets because of the large concentration gradient between the fluoride-free pellet surface and bulk solution and between the pellet surface and the intraparticle pore water. Further fluoride removal took place after fluoride ions diffused into the interior of the pellets via surface and/or pore diffusion. This process was faster (steeper) for the smaller pellet size as the intraparticle diffusion distance was shorter.

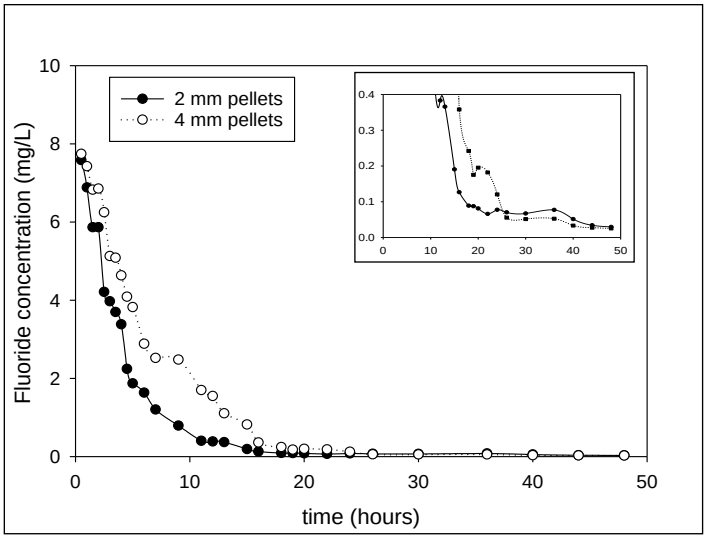

Figure 4.2 Results of kinetic study to determine the rate of fluoride removal in small (2mm diameter) and large pellets (4 mm diameter)

Since the ultimate equilibrium concentration was independent of adsorbent size, the RSSCT approach is deemed appropriate for use with the porous hydroxyapatite ceramics studied in this research.

Continuous-flow column tests

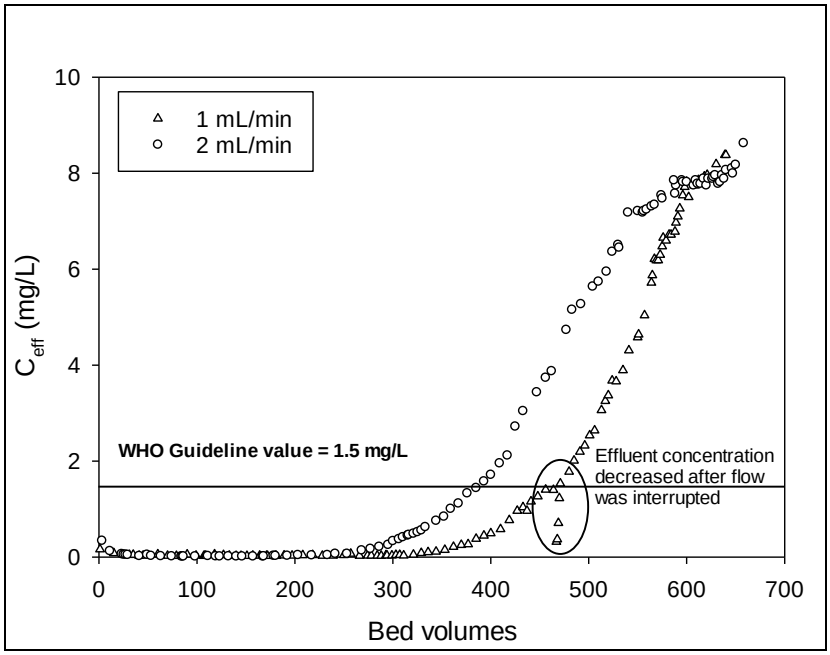

Figure 4.3 Breakthrough curves of small columns with flow rates of 1 mL/min and 2 mL/min (column diameter = 2.5 cm, bed depth = 10 cm)

Two small continuous-flow columns with flow rates of 1 and 2 mL/min were run until exhaustion (i.e., when the effluent concentration C_e reached 85% of (or 0.85 times) C_0). The breakthrough curves, plotting the fluoride concentration in the effluent against bed volumes of each column had the characteristic S-shape (Figure 4.3) commonly reported for adsorbent beds with favorable adsorption isotherms (Brunson and Sabatini, 2014; Du et al. 2016; Tor et al. 2009). The shape of the breakthrough curve is determined by the length of the mass transfer zone (MTZ) that develops in the column. The MTZ is the length of bed needed for uptake of a contaminant (Crittenden et al. 1987b); the bed is assumed to be saturated upstream of the MTZ and unused downstream of it, while the mass transfer of fluoride onto the porous adsorbent takes place in the MTZ. Once the MTZ reaches the downstream end of the column, the fluoride front appears, and the effluent

concentration starts to increase. This was observed after approximately 250 to 300 bed volumes for the columns (Figure 4.3). Before this, the effluent concentration was at or near the detection limit of the ion-selective electrode (0.02 mg/L).

The shape of the breakthrough curves was influenced by the flow rate. The later appearance of fluoride and steeper slope of the 1 mL/min breakthrough curve (Figure 4.3) indicates a shorter mass transfer zone (MTZ) because the longer residence time (determined by the flow rate) allowed more time for the fluoride ions to diffuse into the pores and occupy available adsorption sites. At a higher flow rate (2 ml/min), however, the curve rose earlier and had a more gradual slope and a long 'tail' (which would likely have been more obvious had this column been run until $C_{eff} = C_0$). Likewise, at 2 mL/min, the diffusion-limited adsorption caused an earlier breakthrough as expected for a longer MTZ (). This is consistent with the trends reported by Ghorai and Pant (2005), Marsh and Rodríguez-Reinoso (2006) and Mohan et al. (2017) who observed shorter time to breakthrough with increase in flow rate.

A mass balance was conducted on each column to determine the amount of fluoride adsorbed per gram of ceramic (q) at breakthrough (C_{eff} = 1.5 mg/L) and exhaustion (C_{eff} = 8.5 mg/L), as shown in Table 4.1. The values of q at breakthrough (q_b) were similar for the two columns, but the values of q at exhaustion (q_e) decreased from 11.7 to 10.8 mg/g with increase in flow rate. This is visually confirmed from Figure 4.3 which illustrates less adsorption (area above the curves) for the 2 mL/min column. If the columns had been allowed to run till $C_{eff} = C_0$ = 10 mg/L, it is possible that these values would converge toward the same value – albeit with a long, extended tail for the 2 mL/min case.

Table 4.1 Operational and design parameters of small continuous-flow columns

Parameter	**Q = 2 mL/min**	**Q = 1 mL/min**
EBCT (min.)	24.5	49
Mass of adsorbent (g)	19.4	22.8
Bed volume (mL)	49	49
Bed volumes till breakthrough	390	465
Bed volumes till exhaustion	658	640
q until breakthrough (1.5 mg/L), q_b (mg/g)	9.6	9.8
q until exhaustion (8.5 mg/L), q_e (mg/g)	10.8	11.7
Langmuir isotherm parameters[a]		
$q_{1.5}$	6.0 ± 0.9	
$q_{8.5}$	11.9 ± 2.0	
q_{10}	12.6 ± 1.9	

Note: [a] The values of $q_{1.5}$, $q_{8.5}$ and q_{10} were calculated from batch isotherm data (Nijhawan et al. 2018) using Langmuir isotherm parameters (Q_{max} = 18.2 ± 1.6 mg/g, K = 0.3 ± 0.1). Uncertainties represent standard error of non-linear regression

While the q_e values for both columns lie within the estimated range of $q_{8.5}$ obtained from batch isotherm, the q_b was higher than the batch $q_{1.5}$ (Nijhawan et al. 2018) (Table 4.1). This can be attributed to the fact when C_{eff} = 1.5 mg/L, the early portion of the column bed is in equilibrium with concentrations greater than 1.5 mg/L. In fact, a section of the bed near the influent might be approaching saturation and thus be in equilibrium with the inlet fluoride concentration. Therefore, the q_b value can be thought of as a composite of solid phase fluoride concentrations (q) at local

equilibria, averaged over the entire length of the column, and thus expected to be greater than $q_{1.5}$ obtained from batch studies.

Constant diffusivity (CD) versus proportional diffusivity (PD) RSSCT approaches

The RSSCT approach was tested by designing a larger column and two small columns – designed using the proportional diffusivity (PD) and constant diffusivity (CD) approaches to determine which would predict the breakthrough of the larger column more accurately. The superficial velocity, v_{LC}, and empty bed contact time, $EBCT_{LC,}$ of the large column were 0.24 cm/min and 49 minutes, respectively. The CD column was designed using equations 4.3 and 4.4, while the PD column was designed using equations 4.5 to 4.7. The design parameters for each column are presented in Table 4.2. The bed densities and porosities were similar for all three columns indicating homogeneity in packing density and pore volume with increase in pellet size.

Table 4.2 Operational and design parameters of continuous-flow columns

Parameter	**PD small column**	**CD small column**	**Large column**
Flow rate (mL/min)	2	2.4	4.8
Superficial velocity (cm/min)	0.4	0.48	0.24
EBCT (min.)	24.5	12.3	49
Bed depth (cm)	10	6	12
Bed volume (mL)	49	29.5	236
Bed porosity (%)	72	70	72.5

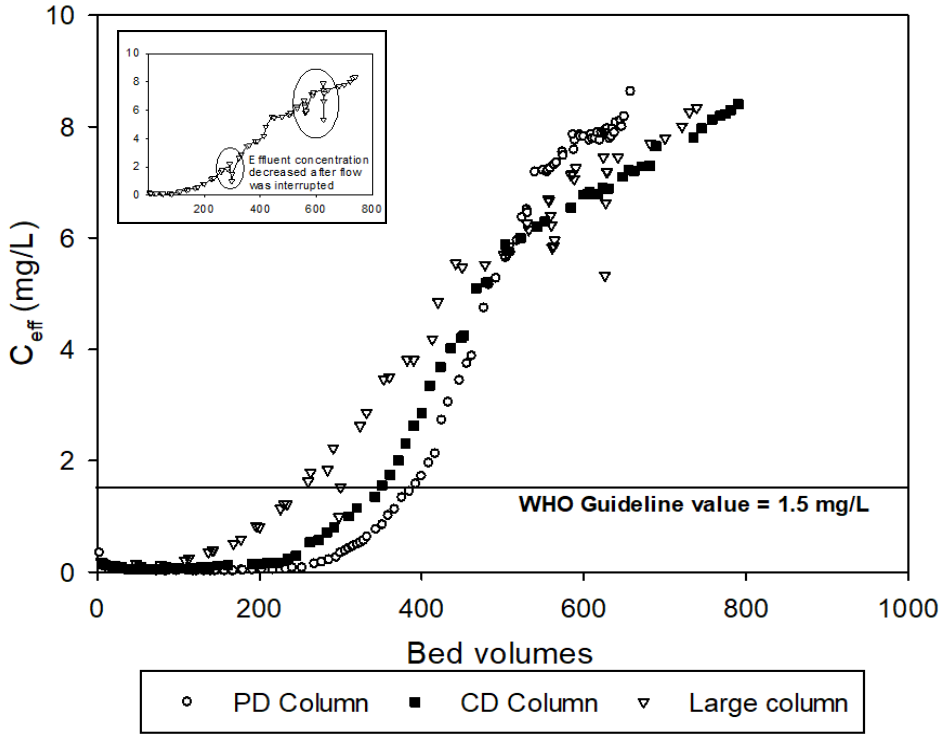

Figure 4.4 Breakthrough curves for a large column and two small (RSSCT) columns designed using the proportional (PD) and constant (CD) diffusivity approaches

The CD approach predicted the breakthrough of the large column better than the PD column, which suggests that the effective intraparticle diffusivity was independent of adsorbent size (an assumption of this approach). However, the three curves begin to converge after approximately 500 bed volumes. This is consistent with the findings of Sperlich et al. (2005) for arsenic removal by granular ferric hydroxide. While the CD RSSCT column was a better predictor of the large column initially, the CD and PD RSSCT breakthrough eventually converged, and both accurately predicted exhaustion of the larger column.

The flow was paused for different durations at multiple points during the large column run to demonstrate the effect of non-equilibrium conditions. As seen in Figure 4.4 inset, interrupting the flow for 48 hours after 290 bed volumes decreased the effluent fluoride concentration from 2.2

mg/L to 0.30 mg/L, an 86% decrease. In comparison, an 18-hour flow interruption after 625 bed volumes only decreased the effluent concentration by 26%, from 7.5 mg/L to 5.3 mg/L. Since this interruption was done further along in the column run, this could be explained by the fact that the system was closer to saturation adsorption and less fewer sites remained available for adsorption.

The flow interruption allowed fluoride ions in the intraparticle region more time to diffuse into the pores of the ceramic pellet, increasing the concentration gradient between the bulk solution and adsorbent surface. A similar phenomenon was observed by Padungthon et al. (2014) who used zirconium-amended anion exchange resins to remove fluoride. The temporary decrease in effluent fluoride concentration indicates that these columns were being operated under non-equilibrium conditions and that intraparticle diffusion plays a significant role in fluoride adsorption.

Effect of flow rate on length of MTZ

A second large column experiment was conducted to test the reproducibility of the results with different flow rates and bed depths, designed to keep the EBCT constant e. A column with a bed depth of 18 cm and flow rate of 7.2 mL/min was chosen to compare to the 12 cm/4.8 mL/min column while maintaining an EBCT of 49 minutes (Table 4.3). The breakthrough curves of both columns are shown in Figure 4.5. The two breakthrough curves have significant overlap because the length of the MTZ increases with increase in flow rate. While the longer column had slightly lower fluoride effluent concentrations initially (first 100 bed volume), the curves started to converge around 150 bed volumes, and both reached exhaustion around 740 bed volumes.

Table 4.3 Operational and design parameters of larger continuous-flow columns

Parameter	**Q = 7.2 mL/min**	**Q = 4.8 mL/min**
EBCT (min.)	49	49
Bed volume (mL)	353	236
Bed depth (cm)	18	12
Mass of adsorbent (g)	158	102
Bed volumes till breakthrough	195	253
Bed volumes till exhaustion	740	739
q till breakthrough (1.5 mg/L), q_b (mg/g)	4.2	5.6
q till exhaustion (8.5 mg/L), q_e (mg/g)	9.8	10.7

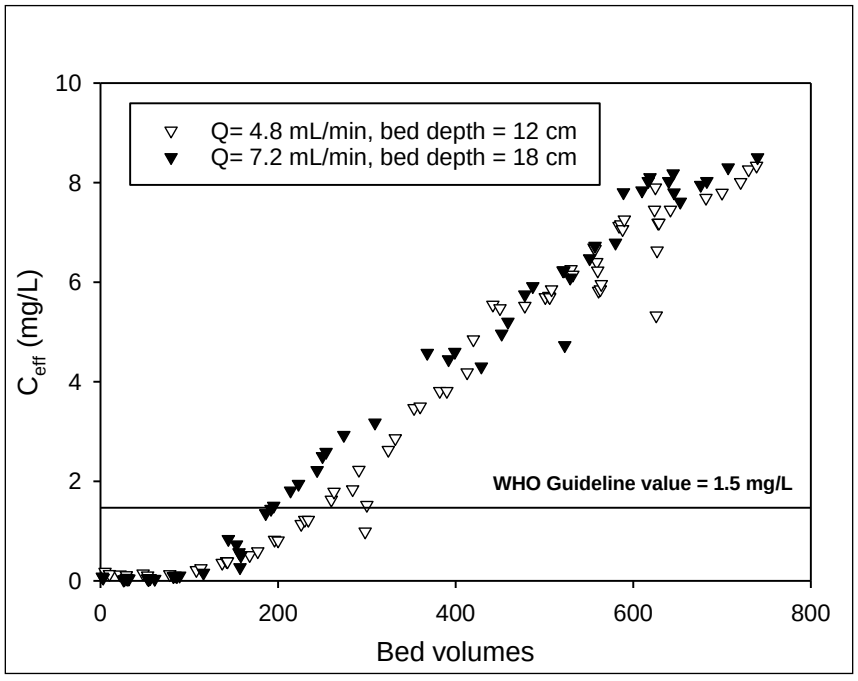

Figure 4.5 Breakthrough curves of columns with EBCT of 49 minutes and flow rates of 4.8 mL/min and 7.2 mL/min

Since the shape of the breakthrough curves was similar for both the columns, and exhaustion occurred after nearly the same number of bed volumes (Table 4.3), these results are consistent with our hypothesis that the length of the MTZ is correlated with the flow rate and superficial velocity in the column and thus that the two column results would be quite similar.

Comparison with other adsorbents and preliminary cost analysis

Comparing the porous hydroxyapatite ceramic with other adsorbents, we observe that it performed 3 to 4 times better than activated alumina and bone char, on a bed volume basis, and comparable to other adsorbents like chemically activated bone (Table 4.4). The ceramics had similar $q_{1.5}$ values and similar bed volumes to breakthrough as compared to chemically activated cow bone (Yami et al. 2016) as well as greater $q_{1.5}$ values and bed volumes to breakthrough than commonly used activated alumina and bone char.

Table 4.4 Comparison of column performance indicators and Langmuir parameters for fluoride adsorbents

Adsorbent	**Bed volumes to breakthrough (C_{eff} = 1.5 mg/L)**	**$q_{1.5}$ (mg/g)**	**Reference**
Activated alumina	70	0.5	Brunson and Sabatini (2014)
Bone char	100	2.1	Brunson and Sabatini (2014)
Chemically activated cow bone	400	4.5 ± 1.8	Yami et al. (2016)
Porous hydroxyapatite ceramics	465	6.0 ± 0.9	This study

As a further step in comparing the porous hydroxyapatite ceramics to the commonly used activated alumina, a preliminary cost analysis was conducted for producing the ceramic media. Based on

bulk costs of chemicals and typical energy consumption values (see Supplementary Information), the cost of the porous hydroxyapatite ceramics was estimated to be $1.63 per kg. This cost compares very favorably with the cost of commercially available activated alumina ($1.50 per kg, Sorg 2014). This combined with the fact that bed volumes to breakthrough were almost seven times greater for the porous hydroxyapatite ceramics (Table 4.4) supports the further evaluation of this adsorbent in pilot and full-scale column and economic studies.

Conclusions

The kinetics of fluoride adsorption on porous hydroxyapatite ceramics were studied through batch and column adsorption tests. In the batch kinetic test, cylindrical pellets of diameter 2 mm and length 3 to 4 mm and diameter 4 mm and length 6 to 8 mm were kept in contact with 10 mg/L fluoride solution for 48 hours. The smaller pellets initially removed fluoride at a faster rate, due to the shorter intra-particle diffusion distances, but the two curves converged after 24 hours and reached the same equilibrium concentration of 0.03 mg/L after 26 hours of reaction time, thus demonstrating the common equilibrium capacity while also confirming the validity of the Rapid Small-Scale Column Tests (RSSCT) approach for these adsorbents.

Fluoride adsorption under continuous-flow column conditions was studied by running two small columns at flow rates of 1 and 2 mL/min. The porous hydroxyapatite ceramics performed better than widely used activated alumina and bone char, measured based on bed volumes to breakthrough ($C_e = 0.15\ C_0$) and exhaustion ($C_e = 0.85\ C_0$). Specifically, the effluent concentration in both the columns was at or below the detection limit of the fluoride selective electrode (0.02 mg/L) for approximately 250 bed volumes, before it started to increase. Eventually, the effluent fluoride concentration reached 1.5 mg/L after 465 and 390 bed volumes for the 1 mL/min and 2

mL/min columns, respectively. Since the adsorbent pellet size and bed depth were kept the same, the breakthrough curve was only influenced by the flow rates of each column. The 2 mL/min column had a faster breakthrough but exhibited a more gradual slope and a long 'tail' because, at higher effluent concentrations, say C_{eff} = 7 mg/L, it had more adsorption capacity left as compared to the 1 mL/min column.

The mass of fluoride adsorbed per gram of the adsorbent was similar for both the columns. The q_e values were 11.7 mg/g at a flow rate of 1 mL/min and 10.8 mg/g at a flow rate of 2 mL/min. This is approaching the value of $q_{8.5}$ (11.9 ± 0.9) obtained from batch adsorption tests (Nijhawan et al. 2018).

The RSSCT approach was validated for the adsorption of fluoride. Two small columns were designed using the constant (CD) and proportional diffusivity (PD) approaches respectively, and their breakthrough curves were compared to that of a large column. The CD approach was a better predictor of the fluoride removal performance suggesting that the effective intra-particle diffusivity is independent of the adsorbent size. On the other hand, the small PD RSSCT column displayed longer time to breakthrough as compared to the larger column. This is comparable to results reported by other researchers who found that the PD RSSCT column often results in longer time to breakthrough. Both the small columns consumed about $1/6^{th}$ the volume of water used by the large column.

Interruption in the column flow at different points in the column run led to a temporary decrease in the effluent fluoride concentration. The effluent fluoride concentration decreased from 2.2 mg/L to 0.30 mg/L when the flow was interrupted for 48 hours after 290 bed volumes. This suggests that the column was being run under non-equilibrium conditions and that intraparticle diffusion

contributes significantly to fluoride removal. During the interruption in flow, the fluoride ions diffused further into the pores of the ceramic pellet creating a concentration gradient between the ceramic surface and bulk fluoride solution. When the flow was restarted, this resulted in adsorption on the now available surface sites.

Two columns with different flow rates but the same EBCT showed similar breakthrough profiles. With increase in flow rate, the length of the MTZ also increased, leading to similar breakthrough curves even though the columns varied in length (12 and 18 cm).

The cost of this ceramic media was found to be approximately $1.63 per kg, which compares favorably with the cost of commercially available activated alumina. The fact that this adsorbent performed six to seven times better than activated alumina makes this cost even more competitive.

These results have implications for the use of this adsorbent in a point-of-use or community-scale treatment system. Continuous-flow column tests with different contact times (and, therefore, superficial velocities), resulted in a marked difference in q_b values ranging from 4.2 to 9.8 mg/g. It is likely that even higher q_b values will be obtained if columns are operated with interrupted flow, thereby, maximizing fluoride loading on to the adsorbent before breakthrough. Therefore, future research should focus on testing adsorption in columns with interrupted loading to determine the optimum hydraulic residence time to maximize the fluoride removal capacity and cost-effectiveness of this material.

Acknowledgements

The authors would like to acknowledge the support of the University of Oklahoma WaTER Center, the School of Civil Engineering and Environmental Science and the Sun Oil Company Endowed Chair.

References

1. Adriano, O. C. and Doner, H. E. (1982). in *Methods of Soil Analysis. Part 2 – Chemical and Microbiological Properties*. Page, A. L., Miller, R. H. and Keeney, D. R. (eds.). Second edition, 449–483, Madison, WI.
2. Arbuckle, W. B., & Ho, Y. F. (1990). Adsorber column diameter: particle diameter ratio requirements. *Research Journal of the Water Pollution Control Federation*, 88-90.
3. Badruzzaman, M., Westerhoff, P., & Knappe, D. R. (2004). Intraparticle diffusion and adsorption of arsenate onto granular ferric hydroxide (GFH). *Water research*, *38*(18), 4002-4012.
4. Brunson, L. R., & Sabatini, D. A. (2009). An evaluation of fish bone char as an appropriate arsenic and fluoride removal technology for emerging regions. *Environmental engineering science*, *26*(12), 1777-1784.
5. Brunson, L. R., & Sabatini, D. A. (2014). Practical considerations, column studies and natural organic material competition for fluoride removal with bone char and aluminum amended materials in the Main Ethiopian Rift Valley. *Science of The Total Environment*, *488*, 580-587.
6. Chen N., Zhang Z., Feng C., Sugiura N., and Chen R. (2010). "Fluoride removal from water by granular ceramic adsorption." *J. Colloid. Interface Sci.*, 348, 579-584.
7. Crittenden, J. C., Berrigan, J. K., & Hand, D. W. (1986). Design of rapid small-scale adsorption tests for a constant diffusivity. *J. Water Pollut. Control Fed.*, *58*(4), 312-319.
8. Crittenden, J. C., Berrigan, J. K., Hand, D. W., & Lykins, B. (1987a). Design of rapid fixed-bed adsorption tests for nonconstant diffusivities. *Journal of Environmental Engineering*, *113*(2), 243-259.

9. Crittenden, J., Hand, D., Arora, H., & Lykins, B. (1987b). Design Considerations for GAC Treatment of Organic Chemicals. *Journal (American Water Works Association), 79*(1), 74-82.
10. Du, J., Sabatini, D. A., & Butler, E. C. (2016). Evaluation of aluminum hydroxide-amended zeolites in fluoride removal: Column filtration and regeneration. *Journal of Environmental Engineering*, *143*(4), 04016092.
11. Fawell, J., Bailey, K., Chilton, J., Dahi, E., & Magara, Y. (2006). *Fluoride in drinking-water*. IWA publishing.
12. Fewtrell, L., Smith, S., Kay, D., & Bartram, J. (2006). An attempt to estimate the global burden of disease due to fluoride in drinking water. *Journal of Water and Health*, *4*(4), 533-542.
13. Ghorai, S., & Pant, K. K. (2005). Equilibrium, kinetics and breakthrough studies for adsorption of fluoride on activated alumina. *Separation and Purification Technology*, *42*(3), 265-271.
14. Grathwohl, P. (2012). *Diffusion in natural porous media: contaminant transport, sorption/desorption and dissolution kinetics* (Vol. 1). Springer Science & Business Media.
15. Hao, O. J., & Huang, C. P. (1986). Adsorption characteristics of fluoride onto hydrous alumina. *Journal of Environmental Engineering*, *112*(6), 1054-1069.
16. Kloos, H., & Haimanot, R. T. (1999). Distribution of fluoride and fluorosis in Ethiopia and prospects for control. *Tropical Medicine & International Health, 4*(5), 355-364.
17. Ku, Y., & Chiou, H. M. (2002). The adsorption of fluoride ion from aqueous solution by activated alumina. *Water, air, and soil pollution*, *133*(1-4), 349-361.

18. Leyva-Ramos, R., Rivera-Utrilla, J., Medellin-Castillo, N. A., & Sanchez-Polo, M. (2010). Kinetic modeling of fluoride adsorption from aqueous solution onto bone char. *Chemical Engineering Journal*, *158*(3), 458-467.
19. Marsh, H., & Rodríguez-Reinoso, F. (2006). Characterization of Activated Carbon. In Marsh, H., & Rodriguez-Reinoso, F. (Eds.), *Activated carbon*, (pp 143-242). London: Elsevier Science.
20. Mlilo, T. B., Brunson, L. R., & Sabatini, D. A. (2009). Arsenic and fluoride removal using simple materials. *Journal of Environmental Engineering*, *136*(4), 391-398.
21. Mohan, S., Singh, D. K., Kumar, V., & Hasan, S. H. (2017). Effective removal of Fluoride ions by rGO/ZrO2 nanocomposite from aqueous solution: fixed bed column adsorption modelling and its adsorption mechanism. *Journal of Fluorine Chemistry*, *194*, 40-50.
22. Nijhawan, A., Butler, E. C., & Sabatini, D. A. (2017). Macroporous hydroxyapatite ceramic beads for fluoride removal from drinking water. *Journal of Chemical Technology and Biotechnology*, 92(8), 1868-1875.
23. Nijhawan, A., Butler, E. C., & Sabatini, D. A. (2018). Hydroxyapatite Ceramic Adsorbents: Effect of Pore Size, Regeneration, and Selectivity for Fluoride. *Journal of Environmental Engineering*, *144*(11), 04018117.
24. Padungthon, S., Li, J., German, M., and SenGupta, A. K. (2014). Hybrid anion exchanger with dispersed zirconium oxide nanoparticles: a durable and reusable fluoride-selective sorbent" *Environ. Eng. Sci.*, 31(7), 360-372.
25. Rase, H.F. (1977*) Chemical Reactor Design for Process Plants, Vol 1: Principles & Techniques*. New York, NY: Wiley and Sons.

26. Sperlich, A., Werner, A., Genz, A., Amy, G., Worch, E., & Jekel, M. (2005). Breakthrough behavior of granular ferric hydroxide (GFH) fixed-bed adsorption filters: modeling and experimental approaches. *Water Research*, *39*(6), 1190-1198.

27. Sorg, T. (2014). Removal of Fluoride from Drinking Water Supplies by Activated Alumina.

28. Tor, A., Danaoglu, N., Arslan, G., & Cengeloglu, Y. (2009). Removal of fluoride from water by using granular red mud: batch and column studies. *Journal of hazardous materials*, *164*(1), 271-278.

29. Verwilghen, C., Rio, S., Nzihou, A., Gauthier, D., Flamant, G., & Sharrock, P. J. (2007). Preparation of high specific surface area hydroxyapatite for environmental applications. *Journal of Materials Science*, *42*(15), 6062-6066.

30. Westerhoff, P., Highfield, D., Badruzzaman, M., & Yoon, Y. (2005). Rapid small-scale column tests for arsenate removal in iron oxide packed bed columns. *Journal of Environmental Engineering*, *131*(2), 262-271.

31. WHO (2011). *Guidelines for drinking-water quality, 4th ed*. World Health Organization. Geneva.

32. Yami, T. L., Chamberlain, J. F., Butler, E. C., & Sabatini, D. A. (2016). Using a high-capacity chemically activated cow bone to remove fluoride: field-scale column tests and laboratory regeneration studies. *Journal of Environmental Engineering*, *143*(2), 04016083.

Supplementary Information

Cost analysis on manufacturing ceramics at industrial scale

Assumptions

i. Chemical costs are bulk prices for a minimum purchase of 20 – 25 metric tons

ii. This operation makes 170 kg of ceramic material daily

iii. The electric kiln is operated for 6 hours daily

iv. The ball mill and sieve shakers are operated for 4 hours daily

v. The US rate of 12 cents per kWh is used to determine electricity costs

1. Capital expenditure

Table S4.1 Equipment costs

Equipment	**Cost (USD)**
Kiln TL20E = 20ft^3 electric kiln	6,650
Ball mill	4,500
Sieve shaker	1,000

2. Operational expenditure

Table S4.2 Wholesale cost of raw materials

Chemical	**Cost per kg (USD/kg)**
Calcium nitrate tetrahydrate	0.09
Ammonium phosphate monobasic	0.12
Ammonium hydroxide, 25 – 28%	0.18
Rice starch	0.15
Soluble starch	1

Total cost of chemicals per kilogram of prepared adsorbent = 1.5 USD

Table S4.3 Energy consumption of equipment and associated costs

Equipment	**Electricity cost per day (for 170 kg ceramics) (USD/day)**	**Electricity cost per kg of ceramics (USD/kg)**
Electric kiln	13.8	0.08
Ball mill	1.0	0.04
Sieve shaker	7.2	0.01

Total cost of material ($USD/kg) = 1.5 + 0.13 = 1.63 USD

Commercially available activated alumina costs 1.5 USD/per kg.

Chapter 5 Conclusions

Despite the widespread use of relatively low-cost fluoride removal technologies, fluoride-impacted drinking water continues to be a health hazard for millions of people worldwide. Limitations of existing removal technologies include low fluoride removal capacity, high cost, leaching of toxic metals and color and odor-causing organic compounds into treated water, lack of cultural acceptability in certain countries, and difficulties in operation and handling because of instability over a wide pH range. The goal of this dissertation was to develop a fluoride adsorbent to address several of these limitations, specifically low fluoride removal capacity, physical and chemical instability at high pH and lack of cultural acceptance.

The specific objectives of this research were to synthesize and characterize porous hydroxyapatite ceramics; evaluate their fluoride removal capacity; and study the impact of parameters such as size of hydroxyapatite particles, size and type of pore-forming materials, pore size, pore volume, synthesis conditions, potential for regeneration, selectivity for fluoride and performance in batch and continuous-flow column systems.

Porous hydroxyapatite ceramics were made by firing mixtures of synthesized hydroxyapatite powders and insoluble and soluble pore forming materials at 1200^{o}C (Chapter 2). Three types of starches – rice, wheat and corn – and cellulose fibers, were used as insoluble pore forming materials. Soluble starch gelatinized in water and acted as a binder for the hydroxyapatite and insoluble starch/cellulose granules, allowing for cohesive, compact shapes before firing. The insoluble starches and cellulose acted as pore formers and created interconnected pores on burning. The result was the formation of a ceramic matrix with porosities in the range of 25 to 45%, depending on the volume ratio of soluble and insoluble starches/cellulose. Since pore diameters

were in the range of 0.11 to 6.9 µm, these ceramics can be considered macroporous. No thermal decomposition or phase change of hydroxyapatite took place during sintering as confirmed by X-ray diffraction (XRD) patterns of the ceramics which showed a pure hydroxyapatite phase (Figure 2.1).

Batch adsorption tests were done to determine the fluoride adsorption capacity of ceramics and the results were fit to the Langmuir isotherm to obtain values of best fit parameters. The maximum fluoride adsorption capacity (q_{max}) ranged from 7 to 12 mg/g (Figure 2.2, Table 2.1). This was higher than or comparable to q_{max} values for activated alumina and bone char reported in the literature.

Ceramics made with insoluble starch were characterized by low porosities (25 to 37%) and relatively lower fluoride uptake (q_{max} values were between 7.4 to 8.6 mg/g). In the absence of insoluble starch, increasing the soluble starch content did not have a statistically significant impact on fluoride uptake. Addition of insoluble starch led to an appreciable increase in fluoride adsorption. The highest adsorption capacity was of the ceramics made with 50% by volume hydroxyapatite and 25% each of soluble and insoluble rice starch, with a porosity of 45%. This was a 1.5 times increase in q_{max} and a three-fold increase in $q_{1.5}$ compared to the ceramics made without 50% hydroxyapatite and 50% soluble starch. Ceramics with more than 25% by volume of insoluble starch disintegrated during handling, possibly because there was insufficient hydroxyapatite to form a solid matrix.

The impact of insoluble starch on fluoride adsorption was explained by examining the pore structure of the ceramics through scanning electron micrographs (Figure 2.3). While ceramics made with only soluble starch as the pore forming material had small closed-off pores, adding

insoluble starch created open and interconnected pores. It is assumed that addition of insoluble starch facilitated higher fluoride uptake by providing more pores for the fluoride ions to diffuse through and a higher surface area for adsorption.

Measuring the open porosity of ceramics gave further insight into the pore forming mechanisms of each type of starch. We compared the open porosities of two ceramics, both with 50% by volume hydroxyapatite and 50% total porosity (with varying contribution of each type of starch to the total porosity). Ceramics made with 50% by volume hydroxyapatite and 50% soluble starch had 31% open porosity. In contrast, ceramics with 50% hydroxyapatite, 25% insoluble starch and 25% soluble starch had 45% open porosity, an increase of 14%. This led to a 57% increase in q_{max} (Table 2.1, 2.2).

The effect of changing the type of pore forming material was evaluated by substituting the insoluble rice starch for wheat starch, corn starch and cellulose fibers. The three types of starch did not result in a statistically significant difference in fluoride adsorption and the $q_{1.5}$ values were in the range of 5.2 to 6.7 mg/g (Table 2.1). However, using cellulose fibers led to a decrease in $q_{1.5}$ which was 2.6 ± 0.5 mg/g. Micrographs of this ceramic revealed fewer open pores compared to ceramics made with the three types of starches (Figure 2.3).

To further explore the role of pore size and its effect on fluoride removal, ceramics with smaller pores were made using smaller hydroxyapatite particles (Chapter 3). It was hypothesized that smaller hydroxyapatite particles would result in smaller pores which would subsequently lead to an increase in specific surface area and fluoride adsorption. A theoretical explanation for this was given by plotting internal surface area against pore radii in the range of 0.1 to 1.5 µm (Figure 3.4). Smaller hydroxyapatite particles (d_{50} of 100 µm, compared to 240 µm used in Chapter 2), were

mixed with 25% each of insoluble rice starch and soluble starch to form porous ceramics. This resulted in a 50% increase in q_{max} from 12.4 mg/g to 18.2 mg/g. The change in $q_{1.5}$ and porosity was negligible (Figure 3.1, Table 3.1).

Further experiments were done on the best performing adsorbent ceramic to study its selectivity for fluoride and potential for regeneration. Batch adsorption tests done in the presence of other ions showed that none of the ions competed with fluoride at concentrations commonly found in groundwater except chloride (Figure 3.6 a). Even then, only very high concentrations of chloride (molar ratio of chloride to fluoride much greater than 1:1) decreased fluoride uptake. Chloride can adsorb onto hydroxyapatite by exchanging with hydroxide ions in the apatite structure, similar to fluoride ions. Natural organic matter (NOM) also competed strongly with fluoride at concentrations above 10 mg/L, or 4.8 mg C/L. These concentrations lie within the reported range of NOM concentrations reported in groundwater, 1- 50 mg C/L (Figure 3.6 b). This interference can either be a result of competition for adsorption sites or the clogging of pores which can hinder intraparticle diffusion of fluoride.

The regeneration potential of these ceramics was evaluated through repeated adsorption and desorption cycles (Figure 3.7). Two sodium hydroxide solutions (0.05 and 0.1 M) were used as regenerating solutions. The ceramics retained 70% of their adsorption capacity after five adsorption cycles [the adsorption capacity decreased from 2.5 mg/g in the first adsorption cycle to 1.75 mg/g after five adsorption cycles when regenerated with 0.1 M sodium hydroxide]. Similar results were obtained for 0.05 M sodium hydroxide. The ceramics did not dissolve even at pH values higher than 12; in contrast, aluminum-based adsorbents form soluble alumino-fluoro complexes at alkaline pH.

Several practical aspects must be considered before adsorbents can be used as a household or community-level treatment technology. The kinetics of fluoride removal were studied to test the performance of hydroxyapatite ceramics in practical settings. This was done through batch and continuous-flow column tests (Chapter 4). Batch kinetic tests revealed that time to reach equilibrium and the equilibrium fluoride concentration were independent of adsorbent size (Figure 4.2). While smaller ceramic pellets initially removed fluoride faster, the curves eventually converged and reached equilibrium after 26 hours. This study confirmed the validity of the Rapid Small-Scale Column Test (RSSCT) approach for scale up of column design.

Cylindrical ceramic pellets of diameter 2 mm and length 3 to 4 mm were packed in a glass column of diameter 2.5 mm and their fluoride removal performance was studied at flow rates of 1 and 2 mL/min, by plotting effluent concentrations against bed volumes treated. The effluent fluoride concentration was at or below the detection limit of 0.02 mg/L for the first 250 bed volumes (Figure 4.3). Eventually, the fluoride concentration in the effluent reached 1.5 mg/L (breakthrough), after 465 and 390 bed volumes for the 1 mL/min and 2 mL/min columns, respectively. The bed volumes to exhaustion ($C_e = 0.85\ C_0$) were similar for both the columns at about 650 bed volumes (Table 4.1). The mass of fluoride adsorbed per gram on to the column was similar at both flow rates. q_e (defined as mass of fluoride per gram of the adsorbent at exhaustion) was between 11 and 12 mg/g while q_b (similarly defined at breakthrough) was close to 10 mg/g for both columns. Values of q_e lie within the range of $q_{8.5}$ estimated from Langmuir fitting of isotherm data. q_b was understandably higher than $q_{1.5}$ since the entire length of the column is not at equilibrium with 1.5 mg/L fluoride at breakthrough. In fact, a large, up-stream portion of the column would be at equilibrium with a higher concentration of fluoride.

The RSSCT approach was tested and validated for fluoride adsorption by porous ceramics. A larger column of diameter 5 cm was packed with pellets of diameter 4 mm and length 4 to 8 mm. Two smaller columns were designed according to the CD and PD RSSCT approaches. The CD approach proved to be a better predictor of the performance of the larger column since there was a greater overlap between the breakthrough curves (Figure 4.4). This implies that the intraparticle diffusivity is independent of adsorbent size. Both the columns consumed about $1/6^{th}$ the volume of water used by the large column. While the CD RSSCT column predicted the breakthrough curve of the larger column more accurately for the first 500 bed volumes, eventually, the CD and PD RSSCT breakthrough curves converged, and both predicted the exhaustion of the larger column.

Column flow was interrupted at different points in the flow which led to a temporary decrease in the effluent concentration which suggests that the column was at non-equilibrium and that intraparticle diffusion contributes significantly to fluoride removal. During the interruption in flow, the fluoride ions diffused further into the porous ceramic pellet creating a concentration gradient between the ceramic surface and bulk fluoride solution. When the flow was restarted, the lowered fluoride concentrations rebounded due to reestablishment of the intra-particle diffusion limited adsorption.

A second larger column with the same EBCT but different flow rate and bed depth was run to determine the effect of flow rate (and thus the superficial velocity) on length of the MTZ. The breakthrough curves had significant overlap (Figure 4.5) thus confirming our hypothesis that length of the MTZ is correlated with the flow rate and superficial velocity in the column.

The takeaway from the kinetic tests was that the EBCT is critical to maximizing the fluoride loading on to the adsorbent, and thus, it's fluoride removal capacity. Column experiments with

different EBCTs resulted in starkly different q_b values, ranging from 4 to 10 mg/g. This has implications for the design and scale up of this adsorbent media. To utilize the fluoride adsorption capacity of this media to its fullest potential, operating the column under interrupted flow conditions might be more useful, if practical, considering that fluoride uptake is diffusion-limited.

A preliminary analysis was done to determine the cost of manufacturing the ceramics on an industrial scale. Based on bulk chemical prices and electricity consumption, the cost was estimated to be $1.63/kg, compared to $1.5/kg for commercially available activated alumina); however, as shown in Chapter 4 (Table 4.4), the ceramic adsorbent treated approximately 7 times more bed volumes to breakthrough than activated alumina. This implies that this media is six to seven times more cost effective than activated alumina.

Recommendation for future research

Three key areas have been identified for future research on fluoride removal using porous hydroxyapatite ceramics. Building on the research presented in this dissertation, the performance of these ceramics should be tested using natural ground water with elevated concentrations of fluoride. Specifically, the optimum pH for fluoride removal and effect of presence of other ions should be evaluated.

The second area of focus is exploring the potential of low-cost pore forming materials. Bio chars obtained from waste materials such as rice husk and saw dust are a cheap alternative to starch. While commercially available activated carbon is relatively expensive, less expensive bio chars with high specific surface area can be made in the laboratory for further investigation into its use as a pore-forming material. This has the potential to further reduce the cost of manufacturing this media at an industrial scale.

Finally, pilot and full-scale experiments should be conducted to explore the technical and economic feasibility of using this adsorbent media to treat fluoride-impacted groundwater. Specifically, future research should focus on designing a pilot-scale treatment system that maximizes the fluoride adsorption capacity while maintaining practical flow rates for use in low-income settings and carry out a detailed cost-estimate for the system.

Appendix A Scanning Electron Micrographs

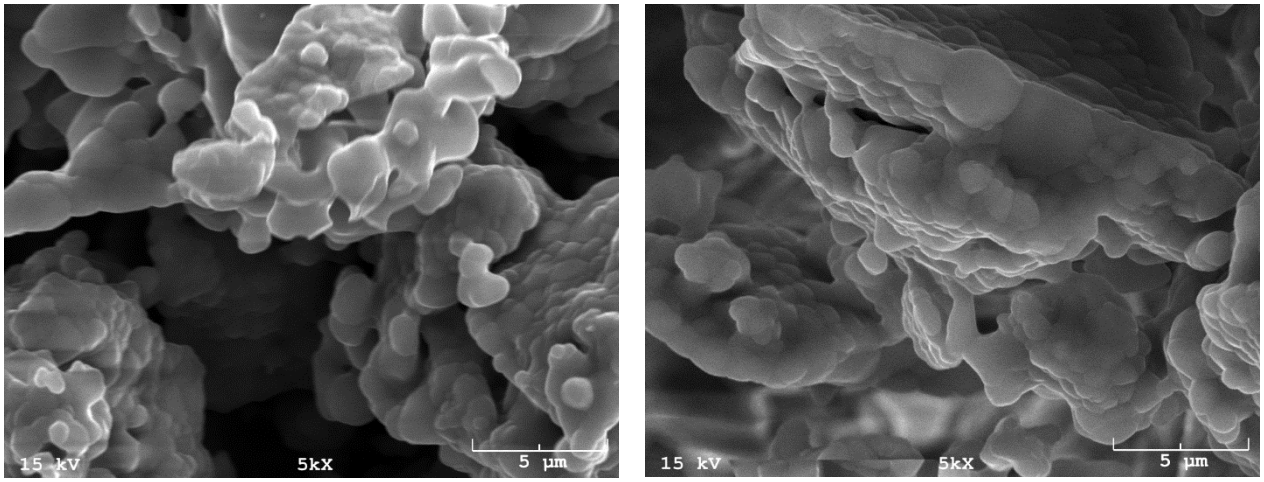

a) b)

Figure A- 1 Scanning electron micrographs of 50-25-25 ceramics made with coarse hydroxyapatite grains (d_{50} = 240 µm) calcined at a) 700 ºC and b) 900 ºC, each containing rice starch and soluble starch as pore forming materials

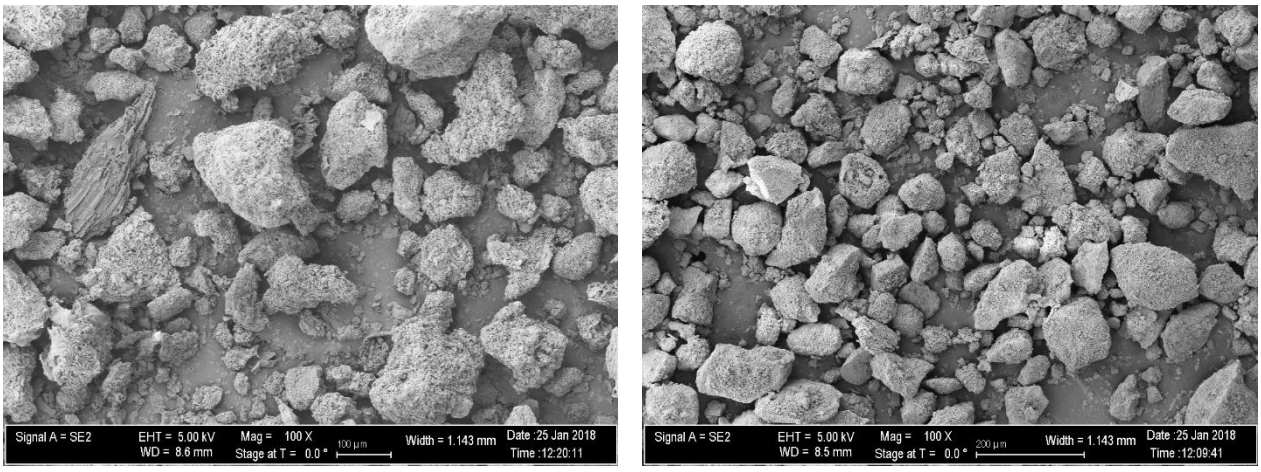

a) b)

Figure A- 2 Scanning electron micrographs of a) coarse hydroxyapatite grains (d_{50} = 240 µm) and b) fine hydroxyapatite grains (d_{50} = 110 µm)